

# 1 **Realization of phosphorylation hypothesis of sleep by** 2 **mammalian CaMKII $\beta$**

3

4 Daisuke Tone<sup>1,\*</sup>, Koji L. Ode<sup>1,2,\*</sup>, Qianhui Zhang<sup>2,\*</sup>, Hiroshi Fujishima<sup>1</sup>, Rikuhiko G.  
5 Yamada<sup>1</sup>, Yoshiki Nagashima<sup>2,3</sup>, Katsuhiko Matsumoto<sup>1</sup>, Zhiqing Wen<sup>2</sup>, Shota Y.  
6 Yoshida<sup>1,8</sup>, Tomoki T. Mitani<sup>1,8</sup>, Rei-ichiro Ohno<sup>2</sup>, Maki Ukai-Tadenuma<sup>1,9</sup>, Junko  
7 Yoshida Garçon<sup>1</sup>, Mari Kaneko<sup>4</sup>, Shoi Shi<sup>1,2</sup>, Hideki Ukai<sup>1,9</sup>, Kazunari Miyamichi<sup>5</sup>,  
8 Takashi Okada<sup>6</sup>, Kenta Sumiyama<sup>7</sup>, Hiroshi Kiyonari<sup>4</sup>, Hiroki R. Ueda<sup>1,2</sup>

9

10 *<sup>1</sup>Laboratory for Synthetic Biology, RIKEN Center for Biosystems Dynamics Research,*  
11 *1-3 Yamadaoka, Suita, Osaka 565-0871, Japan*

12

13 *<sup>2</sup>Department of Systems Pharmacology, Graduate School of Medicine, The*  
14 *University of Tokyo, Hongo 7-3-1, Bunkyo-ku, Tokyo, 113-0033 Japan*

15

16 *<sup>3</sup>Thermo Fisher Scientific K.K., Moriya-cho 3-9, Yokohama, Kanagawa, 221-0022,*  
17 *Japan*

18

19 *<sup>4</sup>Laboratory for Animal Resources and Genetic Engineering, RIKEN Center for*  
20 *Biosystems Dynamics Research, 2-2-3 Minatogima-minamimachi, Chuo-ku, Kobe,*  
21 *Hyogo, 650-0047, Japan*

22

23 *<sup>5</sup>Laboratory for Comparative Connections, RIKEN Center for Biosystems Dynamics*  
24 *Research, 2-2-3 Minatogima-minamimachi, Chuo-ku, Kobe, Hyogo, 650-0047, Japan*

25

26 <sup>6</sup>*Division of Molecular and Medical Genetics, Center for Gene and Cell Therapy, The*  
27 *Institute of Medical Science, the University of Tokyo, Shirokanedai 4-6-1, Minato-city,*  
28 *Tokyo, 108-8639, Japan*

29

30 <sup>7</sup>*Laboratory for Mouse Genetic Engineering, RIKEN Center for Biosystems*  
31 *Dynamics Research, 1-3 Yamadaoka, Suita, Osaka 565-0871, Japan*

32

33 <sup>8</sup>*Graduate school of Medicine, Osaka University, 1-3 Yamadaoka, Suita, Osaka 565-*  
34 *0871, Japan*

35

36 <sup>9</sup>*Present address, International Research Center for Neurointelligence (WPI-IRCN),*  
37 *UTIAS, The University of Tokyo, Hongo 7-3-1, Bunkyo-ku, Tokyo, 113-0033 Japan.*

38

39 \*These authors contributed equally

40

41 Correspondence: [uedah-tky@umin.ac.jp](mailto:uedah-tky@umin.ac.jp) (H.R.U.)

42

43 **ABSTRACT**

44 The reduced sleep duration observed in *Camk2a* and *Camk2b* knockout mice  
45 revealed the role of Ca<sup>2+</sup>/calmodulin-dependent protein kinase II  
46 (CaMKII) $\alpha$ /CAMKII $\beta$  as sleep-promoting kinases and lead to the phosphorylation  
47 hypothesis of sleep. However, the underlying mechanism of sleep regulation by  
48 kinases and protein phosphorylation is largely unknown. Here, we demonstrate that  
49 the phosphorylation states of CaMKII $\beta$  regulates sleep duration and sleep needs.  
50 Importantly, the activation or inhibition of CaMKII $\beta$  can increase or decrease sleep  
51 duration by almost two-fold, supporting the role of CaMKII $\beta$  as a core sleep regulator  
52 in mammals. This sleep regulation depends on the kinase activity of CaMKII $\beta$  in  
53 excitatory neurons. Furthermore, CaMKII $\beta$  mutants mimicking different  
54 phosphorylation states can regulate various sleep steps including sleep induction,  
55 sleep maintenance, and sleep cancelation. Key CaMKII $\beta$  residues responsible for  
56 the mode switch undergo ordered (auto-)phosphorylation. We thus propose that  
57 ordered multi-site phosphorylation of CaMKII $\beta$  underlies multi-step sleep regulation  
58 in mammals.

59

60

## 61 INTRODUCTION

62 A wide range of biological phenomena, including organism-level behaviors, rely on  
63 the regulation of protein activity by phosphorylation. The circadian clock is an  
64 excellent example of the marked role of protein phosphorylation in the regulation of  
65 an organism-level behavior <sup>1-3</sup>. Genetic screening of animal behavior revealed that  
66 the *period* (*per*) gene is a core factor for the circadian clocks <sup>4</sup>. Casein kinase I (CKI)  
67 phosphorylates the PER protein, and a human lineage showing abnormalities in  
68 circadian behavioral rhythms had a single amino acid substitution at the  
69 phosphorylation residue <sup>5</sup>. The phosphorylation of PER by CKI is considered a major  
70 regulator of circadian period length for the following reasons: first, the targeted  
71 mutation of a single phosphorylation residue in PER can bidirectionally change the  
72 period length of the circadian clock <sup>6,7</sup>. Second, the effect is significant, with changes  
73 in CKI-kinase activity resulting in a more than two-fold change in period length, at  
74 least in culture cells <sup>8</sup>.

75

76 The sleep-wake cycle, like the circadian clocks, is a physiological function that  
77 governs the organism-level behavioral rhythms and is believed to regulate synaptic  
78 function <sup>9</sup>. However, the molecular mechanisms regulating the daily amount of sleep  
79 and the transitions between sleep and wake phases are not fully understood.  
80 Genetic screening studies have revealed that protein kinases play an important role  
81 in sleep duration regulation. In particular, knocking out the first sleep-promoting  
82 kinases discovered, *Camk2a* and *Camk2b*, markedly reduced sleep duration in mice  
83 <sup>10</sup>. Subsequent phosphoproteomics studies have shown that the phosphorylation  
84 states of neuronal proteins vary with the sleep-wake cycle and in response to sleep  
85 deprivation <sup>11-13</sup>. The phosphoproteomics profile revealed an alteration of the



86 phosphorylation states of  $\text{Ca}^{2+}$ /calmodulin-dependent protein kinase II  
87 (CaMKII) $\alpha$ /CaMKII $\beta$  and its potential substrates (e.g., Synapsin 1). These results  
88 suggest that CaMKII $\alpha$ /CaMKII $\beta$  plays an important role in mammalian sleep  
89 regulation and support the phosphorylation hypothesis of sleep (the idea that sleep  
90 is regulated by protein phosphorylation).

91

92 The phosphorylation hypothesis of sleep <sup>10,14</sup> assumes that the neural activity  
93 associated with wakefulness acts as an *input* to activate sleep-promoting kinases  
94 such as CaMKII $\alpha$ /CaMKII $\beta$  <sup>10</sup>, SIK1/SIK2/SIK3 <sup>15,16</sup>, and ERK1/ERK2 <sup>17</sup>. Another  
95 prediction is that sleep-promoting kinases may need to *store* some form of  
96 information associated with wakefulness. This is because awakening does not  
97 immediately lead to sleep, but rather *stores* a history of awakening as a sleep need.  
98 As an *output* of sleep regulation, sleep-promoting kinases might induce sleep by  
99 phosphorylating their substrates. CaMKII $\alpha$ /CaMKII $\beta$  has unique features that might  
100 make this kinase suitable for achieving the *input*, *storage*, and *output* mechanism of  
101 sleep regulation. A well-known mechanism of CaMKII $\alpha$ /CaMKII $\beta$  activation is the  
102 intracellular  $\text{Ca}^{2+}$  influx that occurs upon excitatory synaptic input and subsequent  
103 neuronal firing <sup>18,19</sup>. Intracellular  $\text{Ca}^{2+}$  binds to calmodulin (CaM), which binds to  
104 CaMKII $\alpha$ /CaMKII $\beta$  and switches its kinase domain to the exposed open and kinase-  
105 active form. The kinase-active CaMKII $\alpha$ /CaMKII $\beta$  undergoes autophosphorylation  
106 along with phosphorylation of other substrate proteins. T286 (CaMKII $\alpha$ ) and T287  
107 (CaMKII $\beta$ ) are the first residues undergoing autophosphorylation upon activation of  
108 CaMKII $\alpha$ /CaMKII $\beta$ . T286 and T287 phosphorylation switches CaMKII $\alpha$ /CaMKII $\beta$  to  
109 its kinase-active form even in the absence of  $\text{Ca}^{2+}$ /CaM <sup>20-22</sup>. The maintained kinase  
110 activity due to T286 and T287 phosphorylation is called autonomous activity. Finally,

111 the activated CaMKII $\alpha$ /CaMKII $\beta$  phosphorylates several neuronal proteins. The  
112 sequential autoregulation of CaMKII activity serves as a neuronal timer in a minutes  
113 time scale in fruits fly <sup>23</sup>. However, the effect and mechanism of CaMKII $\alpha$ /CaMKII $\beta$   
114 on sleep regulation and duration in mammals have not been rigorously investigated.  
115  
116 Furthermore, the dynamics of sleep-wake are not only characterized by the duration  
117 of sleep, but also by the distribution of sleep and wake episodes. Indeed, *Camk2a*  
118 and *Camk2b* knockout mice are less likely to transition from wake to sleep and from  
119 sleep to wake <sup>10</sup>. This suggests that CaMKII $\alpha$ /CaMKII $\beta$  elicits the transition between  
120 wake and sleep. It should be noted that sleep duration and sleep-wake transition can  
121 be independently regulated: for example, knocking out *orexin* barely affects sleep  
122 duration, but significantly increases the sleep-wake transition <sup>24,25</sup>. Given the  
123 physiological process of the sleep-wake cycle, it is reasonable to assume that  
124 organisms employ multiple and stepwise mechanisms to regulate sleep. It would  
125 begin with sleep induction and switch to sleep maintenance. CaMKII $\alpha$ /CaMKII $\beta$  itself  
126 undergoes multiple and stepwise changes (multi-site autophosphorylation,  
127 dodecameric oligomerization, and conformational changes) <sup>18,26</sup>. Following the  
128 phosphorylation of T286 and T287, the activated kinase catalyzes the  
129 autophosphorylation of residues such as T305 and T306 (CaMKII $\alpha$ ), and T306 and  
130 T307 (CaMKII $\beta$ ). Phosphorylation of these residues inhibits the binding of Ca<sup>2+</sup>/CaM  
131 to CaMKII $\alpha$ /CaMKII $\beta$  <sup>27-29</sup>. The autoregulatory mechanism of CaMKII $\alpha$ /CaMKII $\beta$  may  
132 be more complex than a two-step regulation. It was reported that  
133 autophosphorylation can occur multiple residues other than well-understood  
134 T286/T305/T306 (CaMKII $\alpha$ ) and T287/T306/T307 (CaMKII $\beta$ ) with different efficiency  
135 depending on residues <sup>30</sup> and the dodecameric CaMKII $\alpha$ /CaMKII $\beta$  structure may

136 have many intermediate states <sup>31</sup>. Although the sleep-wake cycle affects the level of  
137 such multi-site autophosphorylation of CaMKII $\alpha$ /CaMKII $\beta$  <sup>11-13,32,33</sup>, little is known  
138 about the actual function of the multi-site autophosphorylation in the regulation of the  
139 sleep-wake cycle. Of the four *Camk2* homologs (i.e., *Camk2a*, *Camk2b*, *Camk2d*  
140 and *Camk2g*), knockout mice of *Camk2b* showed the most pronounced decrease in  
141 sleep duration per day <sup>10</sup>. Thus, this study will focus on CaMKII $\beta$  and aims to  
142 comprehensively analyze the sleep phenotype caused by a series of CaMKII $\beta$   
143 mutants mimicking the different phosphorylation states.

144

145

## 146 **RESULTS**

### 147 **Phosphorylation of CaMKII $\beta$ regulates sleep induction.**

148 To investigate whether CaMKII $\beta$  regulates sleep depending on the phosphorylation  
149 state of CaMKII $\beta$ , we conducted an *in vivo* comprehensive phosphomimetic  
150 screening of CaMKII $\beta$ . Mouse CaMKII $\beta$  protein has 69 serine (S) and threonine (T)  
151 residues that can be the target of autophosphorylation (**Figure 1a**). We assessed  
152 the contribution of these residues to sleep regulation by expressing a series of  
153 phosphomimetic mutants of CaMKII $\beta$ , in which aspartic acid (D) replaced one of the  
154 phosphorylable residues. Each of the 69 CaMKII $\beta$  mutants was expressed under the  
155 control of human *synapsin-1* (*hSyn1*) promoter and delivered in wild-type mice brain  
156 by an adeno-associated virus (AAV) system AAV-PHP.eB<sup>34</sup>, which allows broad  
157 gene expression throughout the brain (**Figure 1b**). The whole-brain expression of  
158 H2B-mCherry reporter under the *hSyn1* promoter delivered by the AAV system was  
159 confirmed by whole-brain imaging using the CUBIC method (**Figure 1c** and **Figure**  
160 **1-figure supplement 1a**). Unless otherwise indicated, we refer to mice with AAV-  
161 mediated expression of CaMKII $\beta$  mutants simply by the mutant name (e.g., T287D  
162 mice). We measured the sleep parameters of the mice expressing mutant CaMKII $\beta$   
163 using a respiration-based sleep phenotyping system, snappy sleep stager (SSS)<sup>24</sup>  
164 (**Figure 1b**). Sleep measurements were started at 8 weeks old following the AAV  
165 administration at 6 weeks old. Mice expressing AAV-induced wild-type (WT)  
166 CaMKII $\beta$  and untreated mice had similar daily sleep durations ( $733.9 \pm 6.1$  and  $724.7$   
167  $\pm 4.3$  min<sup>24</sup>, respectively; all mice phenotypes are reported as mean  $\pm$  SEM). In this  
168 screening, mice expressing T287D, S114D or S109D CaMKII $\beta$  mutants had top  
169 three extended daily sleep duration ( $846.7 \pm 23.7$ ,  $839.7 \pm 14.1$  or  $803.4 \pm 16.2$  min,  
170 respectively), though the phenotype of S109D showed no statistical significance

171 **(Figure 1d)**. Although no statistical significance was obtained for sleep transition  
172 parameters  $P_{WS}$  (probability of transition from wakefulness to sleep) and  $P_{SW}$   
173 (probability of transition from sleep to wakefulness) in this first screening **(Figure 1-**  
174 **figure supplement 2a, b)**, the  $P_{WS}$  of T287D mice was higher than that of WT-  
175 expressing mice, which is opposite to the phenotype of *Camk2b* knockout mice<sup>10</sup>.  
176 There was no correlation between the ensemble of sleep duration and AAV  
177 transduction efficiency among the analyzed mutants **(Figure 1-figure supplement**  
178 **2c)**, indicating that the observed sleep phenotypes can be attributed to the nature of  
179 the introduced mutations rather than to a possible difference in AAV transduction  
180 efficacy.

181 To confirm the reproducibility of the extended sleep duration for T287D,  
182 S114D and S109D mice, we conducted an independent set of experiments. These  
183 confirmed the prolonged sleep duration of T287D mice ( $861.9 \pm 26.1$  min) and the  
184 increase in  $P_{WS}$  **(Figure 1e)**. The extended sleep duration of T287D mice does not  
185 depend on the circadian timing because the mice showed increased sleep duration  
186 at most zeitgeber time of the day **(Figure 1f)**. Besides, this second round of  
187 evaluation did not show a significant increase in the sleep duration of S114D mice  
188 and S109D, although a trend of extended sleep duration was observed for S109D  
189 mutant **(Figure 1-figure supplement 2d and 2e)**. We concluded that T287D  
190 CaMKII $\beta$  is the mutant that robustly increased sleep duration *in vivo*.

191 Replacing T287 with the non-phosphomimetic alanine (A) did not extend  
192 sleep duration ( $701.5 \pm 9.8$  min) **(Figure 1e, f)**. This supports that the  
193 phosphorylation-mimicking property of D caused the sleep duration extension.  
194 Furthermore, the extended sleep duration depends on the kinase activity of CaMKII $\beta$ ,  
195 because the kinase-dead (K43R) version of the T287D mutant (i.e., K43R:T287D)

196 did not extend sleep duration ( $719.8 \pm 12.4$  min). Given that the phosphorylation of  
197 T287 inhibits the interaction between the kinase domain and the regulatory segment  
198 of CaMKII $\beta$  (which leads to the open and kinase-active conformation of the kinase),  
199 the normal sleep duration of K43R:T287D mice suggests that CaMKII $\beta$  with open  
200 conformation alone is insufficient to lengthen sleep duration. We thus propose that  
201 CaMKII $\beta$  induces sleep via T287 phosphorylation and that this process requires the  
202 kinase activity of CaMKII $\beta$ .

203         The robust sleep induction by the T287D mutant suggests that T287  
204 phosphorylation marks the level of sleep need. This has been supported through  
205 previous studies; for example, the level of CaMKII $\alpha$  T286 phosphorylation or  
206 CaMKII $\beta$  T287 phosphorylation follows the expected level of sleep need upon six  
207 hours sleep deprivation and subsequent recovery sleep analyzed by western blotting  
208 <sup>12</sup>. Moreover, the level of CaMKII $\alpha$  T286 phosphorylation follows the expected sleep  
209 need along with normal sleep wake cycle: a previous study showed the circadian  
210 rhythmicity of CaMKII $\alpha$  T286 phosphorylation peaking at the end of the dark (wake)  
211 phase and decreasing throughout the light (sleep) phase <sup>13</sup>. Consistent with this  
212 rhythmicity, another study indicated CaMKII $\alpha$  T286 phosphorylation is higher at the  
213 dark (wake) phase <sup>11</sup>. Because several studies focus on CaMKII $\alpha$  and rely on  
214 western blotting technique, we also examined whether the phosphorylation levels of  
215 T287 in the brain increased upon six hours sleep deprivation by using a quantitative  
216 and targeted selected-reaction-monitoring (SRM) analysis. The SRM analysis  
217 confirmed that sleep deprivation increased T287 phosphorylation of endogenous  
218 CaMKII $\beta$  without changing the amount of total CaMKII $\beta$  (**Figure 1g** and **1h**). In  
219 addition, the phosphorylation level of CaMKII $\alpha$  T286 and CaMKII $\beta$  T287 correlated  
220 well, suggesting that these phosphorylation levels similarly respond to sleep

221 deprivation (**Figure 1-figure supplement 2f, g**).

222

### 223 **Biochemical evaluation of sleep-inducing CaMKII $\beta$ mutants.**

224 To compare the kinase activity and mice sleep phenotypes, we measured  
225 the kinase activity of each mutant *in vitro* using cell lysate system. We prepared cell  
226 extracts of 293T cells overexpressing the CaMKII $\beta$  mutants. Relative expression  
227 level was quantified for each mutant by dot blot (**Figure 1-figure supplement 3a**).  
228 The relative amounts of CaMKII $\beta$  as well as cellular components derived from the  
229 extracts were adjusted by mixing CaMKII $\beta$ -expressing 293T lysate and mock-  
230 transfected 293T lysate. This adjustment process was not applied for the mutants  
231 having <25% expression level compared with wild-type CaMKII $\beta$ . Then, the  
232 enzymatic activity of the expressed CaMKII $\beta$  in the presence and absence of CaM  
233 (**Figure 1-figure supplement 3b**).

234 Most mutants as well as WT exhibit kinase activity only in the presence of  
235 CaM (**Figure 1-figure supplement 3b**). S109D, T242D, and T287D mutants  
236 showed marked enzyme activity even in the absence of CaM. The CaM-independent  
237 kinase activity of T287D is consistent with the constitutive kinase-active property of  
238 T287D. However, the kinase activity of T287D in the presence of CaM is lower than  
239 that of WT. By contrast, S109D and T242D showed no reduction in the kinase activity  
240 in the presence of CaM and the CaM-independent kinase activity is higher than that  
241 of T287D. The reason of this lower T287D activity is currently unknown but might be,  
242 at least in part, due to the inhibitory autophosphorylation that was underway in the  
243 293T cell during the period between the expression of the T287D protein and the  
244 preparation of the cell lysate, and structural thermal-instability elicited by the  
245 detachment of regulatory segment from the kinase domain<sup>35</sup>. Since these inhibitory

246 mechanisms are caused by the constitutive-kinase activation (and/or structural  
247 alteration from close to open conformation) of the enzyme, the final kinase activity  
248 will appear as the sum of positive and negative factors: therefore, it is important to  
249 be careful in discussing the relationship between whether a mutation activates or  
250 inhibits kinase activity based on the one-point relative strength of the  
251 phosphorylation activity alone.

252         Although there are limitations in the biochemical evaluation of kinase activity  
253 in this cell lysate system as described above, it appears reasonable to assume that  
254 mutations, in which CaM-independent activity is detected, have at least the property  
255 of showing CaM-independent phosphorylation activity, unlike the wild-type enzyme.  
256 Similar to the kinase-dead mutation K43R, the mutation that reduces the  
257 phosphorylation activity to a level similar to that of the background from cell extracts  
258 may also be regarded as a reliable phenotype, basically acting in a repressive  
259 manner on the kinase activity. Given that the level of AAV-mediated CaMKII $\beta$   
260 expression is much lower than the level of endogenous CaMKII $\beta$  (**Figure 1-figure**  
261 **supplement 1b**), it would be reasonable to assume that the CaMKII $\beta$  mutants  
262 showing CaM-independent activity affected sleep by exhibiting a dominant  
263 phenotype (e.g., T287D and S109D), even in the presence of abundant endogenous  
264 CaMKII $\alpha$ /CaMKII $\beta$  protein. It is also quite possible that this sleep phenotype is  
265 mediated by the activation of the endogenous CaMKII $\alpha$ /CaMKII $\beta$  by the constitutive-  
266 active mutant. Also, the mutation with reduced kinase activity may not have had a  
267 dominant negative effect on sleep in the presence of higher level of the endogenous  
268 CaMKII $\beta$  due to its low expression level mediated by AAV vector, and thus did not  
269 show a pronounced phenotype in the current screening.

270         It should be noted that while T287D had high kinase activity in the absence of



271 CaM, T242D and especially S109D showed even higher kinase activity in the  
272 absence of CaM. However at least T242D appears not to extend sleep duration and  
273 the effect of S109D on the sleep duration is milder than that of T287D *in vivo*. Hence,  
274 the results of the present kinase assay using a conventional peptide substrate do  
275 not fully account for the quantitative level of sleep induction observed *in vivo*,  
276 suggesting the existence of an additional layer of regulation.

277 Among the kinase-inactive mutants and others, several mutants had  
278 significantly reduced expression levels (e.g., S182) (**Figure 1-figure supplement**  
279 **3a**). Reduced protein expression levels and/or protein stability inherent in such  
280 mutants could also be a reason why these mutants do not exhibit a dominant active  
281 sleep-promoting activity in the screening *in vivo*. The unstable sleep phenotype of  
282 S114D might be related to the unstable/low-expression nature of this mutant at least  
283 in culture cell—as with the kinase activity evaluation, protein expression levels in the  
284 mouse brain do not always correlate with expression levels in 293T cells, and should  
285 be considered carefully though.

286

### 287 **Phosphorylation of CaMKII $\beta$ regulates NREM sleep induction and sleep** 288 **needs.**

289 To further investigate the role of T287 phosphorylation in sleep regulation, we  
290 expressed the CaMKII $\beta$  T287-related mutants under the *Camk2a* promoter<sup>36</sup>, which  
291 is a well-characterized promoter inducing gene expression preferentially to the  
292 excitatory neurons. As **Figures 1e and f** show, the daily sleep duration of T287D  
293 mice was higher than that of WT-expressing mice, which is consistent with the results  
294 obtained with the *hSyn1* promoter. WT, T287A, K43R:T287D, and PBS-  
295 administrated mice had comparable sleep phenotypes (**Figures 2a, b**). As observed

296 in T287D mice with the *hSyn1* promoter, T287D mice with the *Camk2a* promoter had  
297 a significantly higher  $P_{WS}$  (**Figure 2a**), suggesting that the T287-phosphorylated  
298 CaMKII $\beta$  promotes the transition from wakefulness to sleep. We also reproduced the  
299 increased sleep duration by expressing the T287D mutant under the *Camk2b*  
300 promoter cloned in this study (**Figure 2-figure supplement 1a, b**).

301 *Camk2* plays a role in the regulation of the circadian rhythm<sup>37</sup>. To examine  
302 whether the sleep-inducing effect of the CaMKII $\beta$  T287D mutant depends on the  
303 behavioral circadian rhythmicity, we expressed it in *Cry1<sup>-/-</sup>:Cry2<sup>-/-</sup>* and *Per1<sup>-/-</sup>:Per2<sup>-/-</sup>*  
304 double knockout mice (*Cry1/2* DKO and *Per1/2* DKO) using the *Camk2a* promoter.  
305 Both DKO mice lines are deficient in behavioral circadian rhythmicity in constant dark  
306 (DD)<sup>38-41</sup>. Under light/dark (LD) conditions, the daily sleep duration of T287D-  
307 expressing *Cry1/2* DKO and *Per1/2* DKO mice was significantly higher than that of  
308 WT CaMKII $\beta$ -expressing mice (**Figure 2c, d, e, f**). Under constant dark, where both  
309 DKO mice lack a clear circadian behavioral rhythmicity, the sleep duration of T287D-  
310 expressing mice increased irrespective of circadian time across the 24 h (**Figure 2g,**  
311 **h, i, j**). This increased sleep duration under constant dark is associated with  
312 increased  $P_{WS}$ . These results demonstrate that the sleep-inducing effect of the  
313 T287D mutant is independent of behavioral circadian rhythmicity and canonical core  
314 clock genes such as *Cry1/Cry2* or *Per1/Per2*.

315 The sleep-inducing effects of the T287D mutant could be attributed to an  
316 impairment in the proper maintenance of wakefulness. To examine whether the  
317 arousal system in T287D mice is normal, we assessed their responses to external  
318 stimuli. The novel cage environment promotes awakening by stimulating the mice's  
319 exploratory behavior<sup>42</sup>. Cage exchange significantly decreased the sleep duration  
320 of T287D, WT, and PBS-administrated mice compared with the baseline duration

321 **(Figure 2-figure supplement 1c)**, suggesting that the sleep-extending effect of the  
322 T287D mutant is not due to abnormalities in the arousal system.

323 Since the sleep-inducing effect of the T287D mutant depends neither on the  
324 circadian rhythms nor on an abnormal arousal system, it might directly alter sleep  
325 needs, which can be estimated through the delta-wave of an electroencephalogram  
326 (EEG). We recorded EEGs and electromyograms (EMG) of the mice expressing the  
327 CaMKII $\beta$  T287D mutant under the *Camk2a* promoter. The EEG/EMG recordings  
328 revealed that T287D mice had significantly higher daily non-rapid eye movement  
329 (NREM) and REM sleep duration (**Figure 2k, I**) and  $P_{WS}$  (**Figure 2m**) than WT-  
330 expressing mice. This data is consistent with the SSS measurements (**Figure 2a**).  
331 The analysis of transition probabilities between wake, NREM, and REM episodes  
332 revealed a large decrease ( $p < 0.001$ ) in wake maintenance (W to W) and increase  
333 ( $p < 0.001$ ) in the transitions from wake to NREM (W to N) compared with WT-  
334 expressing mice (**Figure 2n**). These results suggest that the T287 phosphorylation  
335 of CaMKII $\beta$  induces sleep by increasing wake to NREM transitions. Besides, we  
336 confirmed that T287D mice had significantly higher delta power and slow power  
337 during sleep episodes (**Figure 2o** and **Figure 2-figure supplement 1d**), suggesting  
338 elevated sleep needs. We obtained similar EEG/EMG recordings with mice  
339 expressing T287D mutant under the *hSyn1* promoter (**Figure 2-figure supplement**  
340 **1e-j**). These results demonstrate that T287-phosphorylated CaMKII $\beta$  provokes  
341 physiological sleep needs and acts on the transition from wake to NREM sleep.

342

343 **Phosphorylation of CaMKII $\beta$  in excitatory neurons regulates sleep induction.**

344 A potential limitation of the use of *Camk2a* promoter is that the expression is highly  
345 enriched in excitatory neurons but not exclusively localized<sup>36</sup>. We then investigated

346 the neuronal cell types responsible for the CaMKII $\beta$ -mediated sleep induction by  
347 using other strategy using AAVs carrying double-floxed inverted open reading frame  
348 (DIO) constructs and mouse lines expressing *Cre* recombinases in specific neurons  
349 (*Cre*-mice) (**Figure 3a**). CaMKII $\beta$  T287D expression in *Vglut2*-specific neurons  
350 significantly increased sleep duration compared to the WT CaMKII $\beta$ -expressing mice  
351 (**Figure 3b, c**), while expression of the T287D mutant in *Gad2*-specific neurons did  
352 not affect sleep phenotype (**Figure 3d, e**). These results confirm that glutamatergic  
353 excitatory neurons are involved in the sleep promotion by the CaMKII $\beta$  T287D  
354 mutant.

355

### 356 **Kinase activity of CaMKII $\beta$ bidirectionally regulates sleep.**

357 Having the different efficacy of sleep-inducing activity among the biochemical  
358 constative-active CaMKII $\beta$  mutants (e.g., T287D and S109D), we next sought to  
359 confirm the relationship between the CaM-independent enzymatic activity of  
360 CaMKII $\beta$  and sleep promotion by using another type of constitutive-active CaMKII $\beta$ .  
361 To this end, we used CaMKII $\beta$  deletion mutant that lacks the C-terminal half involving  
362 the regulatory segment, linker region, and oligomerization domain <sup>43</sup>). The CaMKII $\beta$   
363 deletion mutant is constitutively active due to the exposed kinase domain but does  
364 not retain T287 and subsequent residues (**Figure 4a**). Similar to T287D mice, mice  
365 expressing the deletion mutant (del) showed an extended sleep duration and  
366 increased  $P_{WS}$ . The extended sleep duration depends on the kinase activity because  
367 mice expressing the deletion mutant with the K43R point mutation (K43R:del) and  
368 the WT-expressing mice had similar sleep phenotypes (**Figure 4b, c**). These results  
369 support that the constitutive kinase activity of CaMKII $\beta$  induces sleep. Furthermore,  
370 sleep induction by CaMKII $\beta$  does not require the dodecameric structure of CaMKII $\beta$

371 or the regulatory segment and the linker region.

372 We carried out a complementary approach by inhibiting the kinase activity of  
373 endogenous CaMKII. We used autocamide inhibitory peptide 2 (AIP2), which  
374 inhibits the enzyme activity of CaMKII $\alpha$  and CaMKII $\beta$  by binding to the kinase domain  
375 and inhibiting the substrate-enzyme interaction (**Figure 4d**)<sup>44,45</sup>. Mice expressing  
376 the mCherry-fused AIP2 exhibited a decreased sleep duration and  $P_{WS}$  along with  
377 an increased  $P_{SW}$  compared with mice expressing the inactive mutant of AIP2  
378 (RARA) (**Figure 4e, f**), demonstrating that the CaMKII $\alpha$ /CaMKII $\beta$  kinase activity is  
379 critical for normal sleep induction and maintenance. These results were consistent  
380 with the phenotype of *Camk2a* or *Camk2b* knockout mice<sup>10</sup>, except for the  $P_{SW}$   
381 change: the genetic knockout of *Camk2a* or *Camk2b* slightly decreased  $P_{SW}$ . This  
382 difference might account for the postnatal and kinase activity targeted inhibition of  
383 CaMKII $\alpha$ /CaMKII $\beta$  by AIP2 expression.

384 We further investigated the architectural and qualitative sleep changes under  
385 suppressed CaMKII $\alpha$ /CaMKII $\beta$  activity. The EEG/EMG recording of mice expressing  
386 AIP2 showed a significant decrease in NREM and REM sleep duration (**Figures 4g-**  
387 **i**). The increased transition probability from NREM/REM to wake and decreased  
388 transition to keep NREM and REM episodes in AIP2-expressing mice suggested that  
389 CaMKII $\alpha$ /CaMKII $\beta$  inhibition impaired the maintenance mechanism of NREM/REM  
390 sleep (**Figure 4j**). There was no significant change in normalized delta power during  
391 NREM sleep (**Figure 4-figure supplement 1a, b**). Note that there were differences  
392 in the waveforms of the EEG represented by the increased power of slow-wave  
393 oscillations (0.5 Hz–1 Hz) in all three states of vigilance (**Figure 4-figure**  
394 **supplement 1c**), though no difference was observed in the local field potential  
395 recordings of awaking mice cortex with the adult deletion of both *Camk2a* and

396 *Camk2b*<sup>46</sup>. Consistent with the phenotype of AIP2-expressed mice, EEG/EMG  
397 analysis showed that *Camk2b* knockout mice had decreased NREM and REM  
398 duration (**Figure 4-figure supplement 1d-g**) as well as decreased  $P_{SW}$ . The  
399 knockout mice were established in previous study<sup>10</sup> but not analyzed for the sleep  
400 phenotype by EEG/EMG recordings. *Camk2b* knockout mice might have a  
401 decreased delta power, although we could not conclude on this because the changes  
402 in delta power depend on the normalization procedure of the EEG power spectrum  
403 (**Figure 4-figure supplement 1h-k**). The reduced sleep duration in SSS by AIP2-  
404 expression or *Camk2b* knockout can be attributed to the reduced NREM sleep  
405 because NREM sleep constitutes the most portion of total sleep time, though  
406 CaMKII $\alpha$ /CaMKII $\beta$  may also have a role in the control of REM sleep as observed in  
407 reduced REM sleep duration in these EEG/EMG recordings.

408

#### 409 **Multi-site phosphorylation of CaMKII $\beta$ can cancel sleep induction.**

410 Supposing that the autophosphorylation of T287 in CaMKII $\beta$  encodes information on  
411 sleep need, the encoded information should not be decoded when it is not required.  
412 We thus investigated whether the phosphorylation of additional residues could  
413 cancel the sleep-inducing function of T287-phosphorylated CaMKII $\beta$ . To this end, we  
414 created a series of double-phosphomimetic mutants of CaMKII $\beta$ , in which besides  
415 T287, we mutated one of the remaining 68 S or T residues to D. The screening of  
416 these double-phosphomimetic mutants *in vivo* identified several mutants that exhibit  
417 a sleep phenotype similar to WT-expressing mice (**Figure 5a, Figure 5-figure**  
418 **supplement 1a-b**). In other words, the additional D mutation cancels the sleep-  
419 inducing effect of T287D. We focused on the five mutants (+S26D, +S182D, +T177D,  
420 +T311D, and +S516D; hereafter, we refer to the double-mutants by the additional

421 mutated residue preceded by a plus sign) with the top five closest sleep parameters  
422 to WT, even if they had transduction efficiencies comparable to that of T287D (**Figure**  
423 **5-figure supplement 1c-e**). To confirm that the observed phenotype of these five  
424 mutants came from the phosphomimetic property of D, we evaluated the phenotypes  
425 of non-phosphomimetic A mutants. The +S26A, +S182A, and +T311A mutants lost  
426 the effect of the D substitution, supporting the idea that phosphorylation of S26, S182,  
427 and T311 cancels the sleep-inducing effect of the co-existing T287 phosphorylation.  
428 On the other hand, the sleep phenotypes of +T516A and +T177A mice were similar  
429 to those of +T516D, +T177D, and WT mice (**Figure 5b, c**). This indicates that both  
430 A and D substitutions for these residues disturb sleep inducing effect of co-existing  
431 T287D mutation and thus the effect of D mutant may not rely on its phosphomimetic  
432 property.

433

#### 434 **Biochemical evaluation of double-phosphomimetic CaMKII $\beta$ mutants.**

435 We next evaluated the kinase activity of double-phosphomimetic CaMKII $\beta$   
436 mutants. Consistent with the result of single D mutants kinase assay (**Figure 1-**  
437 **figure supplement 2g**), T287D single mutant showed CaM-independent kinase  
438 activity and the level of CaM-dependent kinase activity is lower than that of wild-type  
439 (**Figure 5-figure supplement 1f**). Most of the double D mutants locates around the  
440 T287D suggesting that most of the second phosphomimetic mutations do not affect  
441 the kinase activity of T287D mutant significantly. It can also be seen that there is a  
442 correlation between CaM-dependent and CaM-independent kinase activity for  
443 T287D and double D mutants. We do not exclude the possibility that this  
444 variation/correlation is due to incomplete correction of relative CaMKII $\beta$  levels in the  
445 cell extracts using dot blot (**Figure 5-figure supplement 1g**).



446           However, several mutants showed phosphorylation activity that was markedly  
447 different from T287D, to an extent that is difficult to be explained by the technical  
448 limitations of adjusting expression levels. Mutants located at the left-bottom corner  
449 of **Figure 5-figure supplement 1f** had negligible kinase activity similar to kinase  
450 dead K43R mutant. +T311D mutant impaired the kinase activity in the absence of  
451 CaM compared to T287D, but the kinase activity in the presence of CaM is similar  
452 to T287D, suggesting that +T311D mutant abolished the constitutive-active property  
453 of T287D single mutant but the kinase activity is not abolished significantly. +S71D  
454 showed markedly higher kinase activity in the presence and absence of CaM. The  
455 dot blot quantification (**Figure 5-figure supplement 1g**) indicated that +S71D  
456 showed elevated expression level in 293T, but the kinase assay using the cell lysates  
457 with adjusted CaMKII $\beta$  expression level suggests that the apparent catalytic rate  
458 constant for the kinase reaction of +S71D mutant is also elevated compared with  
459 T287D single mutant.

460           The comparison between kinase assay and double D mutant screening in vivo  
461 further supports that the constitutive and CaM-independent kinase activity is one of  
462 the factors responsible for the sleep-inducing effect and its cancellation. +S26D,  
463 +T47D, +T177D, +S182D, +T311D, and +T516D are the top 5 potential T287D-  
464 canceling mutants suggested by the AAV-based screening (**Figure 5a**). At least four  
465 of these five mutants had impaired kinase activity in the absence of CaM (i.e., +S26D,  
466 +T47D, +T177D, +S182D, and +T311D), and +T516D also showed reduced kinase  
467 activity compared with T287D mutant. The fact that +T311 shows kinase activity in  
468 the presence of CaM might indicate that the CaM-independent kinase activity is  
469 rather more important for the sleep phenotype in our AAV-based in vivo screening.  
470 Among these five mutants, four mutants (+S26D, +T47D, +S182D, +T311D, and



471 +T516D) except for +T177D showed reduced expression level in 293T cells, and  
472 thus we could not evaluate the apparent catalytic rate constant for these low-  
473 expressed mutants. It is highly possible that the sleep cancelation effect of these  
474 mutants is mediated by the reduced expression level rather than the reduced  
475 catalytic constant, although there should be a considerable difference between  
476 protein expression levels in human cultured cell line and those in mice brain.

477 It should be noted that there are several mutants showing kinase activity that  
478 cannot be fully reconciled with the results of AAV-based screening *in vivo*. For  
479 example, although sleep canceling mutants (e.g., +S26D, +T47D etc) had the  
480 reduced kinase activity especially in the absence of CaM, there are also several  
481 mutants showing the very low kinase activity (e.g., +T8D, +S81D etc) but exhibit  
482 sleep-promotion effect comparable to the level of T287D single mutant. The reasons  
483 of these differences between *in vivo* phenotype and *in vitro* kinase activity are  
484 currently unknown.

485

#### 486 **Multi-site phosphorylation of CaMKII $\beta$ regulates sleep stabilization.**

487 Sleep duration and probabilities between sleep and awake phase switching (i.e.,  $P_{WS}$   
488 and  $P_{SW}$ ) can be altered independently. For example, both  $P_{WS}$  and  $P_{SW}$  can have  
489 increased value without markedly changing sleep duration as observed in *Hcr1*  
490 knockout mice<sup>24</sup>. The sleep-wake dynamics underlying the extended sleep duration  
491 can be subdivided into two types by using  $P_{WS}$  and  $P_{SW}$ : one is increased sleep  
492 “induction” activity characterized by an increase in  $P_{WS}$  (higher probability of  
493 switching from awake phase to sleep phase). The other is increased sleep  
494 “maintenance” activity characterized by decrease  $P_{SW}$  (lower probability of switching  
495 from sleep phase to awake phase). The T287D single mutant increases  $P_{WS}$ , which

496 can be categorized as an elevated sleep induction activity. Interestingly, we noticed  
497 that several double-mutants showed extended sleep duration due to an elevated  
498 sleep maintenance activity rather than sleep induction activity. **Figure 6a** shows the  
499 double-mutants plotted according to their  $P_{SW}$  and  $P_{WS}$ . The "T287D-canceling"  
500 mutants such as +S26D, +S182D, and +T311D locate close to WT. Notably, several  
501 mutants such as +T306D and +T307D locate at the bottom-left corner of the  $P_{SW}$ -  
502  $P_{WS}$  plot, indicating that these mutants had lower  $P_{WS}$  and  $P_{SW}$  compared with single  
503 T287D mutants. In other words, the extended sleep duration of these double-  
504 mutants can lie in the increased sleep maintenance activity (i.e., decreased  $P_{SW}$ )  
505 rather than sleep induction activity. The double mutants locate at the bottom-left  
506 corner can be categorized through clustering analysis indicated as "cluster III"  
507 (**Figure 6-figure supplement 1a**). Among the seven double mutants categorized as  
508 cluster III, T287D:T306D, T287D:T307D, and T287D:S534D robustly exhibited  
509 prolonged sleep duration, unchanged  $P_{WS}$ , and reduced  $P_{SW}$  compared with WT-  
510 expressing mice in the independent experiment (**Figure 6b** and **Figure 6-figure**  
511 **supplement 1b, c**). As the reduced  $P_{SW}$  suggests, these three mutants prolonged  
512 sleep episode duration, indicating that they stabilize sleep (**Figure 6c**). We focused  
513 on the sleep maintenance function of T306 and T307 because these residues are a  
514 well-known autonomous negative-feedback control for CaMKII $\beta$  kinase activation.  
515 We substituted these residues with the non-phosphomimetic residue alanine. The  
516 T287D:T306D:T307D and T287D:T306A:T307A mice both exhibited extended sleep  
517 duration compared to the WT (**Figure 6d**). As with T287D single mutant, the  
518 prolonged sleep duration for the T287D:T306A:T307A can be explained by an  
519 increase in  $P_{WS}$  (i.e., sleep induction). However, the T287D:T306D:T307D mice  
520 showed decreased  $P_{WS}$  and  $P_{SW}$ , indicating that the extended sleep duration can be

521 explained by sleep maintenance rather than the sleep induction (**Figure 6d and**  
522 **Figure 6-figure supplement 1d, e**). In support of this, T287D:T306D:T307D  
523 showed prolonged sleep episode duration (**Figure 6e**). The difference between  
524 T287D, T287D:T306D:T307D and T287D:T306A:T307A can be clearly visualized in  
525 the  $P_{WS}$  and  $P_{SW}$  plot (**Figure 6d**). A similar relationship can be observed between  
526 T287D:T306D and T287D:T306A mutants.

527 We analyzed the architectural changes of sleep caused by the sleep-  
528 stabilizing mutant T287D:T306D:T307D using EEG/EMG recordings. The results  
529 showed an increase in NREM and REM sleep duration (**Figure 6f and 6g**), a  
530 significant decrease in  $P_{SW}$ , and no significant change in  $P_{WS}$  (**Figure 6h**), which is  
531 consistent with the SSS analysis. These mice had higher NREM to NREM and REM  
532 to REM transition probabilities than WT-expressing mice. However, unlike T287D,  
533 this mutant did not increase the wake to NREM transition probability (**Figure 6i and**  
534 **Figure 2-figure supplement 1h**), suggesting that the additional phosphorylation(s)  
535 of T306 and/or T307 stabilize NREM and REM sleep. Mice expressing the  
536 T287D:T306D:T307D mutant and those expressing WT had similar delta power, but  
537 the mutant increased slow power (**Figure 6j and Figure 6-figure supplement 1f**).  
538 Thus, phosphorylation of T306/T307 also seems to elevate sleep need levels.

539 Phosphorylation of T306 and T307 in CaMKII $\beta$  suppresses the kinase  
540 activity by inhibiting CaM binding<sup>27,47</sup>. To test whether the sleep maintenance  
541 function of the T287D:T306D:T307D mutant depends on its enzyme activity, we  
542 examined the sleep phenotype of mice expressing its kinase-dead version  
543 (K43R:T287D:T306D:T307D) and found that these mice did not exhibit a sleep-  
544 stabilizing phenotype. They had similar sleep parameters to the WT (**Figure 6-figure**  
545 **supplement 1g**). Furthermore, the T287A:T306D:T307D mutant, in which T287 was

546 replaced by a non-phosphomimetic A, also resulted in similar sleep parameters to  
547 WT. These results suggest that the sleep maintenance function of CaMKII $\beta$  with  
548 phosphorylated T306 and T307 depends on its enzyme activity and that this function  
549 requires T287 phosphorylation. We thus propose that multi-site phosphorylation of  
550 CaMKII $\beta$  (residues T287, T306, and T307) converts the sleep-inducing effect of  
551 T287-phosphorylated CaMKII $\beta$  into a sleep maintenance activity.

552

### 553 **Biochemical evaluation of sleep-stabilizing CaMKII $\beta$ mutants.**

554 We then examined *in vitro* kinase activity of these sleep-stabilizing multiple  
555 D mutants and corresponding A mutants (**Figure 6-figure supplement 2a and b**).  
556 Consistent with the role of phosphorylation at T306 and T307 for the inhibition of the  
557 interaction with Ca<sup>2+</sup>/CaM to CaMKII $\beta$ , mutants having the D substitution at either of  
558 T306 or T307 (i.e., T306D, T307D, T306D:T307D, T287D:T306D, T287D:T307D,  
559 T287D:T306D:T307D) showed reduced kinase activity in the presence of CaM. On  
560 the other hand, any mutants having the T287D mutation including sleep-stabilizing  
561 mutants annotated in AAV-based analysis (i.e., T287D:T306D and  
562 T287D:T306D:T307D) showed CaM-independent kinase activity compared with  
563 wild-type. This is also consistent with the role of T306/T307 phosphorylation because  
564 these phosphorylation does not actively inhibit the kinase activity of CaMKII $\beta$ , and  
565 thus the CaM-independent activity of T287D mutant should be maintained if T287D  
566 is combined with T306D and/or T307D. The CaM-independent kinase activity was  
567 more evident with another substrate called autocalmitide-2 (**Figure 6-figure**  
568 **supplement 2b**).

569 By contrast, kinase activity of mutants having the A substitution at T306 or  
570 T307 will need to be carefully interpreted. Introducing A substitution to either or both

571 of T306 and T307 results in the CaM-independent kinase activity without having the  
572 T287D mutation (i.e., T306A, T307A, or T306A:T307A). We speculate that such  
573 CaM-independent activity might be caused by autophosphorylation of CaMKII $\beta$  in  
574 the 293T cell. 293T cell expresses endogenous CaM protein. Although the cell-  
575 endogenous CaM is not sufficient to fully activate the over-expressed CaMKII $\beta$ , it is  
576 reasonable to assume that there is a background level of CaM-dependent activation  
577 of CaMKII $\beta$  in the 293T cells. Because T306A or T307A mutation impairs the auto-  
578 inhibitory mechanism, the T306A, T307A, or T306A:T307A mutants would be more  
579 susceptible to CaMKII $\beta$  activation, which occurs at a lower efficiency in the 293T cell.  
580 Therefore, by the time 293T cell lysates are prepared, some portion of T306A, T307A,  
581 or T306A:T307A mutants may already be in an autonomously activated state with  
582 autophosphorylation at T287 residue.

583

584 **Ordered multi-site phosphorylation of CaMKII $\beta$  underlies multi-step sleep**  
585 **regulation.**

586 The above *in vivo* analysis proposes that different CaMKII $\beta$  phosphorylation states  
587 can induce sleep (T287), maintain sleep (T287:T306:T307), and cancel sleep  
588 promotion (S26:T287, S182:T287, and T287:T311). We assumed that  
589 phosphorylation at T287 precedes the other phosphorylations. We then aimed to  
590 biochemically confirm the ordered multi-site phosphorylation. We analyzed the time  
591 course changes in the phosphorylation levels of each sleep-controlling residues in  
592 CaMKII $\beta$  (S26, S182, T287, T306, T307, and T311). The purified CaMKII $\beta$  was  
593 incubated with CaM under four conditions with different concentrations of Ca<sup>2+</sup> in the  
594 reaction buffer. Condition #1: 0 mM Ca<sup>2+</sup> and 10 mM EGTA, supposing the presence  
595 of a negligible amount of free Ca<sup>2+</sup>. Condition #2: 0 mM Ca<sup>2+</sup>, supposing the

596 presence of low  $\text{Ca}^{2+}$  concentration, possibly coming from the purified CaMKII $\beta$   
597 and/or CaM. Condition #3: 0.5 mM  $\text{Ca}^{2+}$ , assuming a sufficient amount of free  $\text{Ca}^{2+}$   
598 to activate CaMKII $\beta$ . Condition #4: 0.5 mM  $\text{Ca}^{2+}$  and 10 mM EGTA at 5 min, where  
599 EGTA was added 5 min after incubation started. This type of condition induces the  
600 phosphorylation of T305 and T306 upon CaMKII $\alpha$  activation <sup>48,49</sup>. Although we could  
601 detect the peak corresponds to S182 phosphorylation appeared during the CaMKII $\beta$   
602 incubation, it is hard to clearly separate the chromatogram of the peptide with S182  
603 phosphorylation and that with the adjacent T177 phosphorylation (**Figure 7-figure**  
604 **supplement 1a**), so the quantification value of pS182 presented below include the  
605 signal from pT177 peptides.

606 **Figure 7a** indicates that T287 phosphorylation occurs in the presence of 0.5  
607 mM  $\text{Ca}^{2+}$  (conditions #3 and #4), but not in the absence of explicitly added  $\text{Ca}^{2+}$  in  
608 the reaction buffer (conditions #1 and #2). The level of phosphorylation reaches a  
609 saturation level 5 min after CaM addition. Under condition #3, S26 and S182  
610 phosphorylations follow T287 phosphorylation. However, conditions #1 and #4 do  
611 not phosphorylate these residues.

612 On the other hand, T306 and T307 remain unphosphorylated in the presence  
613 of a high amount of  $\text{Ca}^{2+}$  and CaM (condition #3). Shielding the  $\text{Ca}^{2+}$  after CaMKII $\beta$   
614 activation (condition #4) triggered T306 and T307 phosphorylation. This is consistent  
615 with previous studies suggesting that the stable binding of  $\text{Ca}^{2+}$ /CaM renders T306  
616 and T307 inaccessible to the kinase domain of CaMKII $\beta$ , and their phosphorylation  
617 requires the temporal removal of  $\text{Ca}^{2+}$ /CaM from the kinase <sup>48-51</sup>. We also confirmed  
618 that the optimal  $\text{Ca}^{2+}$  concentration for T306 and T307 phosphorylation is lower than  
619 that for T287 phosphorylation: gradual phosphorylation of T306 and T307 occurs in  
620 the absence of apparent  $\text{Ca}^{2+}$  in the reaction buffer (condition #1 and #2) <sup>47,52</sup>. The

621 low  $\text{Ca}^{2+}$  concentration condition also promotes T311 phosphorylation, which is  
622 spatially close to T306 and T307. The time course of T311 phosphorylation in  
623 condition #2 is different from that of T306 and T307 phosphorylation: the  
624 phosphorylation of T311 peaked 5 min after CaM addition and then decreased,  
625 presumably because of the progressive phosphorylation of T306 and T307. It is  
626 unlikely that a misregulated,  $\text{Ca}^{2+}$ /CaM-independent kinase activity phosphorylated  
627 T306, T307, and T311 under low  $\text{Ca}^{2+}$  concentration conditions because chelating  
628  $\text{Ca}^{2+}$  with EGTA abolishes the appearance of double-phosphorylated  
629 T306/T307/T311 peptides (condition #1; ppT306/T307/T311). In summary, the  
630 biochemical analysis suggests that T287 phosphorylation initiates the ordered  
631 phosphorylation of S26, S182, T306, T307, and T307 (**Figure 7-figure supplement**  
632 **1b**) at least in our *in vitro* experimental condition.

633 With the ordered phosphorylation events observed *in vitro*, the CaMKII $\beta$  might  
634 reach multi-phosphorylated states such as pS26:pT287:pT306:pT307,  
635 pS182:pT287:pT306:pT307, or pT287:pT306:pT307:pT311 *in vivo*. To investigate  
636 the effect of such multi-phosphorylated states in sleep regulation, we expressed  
637 CaMKII $\beta$  mutants mimicking quadruple-phosphorylation in mice. Inclusion of S26A  
638 or S182A to the T287D:T306D:T307D recapitulated the sleep maintenance function  
639 observed in T287D:T306D:T307D mutant (**Figures 7b, c** and **Figure 7-figure**  
640 **supplement 1c, d**), with decreased  $P_{\text{SW}}$  and a prolonged sleep episode duration.  
641 On the other hand, the substitution of in S26 or S182 to D resulted in the loss of the  
642 sleep maintenance function. The mutant with the T311D substitution added to the  
643 T287D:T306D:T307D retained sleep maintenance activity (**Figure 7-figure**  
644 **supplement 1e**). Therefore, the sleep induction and maintenance effect of CaMKII $\beta$   
645 elicited by T287 phosphorylation followed by T306 and T307 phosphorylation

646 appears to be terminated by S26 and S182 phosphorylation, which also follows T287  
647 phosphorylation. Based on these results, we propose that the ordered multi-  
648 phosphorylation states of CaMKII $\beta$  underly the sleep regulation steps, namely the  
649 induction (pT287), the maintenance (pT287/pT306/pT307), and the cancelation  
650 (pS182 or pS26). These multi-site phosphorylation states might be connected, and  
651 finally completed as a cycle by the turnover of phosphorylated CaMKII $\beta$  promoted  
652 by the protein destabilization effect of S182 or S26 phosphorylation (**Figure 7d**).  
653



## 654 Discussion

655 In this study, we demonstrated that the conditional induction or inhibition of CaMKII $\beta$   
656 kinase activity could bidirectionally increase or decrease mammalian sleep duration.  
657 The bidirectional effect as well as the near two-fold difference in sleep duration  
658 caused by the activation (e.g., 936.7  $\pm$  22.6 min; **Figure 2a**) and inhibition (e.g.,  
659 554.1  $\pm$  21.2 min; **Figure 4e**) of CaMKII $\beta$  further supports the role of CaMKII $\beta$  as a  
660 core sleep regulator, rather than auxiliary inputs that either induce or inhibit sleep  
661 upon environmental responses. Assuming the role of CaMKII $\beta$  as one of the core  
662 kinases in the sleep control, the next question would be how CaMKII $\beta$  relates to  
663 other phosphorylated enzymes, such as CaMKII $\alpha$ <sup>10</sup>, SIK1/SIK2/SIK3<sup>15,16</sup>, and  
664 ERK1/ERK2<sup>17</sup>, to shape the phosphorylation signaling network for sleep regulation.

665 The postnatal conditional expression of CaMKII $\beta$  and its inhibitor changes the  
666 sleep phenotype, which rules out, at least in part, neuronal developmental  
667 abnormality potentially caused by the embryonic knockout of *Camk2b*<sup>53</sup>. Although  
668 the embryonic double knockout of *Camk2a/Camk2b* caused developmental effects  
669<sup>46</sup>, the sleep reduction caused by the conditional expression of CaMKII inhibitor AIP2  
670 supports that the reduction of kinase activity reduced sleep duration in the *Camk2a*  
671 KO and *Camk2b* KO mice<sup>10</sup>, not the neuronal structural abnormality potentially  
672 caused by the gene knockout. Given the inducible adult deletion of both *Camk2a*  
673 and *Camk2b* resulted in lethal phenotype<sup>46</sup>, our AIP2 expression condition would  
674 only partially inhibit the kinase activity of CaMKII $\alpha$  and CaMKII $\beta$ .

675 Third, the effect of AIP2 and kinase-inhibitory CaMKII $\beta$  mutants (e.g., K43R  
676 and S26D) indicate that the sleep-promoting effect of activated CaMKII $\beta$  comes from  
677 the enzymatic activity of CaMKII $\beta$  (**Figure 4**). The sleep-promoting effect of the  
678 truncated CaMKII $\beta$  kinase domain further indicates that CaMKII $\beta$  oligomerization is

679 not necessary for the sleep-promoting effect. This is in stark contrast with the non-  
680 enzymatic role of CaMKII $\beta$  through its interaction with F-actin <sup>54,55</sup>. The truncated  
681 CaMKII $\beta$  used in this study lacks the actin binding domain. Another well-known  
682 binding partner of CaMKII $\alpha/\beta$  is NR2B <sup>56</sup>, which has a low affinity for monomeric  
683 CaMKII $\alpha$  <sup>57</sup>. Therefore, the potent sleep-inducing effect of truncated CaMKII $\beta$   
684 suggests that other downstream targets (such as phosphorylation substrates) are  
685 responsible for the sleep-inducing effect of CaMKII $\beta$ . Future research should focus  
686 on identifying such downstream targets, but at least the present study excludes the  
687 core circadian transcription factors and functional transcription-translation circadian  
688 feedback loop as downstream factors of CaMKII $\beta$  sleep promotion (**Figure 2**).

689 Finally, comparing phosphorylation-mimicking mutants and non-  
690 phosphorylation-mimicking mutants allowed us to attribute the effect of  
691 phosphorylation to the negative charge mimicked by the D residue or to any other  
692 effect caused by the mutation. As observed in the SIK3 phosphorylation site S551  
693 <sup>58</sup>, D and A mutations sometimes yield similar results (e.g., increased sleep), making  
694 it difficult to conclude that the D mutation mimics phosphorylation. For residues  
695 analyzed in **Figure 7a**, we showed that A and D mutants had different effects in sleep  
696 regulation *in vivo*, suggesting that the phosphorylation states of these sites in  
697 CaMKII $\beta$  can regulate sleep. To the best of our knowledge, this is the first conclusive  
698 demonstration of phosphorylation-dependent sleep regulation at single residue level.  
699 Besides, these residues are autophosphorylation substrates, at least *in vitro*. These  
700 results suggest that the multi-step effects of CaMKII $\beta$  on sleep induction, sleep  
701 maintenance, and sleep promotion cancelation can be attributed to the properties of  
702 the CaMKII $\beta$  with multiple (auto-)phosphorylation patterns.

703 The sleep-promoting effect observed with *Vglut2-Cre* but not *Gad2-Cre*

704 **(Figure 3)** suggests that CaMKII $\beta$  promotes sleep by acting on excitatory neurons  
705 rather than inhibitory neurons and glial cells. However, these data do not exclude  
706 the possibility of the contribution of non-excitatory neurons and glial cells for  
707 CaMKII $\beta$ -dependent sleep regulation because the Cre-expression specificity may  
708 not be perfectly selective to desired cell types. Furthermore, endogenous *Camk2b*  
709 is widely expressed in neurons and constitutes ~1.3% of postsynaptic density<sup>59</sup> and  
710 glial cells also express *Camk2b*<sup>60</sup>. Future research will have to precisely elucidate  
711 where CaMKII $\beta$  exerts its sleep function in terms of both neuronal cell types and  
712 brain regions as well subcellular localization. In the data shown in **Figure 3b**,  
713 focused expression of T287D to *Vglut2-Cre* positive cells might induce the sleep  
714 maintenance activity (i.e., extended sleep duration and low  $P_{SW}$ ) in addition to the  
715 sleep induction activity (i.e., high  $P_{WS}$ ), suggesting that different types of neurons  
716 might be involved in the sleep induction or maintenance activities to different degrees.  
717 Notably, homeostatic regulation of sleep/wake-associated neuronal firing was  
718 recapitulated in cultured neuron/glial cells<sup>61,62</sup>. Given the ubiquitous and abundant  
719 expression of CaMKII $\beta$  in neurons, investigating the relationship between sleep  
720 homeostasis in cultured neurons/glial cells and CaMKII $\beta$  phosphorylation states  
721 would reveal valuable information about the ubiquitous and cell-type specific function  
722 of CaMKII $\beta$  in the sleep control.

723 Multi-site phosphorylation encodes complex biochemical systems such as the  
724 sequential triggering of multiple events and the integration of multiple signals (such  
725 as AND logic gates)<sup>63,64</sup>. One of the most intriguing properties of CaMKII is the multi-  
726 site autophosphorylation combinations that regulate kinase activity and protein-  
727 protein interactions. In this study, we conducted comprehensive mutagenesis of  
728 single or multiple potentially (auto-)phosphorylatable residues. We revealed that the

729 phosphorylation of kinase-suppressive residues can cancel the sleep-promoting  
730 effect of the active T287-phosphorylated CaMKII $\beta$  (**Figure 5**). Sleep-suppressing  
731 mechanisms may include CaMKII $\beta$  destabilization (e.g., through S182  
732 phosphorylation) and other biochemical mechanisms inhibiting either the kinase  
733 activity or the CaMKII $\beta$ -substrates interaction. The combination of sleep-promoting  
734 and sleep-suppressing phosphorylations of CaMKII $\beta$  may underlie the mechanism  
735 regulating sleep need to an appropriate level, depending on the animal's internal  
736 conditions and external environments. Considering this, it would be interesting to  
737 quantify the phosphorylation level of each residue (other than T287) in response to  
738 signals causing acute and chronic changes in the sleep-wake cycle (such as  
739 inflammation and stress).

740       Next, we found that combining phosphomimetic mutations of T306D and  
741 T307D to T287D (i.e., T287D:T306D:T307D) does not affect sleep duration  
742 (compared with the T287D single mutation) but causes unexpected differences in  
743 sleep maintenance and sleep induction (**Figure 6**). The transition probabilities ( $P_{WS}$   
744 and  $P_{SW}$ ) allowed us to quantify these interesting differences. For example, the  
745 T287D mutant has a higher  $P_{WS}$ , suggesting that T287 phosphorylation plays a role  
746 in sleep induction. On the other hand, the T287D:T306D:T307D mutant has a lower  
747  $P_{SW}$ , suggesting that T287/T306/T307 phosphorylation plays a role in sleep  
748 maintenance. The autophosphorylation of T306 and T307 has a well-known  
749 inhibitory effect on the CaMKII $\beta$ -CaM interaction <sup>27,28</sup>, creating an auto-inhibitory  
750 feedback regulation of CaMKII $\beta$ . CaMKII $\beta$  deletion mutant shares some properties  
751 with T287D:T306D:T307D; both mutants lost the CaMKII $\beta$ -CaM interaction and have  
752 the CaM-independent kinase activity. Nevertheless, T287D:T306D:T307D has the  
753 sleep maintenance activity while the deletion mutant shows sleep induction activity.

754 Thus, the mechanism of sleep maintenance by T287D:T306D:T307D may not be  
755 attributed to the loss of CaMKII $\beta$ -CaM interaction itself. The outcome of CaMKII $\beta$   
756 kinase activity with different phosphorylation patterns and molecular mechanisms  
757 underlying the sleep induction/maintenance activities are currently unknown. Recent  
758 studies suggested that the phosphorylation of T305/T306 of CaMKII $\alpha$  promotes the  
759 dissociation of CaMKII $\alpha$  dodecamer<sup>65</sup>. Another study demonstrated that the same  
760 phosphorylation promotes the translocation of CaMKII $\alpha$  from the spine to dendrite<sup>66</sup>.  
761 It is plausible that different patterns of multi-site phosphorylation or combination of D  
762 mutants of CaMKII $\beta$  affect sleep induction/maintenance through the different  
763 interactions of endogenous CaMKII $\alpha$ /CaMKII $\beta$  and neuronal proteins.

764 We also showed that other sleep-controlling residues (such as S26, S182,  
765 and T311) also undergo autophosphorylation (**Figure 7a**). S26 autophosphorylation  
766 occurs in CaMKII $\gamma$ <sup>67</sup> and suppresses the kinase activity<sup>68</sup>, which is consistent with  
767 our results in CaMKII $\beta$ . The other phosphoproteomics study identified S25  
768 autophosphorylation in CaMKII $\alpha$ <sup>30</sup>. Although the level of phosphorylation at S25 was  
769 indicated for ~5% of total CaMKII $\alpha$  at 4 min incubation time<sup>30</sup>, it is possible that the  
770 level of this phosphorylation continuously increases given the slow dynamics of  
771 autophosphorylation at S26 of CaMKII $\beta$  found in this study. We also note that peptide  
772 phosphorylated with S26 can be found *in vivo* brain sample<sup>12</sup> (**Figure 7-figure**  
773 **supplement 1f**), although it is unable to distinguish CaMKII isoforms because of the  
774 identical sequence around S26 phosphorylation site. Reports suggest that T311  
775 autophosphorylation occurs in CaMKII $\beta$ <sup>30</sup> and that the phosphorylation level of the  
776 corresponding residue in CaMKII $\alpha$  was reduced during the dark phase (mostly  
777 awake phase in mice)<sup>11</sup>. The T311 phosphorylation was also detected in the other  
778 set of phosphoproteomic analyses of *in vivo* mice brains<sup>12</sup>, although sequence

779 identity around the T311 residue makes it difficult to distinguish CaMKII $\alpha$  and  
780 CaMKII $\beta$ . These phosphoproteomics analyses support the possible role of  
781 phosphorylation at S26 or T311 in the regulation of CaMKII $\alpha$ /CaMKII $\beta$  in mice brains  
782 *in vivo*. To the best of our knowledge, our study is the first to report the  
783 autophosphorylation of S182. Furthermore, S26 and S182 autophosphorylation are  
784 slower than that of T287 (**Figure 7a**), consistent with the fact that these residues are  
785 not exposed on the surface and thus a kinase cannot easily access to these residues.  
786 The mammalian circadian clock regulation appears to use the non-canonical and  
787 inefficient phosphorylation residue to encode slower dynamics of circadian clock  
788 peacemaking<sup>69,70</sup>; it should be rigorously tested whether non-canonical  
789 autophosphorylation residues such as S26 and S182 plays a role in the regulation  
790 of normal sleep regulation *in vivo* through the knockout/knockdown rescue  
791 experiment by re-expressing the unphosphorylatable A mutations at corresponding  
792 residues. Through such rescue experiments, it would be possible to approach the  
793 question not covered by the current study: whether the sleep cancellation effect is  
794 related to the transition from sleep to awake phase in the natural sleep-wake cycle,  
795 or to the cancellation of additional sleep needs upon unusual input such as sleep  
796 deprivation.

797       Considering this sequential autophosphorylation of sleep-controlling residues,  
798 we aligned the different sleep-promoting effects elicited by each phosphorylation  
799 state with the autophosphorylation events (**Figure 7d**). The expected sleep  
800 regulation sequence is physiologically plausible: the increased transition rate from  
801 awake to sleep phase, the induced sleep is stabilized, and then the sleep-promoting  
802 effect is canceled. The cancelation may include complete erasure of multi-site  
803 phosphorylation through the destabilization of CaMKII $\beta$ . Because both CaMKII $\alpha$  and

804 CaMKII $\beta$  are involved in sleep control and have overlapping roles in the control of  
805 neural plasticity, the mechanism we found in this study may be shared by CaMKII $\alpha$   
806 as well as CaMKII $\beta$ . On the other hand, it is also known that there are differences in  
807 the dynamics of phosphorylation of T306 and T307 between CaMKII $\alpha$  and CaMKII $\beta$   
808 <sup>49</sup>, and it will be interesting to investigate how these differences at the molecular level  
809 affect sleep-wake regulation.

810 This sequence is hypothetical at this stage, and it is still unknown whether the  
811 same CaMKII $\beta$  molecule regulates the sequential events or different CaMKII $\beta$   
812 molecules with distinct phosphorylation states operate individually. It is also possible  
813 that phosphorylation on several non-canonical autophosphorylation residues (e.g.,  
814 S26 and S182) is mediated by different kinases, and several residues may be rather  
815 effectively phosphorylated during the awake phase as observed in the T310  
816 (CaMKII $\alpha$ ) or T311 (CaMKII $\beta$ ) residues. The obvious next question might be: how  
817 are the sleep-driven and wake-driven multi-site phosphorylation of each CaMKII $\beta$   
818 molecule integrated and organized by autophosphorylation and phosphorylation by  
819 other kinases, such that robust and flexible cycle of sleep induction, maintenance  
820 and subsequent transition from sleep to awake phase. Also, the multi-site  
821 phosphorylation status of CaMKII $\beta$  might be the key to understand the connection  
822 between the sleep-wake cycle and its physiological significance. Indeed,  
823 phosphorylation mimicking or non-phosphorylation mimicking mutants of CaMKII $\alpha$ /  
824 CaMKII $\beta$  have been shown to elicit defects in neuronal plasticity and some type of  
825 learning. Because it is well understood that the sleep-wake cycle affects the learning  
826 process, CaMKII $\beta$ -expressing mice with changes in sleep phenotype may also have  
827 changes in learning phenotype. In this case, it would be interesting to ask whether  
828 the changes in learning phenotype are simply due to sleep abnormalities or whether

829 CaMKII $\beta$  plays a more direct role in these relationships as a molecule that controls  
830 both sleep and learning processes.

831 In summary, we showed that CaMKII $\beta$  kinase activity promotes mammalian  
832 sleep by acting on the excitatory neurons. We propose that the ordered multi-site  
833 phosphorylation and kinase activity of CaMKII $\beta$  compose the *input* (exposure of the  
834 kinase domain), *storage/processing* (T287 and following phosphorylations), and  
835 *output* (substrate phosphorylation) mechanism of sleep need in mammals. Hence,  
836 this could be the molecular mechanism of the phosphorylation hypothesis of sleep  
837 in mammals.

838

839



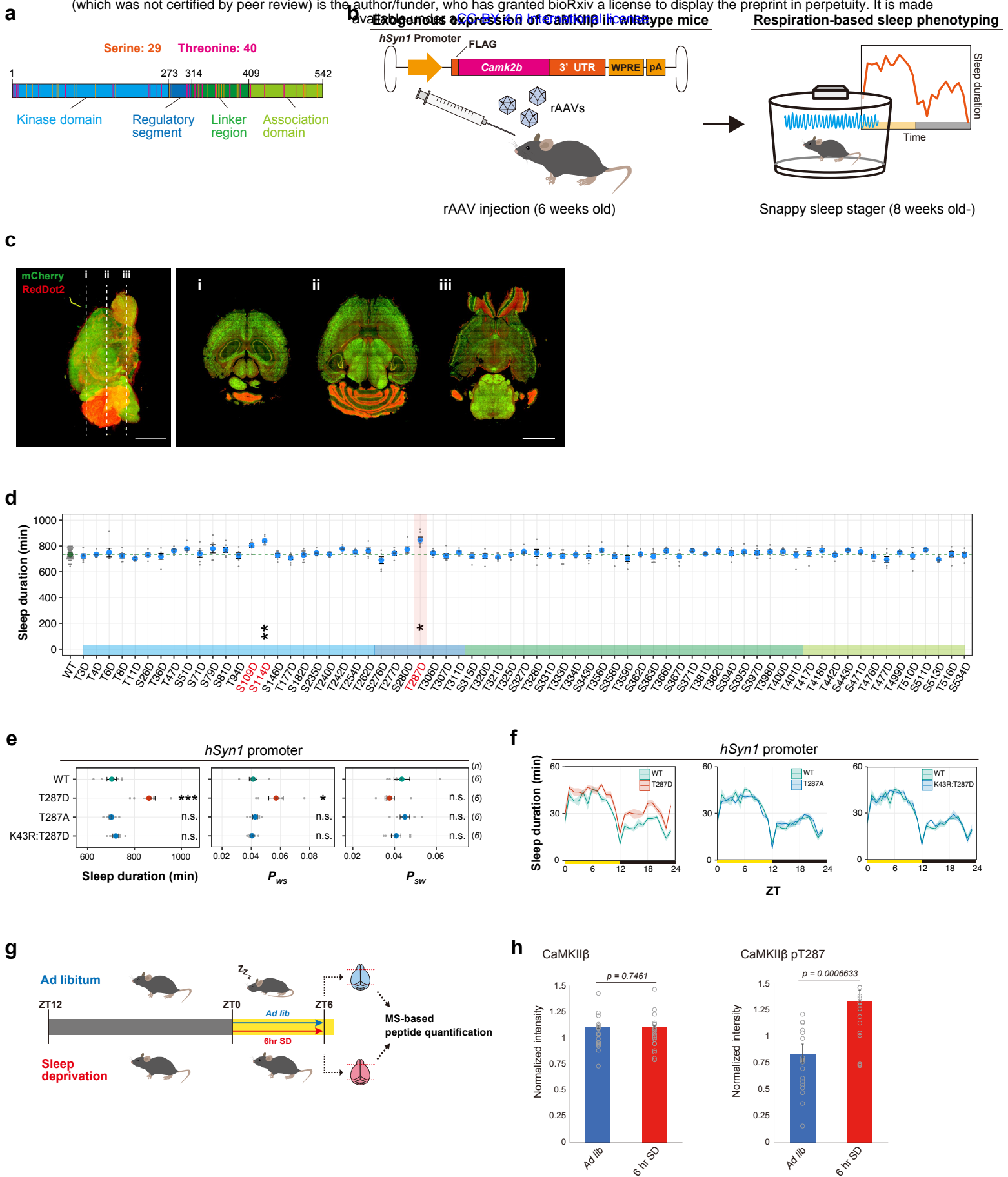


Figure 1

## 840 **FIGURE LEGENDS**

### 841 **Figure 1. Phosphorylation of CaMKII $\beta$ regulates sleep induction**

842 **(a)** The 29 serine and 40 threonine residues throughout CaMKII $\beta$ . Orange and  
843 magenta lines represent serine and threonine residues, respectively. Color-coded  
844 regions indicate the functional domains of CaMKII $\beta$ .

845 **(b)** Schematic diagram of AAV-based CaMKII $\beta$  expression and respiration-based  
846 sleep phenotyping. UTR: untranslated region. pA: polyA.

847 **(c)** Representative cross-sectional images of the brain of mice expressing H2B-  
848 mCherry under the *hSyn1* promoter by the AAV. Data were acquired by whole brain  
849 imaging with RedDot2 counterstaining, and detailed images of each brain region are  
850 shown in **Figure 1-figure supplement 1a**. Scale bars, 5 mm.

851 **(d)** Daily sleep duration of mice expressing CaMKII $\beta$  phosphomimetic mutants (n =  
852 6–10) in the presence of endogenous wildtype CaMKII $\beta$ . The represented value is  
853 the average of SSS measurements over six days. The dashed green line represents  
854 the average sleep duration of wild-type CaMKII $\beta$ -expressing mice (WT, n = 48).  
855 Multiple comparison test was performed against WT.

856 **(e-f)** Sleep/wake parameters **(e)** and sleep profiles **(f)** of mice expressing T287-  
857 related CaMKII $\beta$  mutants, averaged over six days. Measurements are independent  
858 of those in **(d)**. Sleep duration is the total sleep duration in a day,  $P_{WS}$  and  $P_{SW}$  are  
859 the transition probabilities between wakefulness and sleep. The shaded area  
860 represents the SEM. Multiple comparison test was performed against WT. ZT:  
861 zeitgeber time.

862 **(g)** Sleep deprivation and peptide quantification procedures. The brains of the sleep-  
863 deprived and control mice were collected for MS-based peptide quantification.

864 **(h)** Total CaMKII $\beta$  and T287-phosphorylated peptides from brains of sleep-deprived  
865 and control mice, analyzed by SRM quantitative mass spectrometry.  
866 Error bars: SEM. \* $p < 0.05$ , \*\* $p < 0.01$ , \*\*\* $p < 0.001$ , n.s.: no significance.

867

868 **Figure 1-source data 1**

869 Source data for Figure 1d, e, f.

870

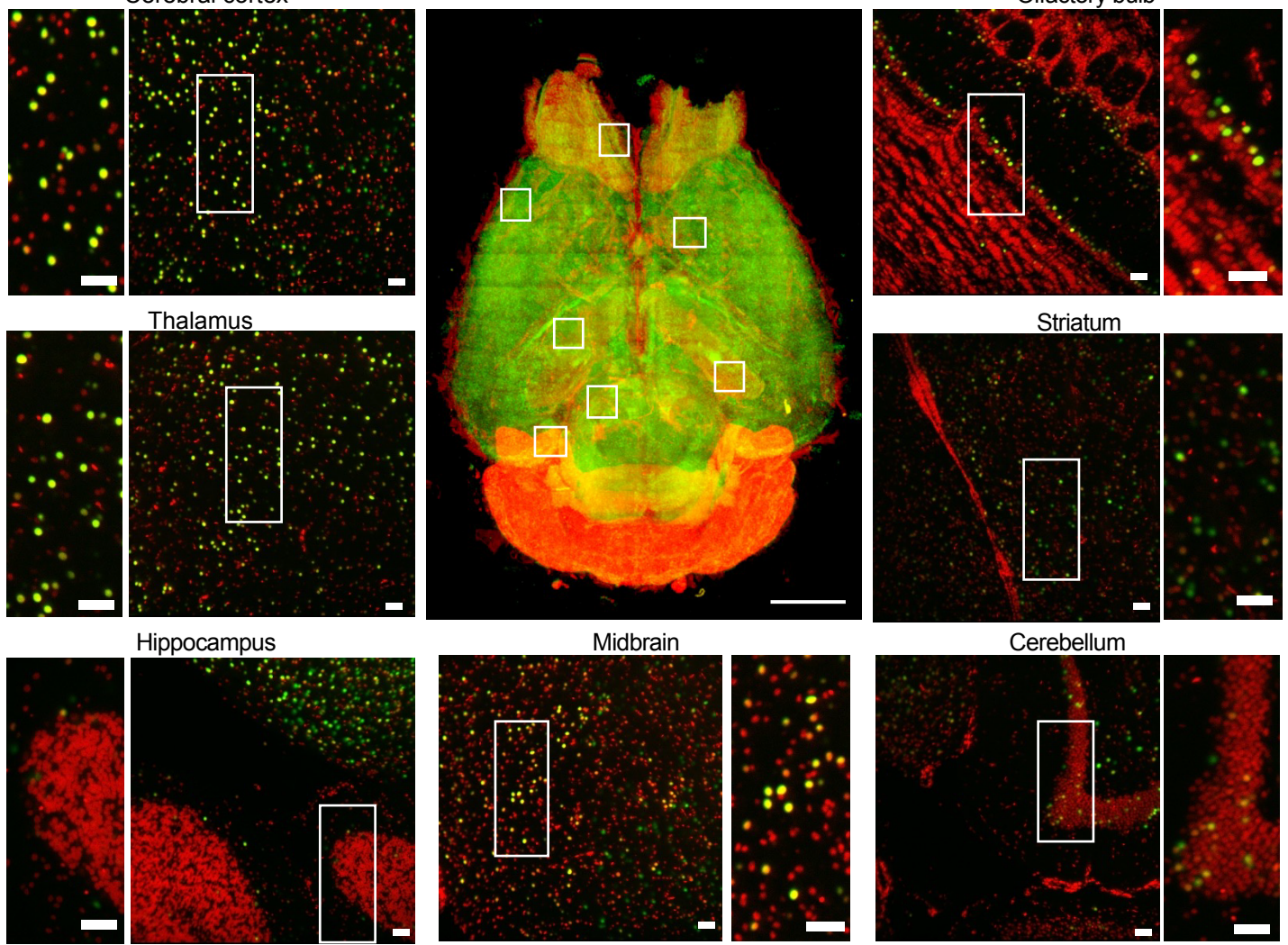
871 **Figure 1-source data 2 and 3**

872 Source data for Figure 1h.

873

874

**a**



**b**

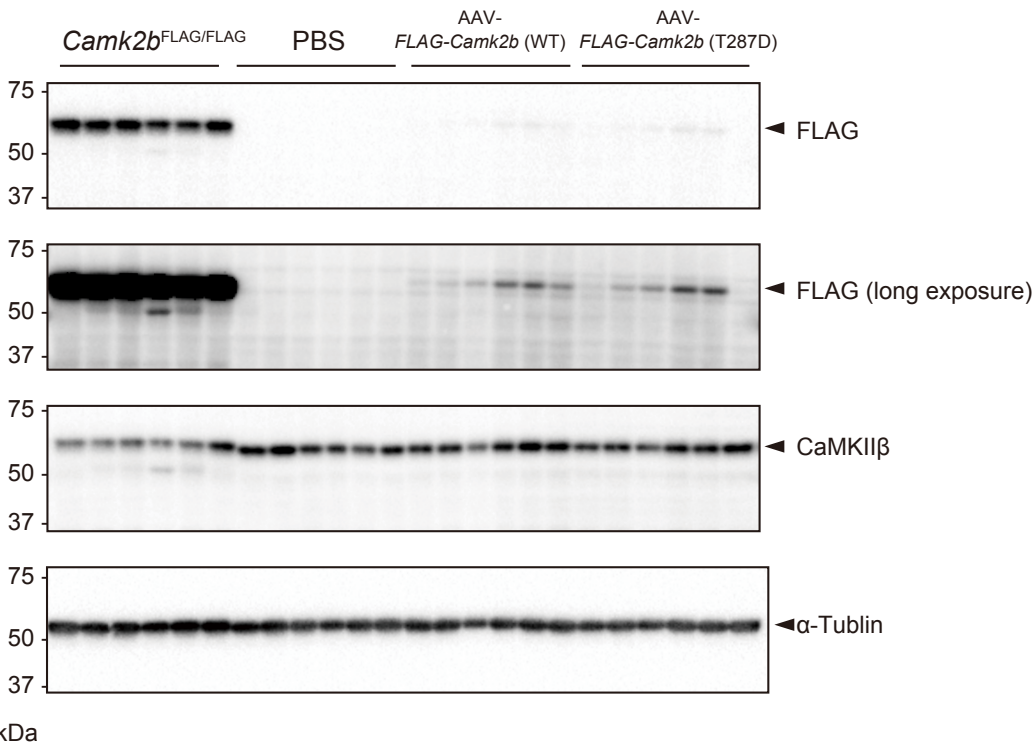


Figure 1-figure supplement 1

875 **Figure 1-figure supplement 1. Expression of the CaMKII $\beta$  throughout the**  
876 **brain by AAV-PHP.eB**

877 **(a)** Volume-rendered and single-plane images of the brain expressing H2B-mCherry  
878 under *hSyn1* promoter by the AAV (mCherry, green) counterstained with RD2 (red).  
879 A volume-rendered image is shown in the center. Single-plane and magnified images  
880 are shown for cerebral cortex, thalamus, hippocampus, midbrain, cerebellum,  
881 striatum, and olfactory bulb. Scale bar in the center image, 3 mm; other scale bars,  
882 100  $\mu$ m.

883 **(b)** Expression levels of endogenous CaMKII $\beta$  and AAV-mediated transduced  
884 CaMKII $\beta$  in the brain. *Camk2b*<sup>FLAG/FLAG</sup> represents homo knock-in mice in which the  
885 FLAG tag was inserted into the endogenous *Camk2b* locus. PBS: PBS-  
886 administrated mice. Immunoblotting against FLAG-tagged protein indicates that  
887 AAV-mediated expression of CaMKII $\beta$  is lower than the expression level of  
888 endogenous CaMKII $\beta$ .

889

890 **Figure 1-figure supplement 1-source data 1**

891 Uncropped blot images for Figure 1-figure supplement 1b.

892

893 **Figure 1-figure supplement 1-source data 2**

894 Raw blot images for Figure 1-figure supplement 1b.

895



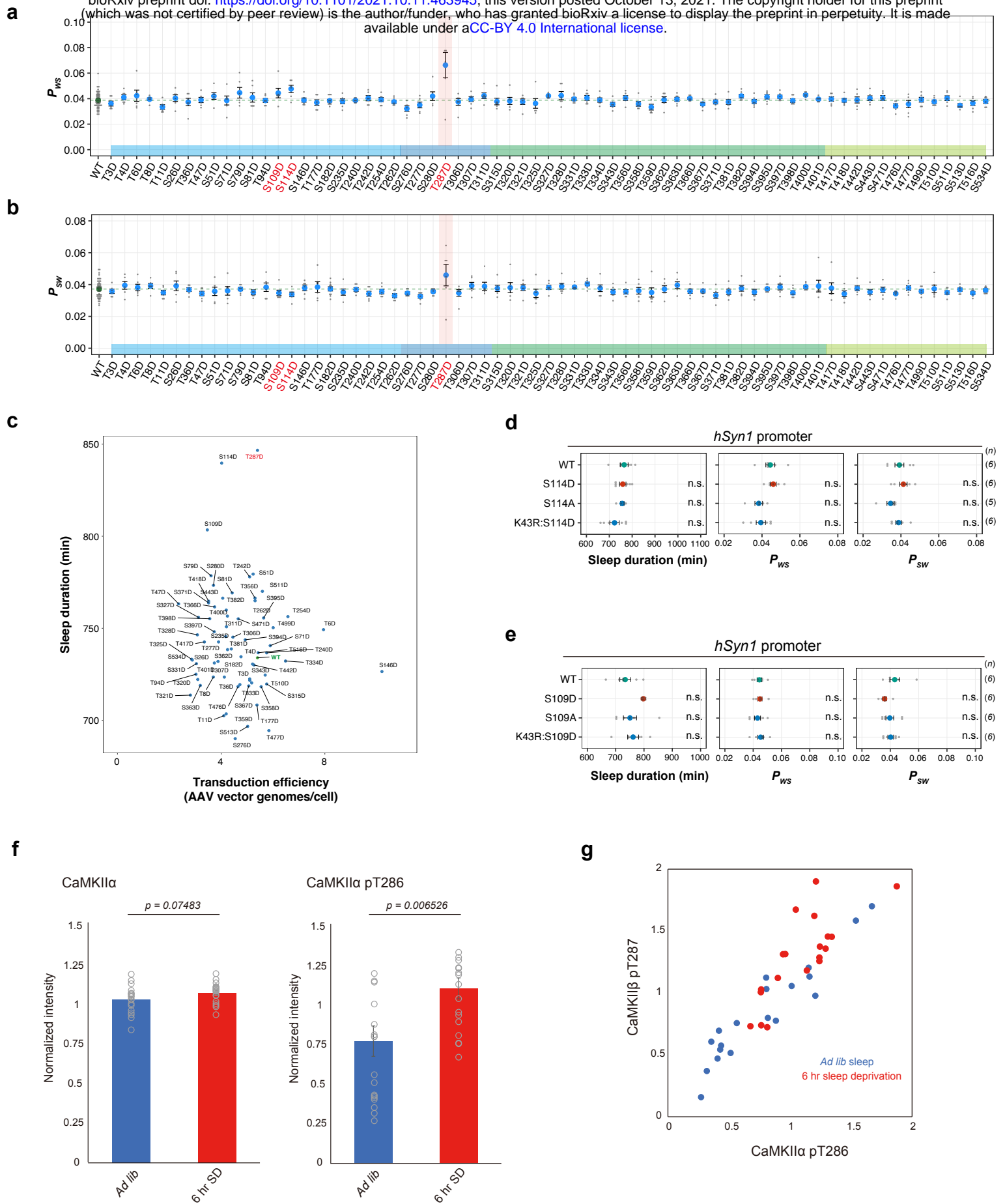


Figure 1-figure supplement 2

896 **Figure 1-figure supplement 2. Phosphorylation of CaMKII $\beta$  regulates sleep**  
897 **induction**

898 **(a)** Daily  $P_{WS}$  **(a)** and  $P_{SW}$  **(b)** of mice expressing the CaMKII $\beta$  phosphomimetic  
899 mutants (n = 6–10) shown in **Figure 1c**, averaged over six days. Dashed green lines  
900 represent averaged  $P_{WS}$  **(a)** and  $P_{SW}$  **(b)** of mice expressing wild-type CaMKII $\beta$  (WT,  
901 n = 48). The multiple comparison test revealed no significant differences between  
902 mutants and WT.

903 **(c)** Calculated transduction efficiency plotted against sleep duration. Transduction  
904 efficiency is an estimation of the number of AAV vector genomes present per cell in  
905 a mouse brain. After the SSS measurements, we purified the AAV vector genomes  
906 from the mice brains and then quantified them with a WPRE-specific primer set and  
907 normalized to mouse genomes.

908 **(d-e)** Sleep/wake parameters of mice expressing S114-related CaMKII $\beta$  mutants **(d)**  
909 and S109-related CaMKII $\beta$  mutants **(e)**, averaged over six days. The shaded areas  
910 represent SEM. Multiple comparison test was performed against wild-type CaMKII $\beta$ -  
911 expressing mice (WT).

912 **(f)** Total CaMKII $\alpha$  and T286-phosphorylated peptides from brains of sleep-deprived  
913 and control mice, analyzed by SRM quantitative mass spectrometry. Error bars: SEM

914 **(g)** Correlation of phosphorylation of CaMKII $\alpha$  T286 and CaMKII $\beta$  T287 in each brain.  
915 Each point corresponds to the quantification value obtained from individual mouse  
916 brain.

917 Error bars: SEM, \*p < 0.05, \*\*p < 0.01, \*\*\*p < 0.001, n.s.: no significance.

918

919 **Figure 1-figure supplement 2-source data 1**

920 Source data for Figure 1-figure supplement 2d, e, f

921

922 **Figure 1-source data 2 and 3**

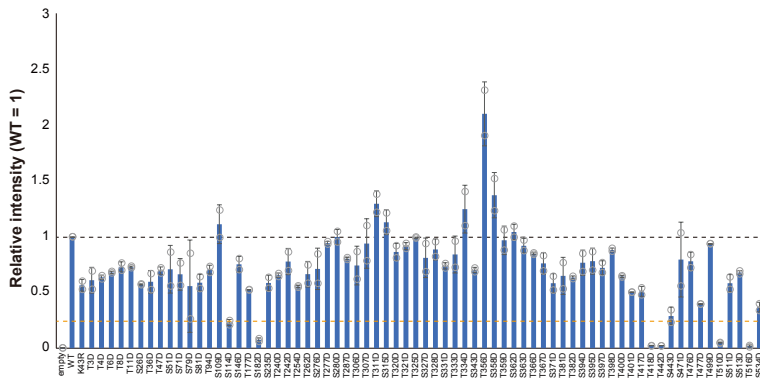
923 These source data include source data for Figure 1-figure supplement 2f and 2g.

924

925



**a**



926 **Figure 1-figure supplement 3. Biochemical evaluation of sleep-inducing**

927 **CaMKII $\beta$  mutants.**

928 **(a)** Expression levels of each mutant in the cell extracts used for the measurements  
929 shown in **(b)**. The expression level of each mutant was normalized relative to WT  
930 (black dashed line). The orange dashed line indicates 25% of the WT expression  
931 level. The represented values are the mean  $\pm$  SD (n = 2, independent experiments).

932 **(b)** *In vitro* kinase activity of CaMKII $\beta$  phosphomimetic mutants. Phosphorylation (%)  
933 indicates the percentage of the phosphorylated substrate relative to the total peptide  
934 in the presence or absence of CaM. The represented values are the mean  $\pm$  SD (n  
935 = 2, independent experiments). The mutants with blue labels exhibited < 25% lower  
936 expression than the WT in both trials. The mutants with green labels exhibited < 25%  
937 lower expression than the WT in one of the two trials.

938

939 **Figure 1-figure supplement 3-source data 1**

940 Source data for Figure 1-figure supplement 3a, b.

941

942

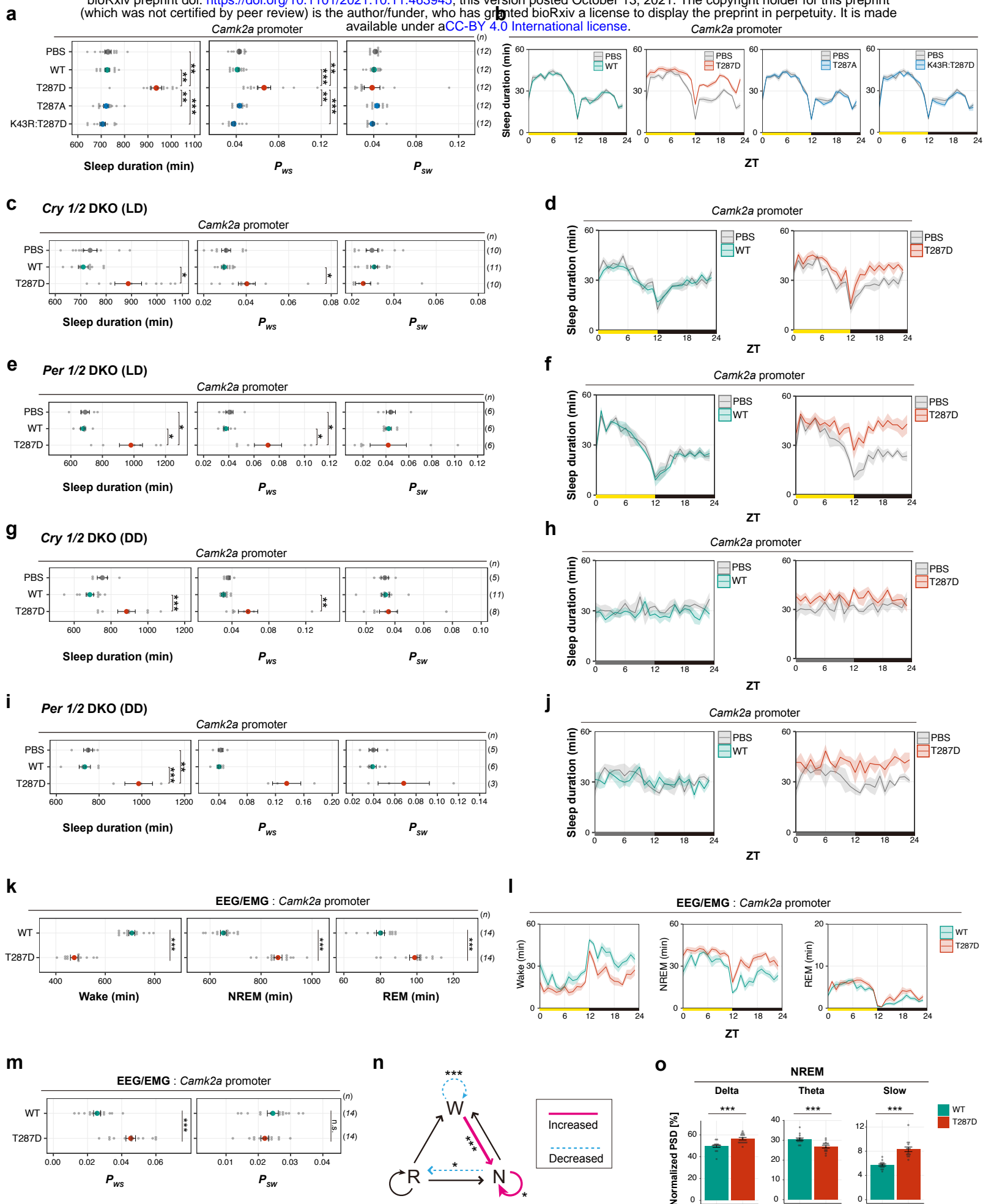


Figure 2

943 **Figure 2. Phosphorylation of CaMKII $\beta$  regulates NREM sleep induction and**  
944 **sleep needs**

945 **(a-b)** Sleep/wake parameters **(a)** and sleep profiles **(b)** of mice expressing CaMKII $\beta$   
946 T287-related mutants under the *Camk2a* promoter, averaged over six days. Shaded  
947 areas represent SEM. Multiple comparison test was performed against PBS-injected  
948 control mice (PBS).

949 **(c-f)** Sleep/wake parameters and sleep profiles, averaged over four days, of *Cry1/2*  
950 DKO mice **(c and d)** and *Per1/2* DKO mice **(e and f)** expressing wild-type CaMKII $\beta$   
951 (WT) or the T287D mutant under the light/dark condition. Multiple comparison tests  
952 were performed between all individual groups.

953 **(g-j)** Sleep/wake parameters, averaged over four days, of *Cry1/2* DKO mice **(g and**  
954 **h)** and *Per1/2* DKO mice **(i and j)** expressing wild-type CaMKII $\beta$  (WT) or the T287D  
955 mutant under constant dark. Multiple comparison tests were performed between all  
956 individual groups.

957 **(k-m)** Sleep phenotypes **(k and m)** and sleep profiles **(l)** measured by EEG/EMG  
958 recordings for mice expressing CaMKII $\beta$  (WT) or the T287D mutant.

959 **(n)** Differences in transition probabilities (between wakefulness (W), NREM sleep  
960 (N), and REM sleep (R)) between mice expressing WT CaMKII $\beta$  or the T287D  
961 mutant. Magenta lines and dashed blue lines indicate when the values for the  
962 T287D-expressing mice are significantly ( $p < 0.05$ ) higher and lower, respectively.

963 **(o)** NREM power density in typical frequency domains of mice expressing WT  
964 CaMKII $\beta$  or the T287D mutant.

965 Error bars: SEM, \* $p < 0.05$ , \*\* $p < 0.01$ , \*\*\* $p < 0.001$ , n.s.: no significance.

966

967 **Figure 2-source data 1**

968 Source data for Figure 2a-o

969

970

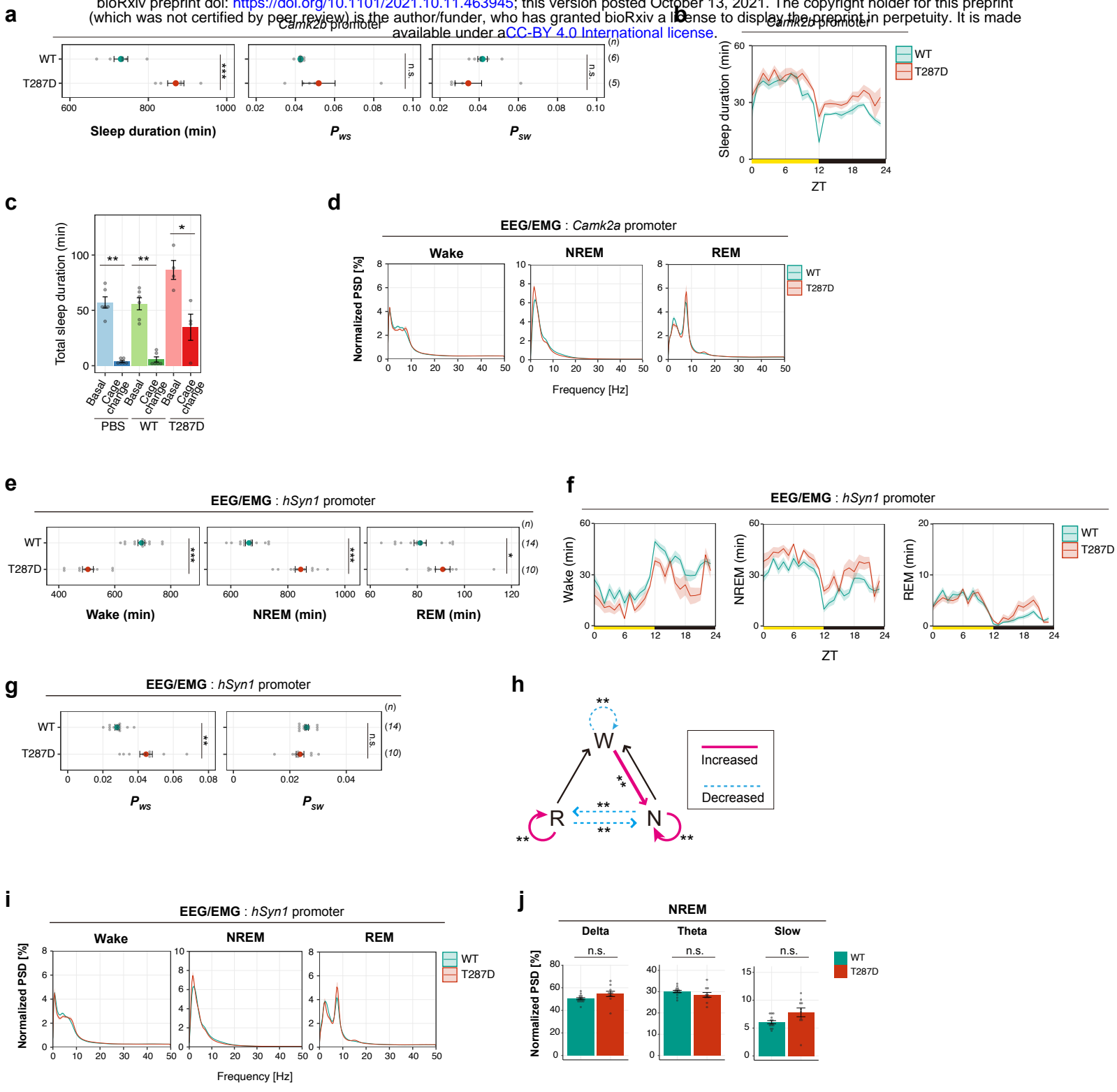


Figure 2-figure supplement 1

971 **Figure 2-figure supplement 1. Phosphorylation of CaMKII $\beta$  regulates NREM**  
972 **sleep induction and sleep needs**

973 **(a-b)** Sleep/wake parameters **(a)** and sleep profiles **(b)**, averaged over six days, of  
974 mice expressing WT CaMKII $\beta$  or the T287D mutant (T287D) under the *Camk2b*  
975 promoter.

976 **(c)** Total sleep duration from ZT0 to ZT2 of mice expressing wild-type CaMKII $\beta$  (WT,  
977 n = 6) and the CaMKII $\beta$  T287D mutants (T287D, n = 4) after cage change at ZT0.  
978 PBS: PBS-injected control mice (n = 6). “Basal” represents the sleep duration from  
979 ZT0 to ZT2 averaged over three days before the day of the cage change.

980 **(d)** EEG power spectra of mice expressing WT CaMKII $\beta$  or the T287D mutant under  
981 the *Camk2a* promoter.

982 **(e-g)** Sleep parameters **(e and g)** and sleep profiles **(f)** measured by EEG/EMG  
983 recordings for mice expressing CaMKII $\beta$  WT or the T287D mutant under the *hSyn1*  
984 promoter.

985 **(h)** Differences in transition probabilities (between wakefulness (W), NREM sleep  
986 (N), and REM sleep (R)) between WT CaMKII $\beta$  or T287D-expressing mice under the  
987 *hSyn1* promoter. Magenta lines and dashed blue lines indicate when the values for  
988 the T287D-expressing mice are significantly ( $p < 0.05$ ) higher and lower, respectively.

989 **(i-j)** EEG power spectra **(i)** and NREM power density in typical frequency domains  
990 **(j)** of mice expressing WT CaMKII $\beta$  or the T287D mutant under the *hSyn1* promoter.

991 Error bars: SEM, \* $p < 0.05$ , \*\* $p < 0.01$ , \*\*\* $p < 0.001$ , n.s.: no significance.

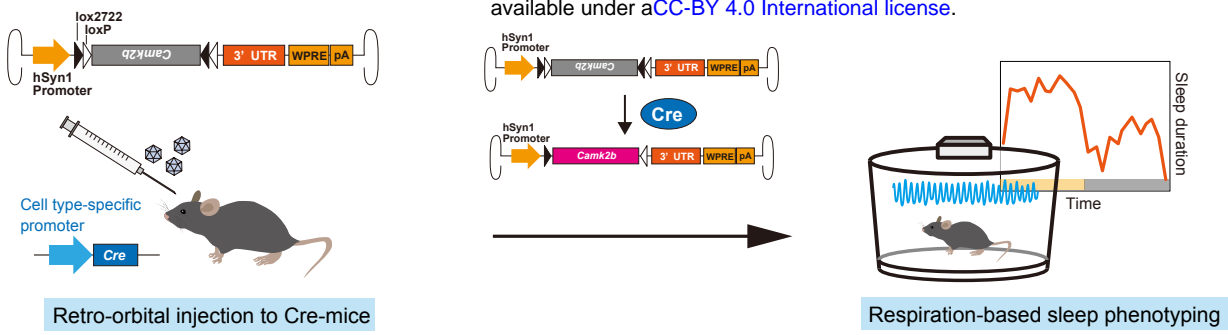
992

993 **Figure 2-figure supplement 1-source data 1**

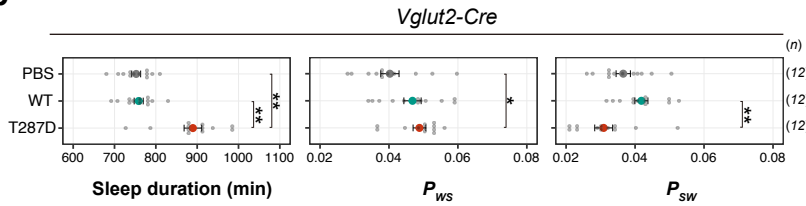
994 Source data for Figure 2-figure supplement 1a-j

995

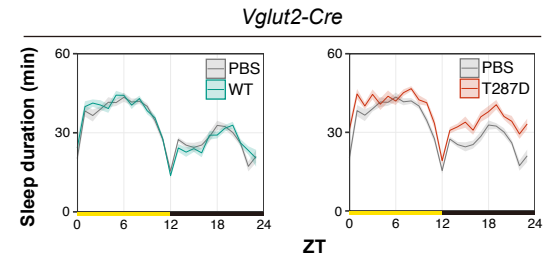
**a**



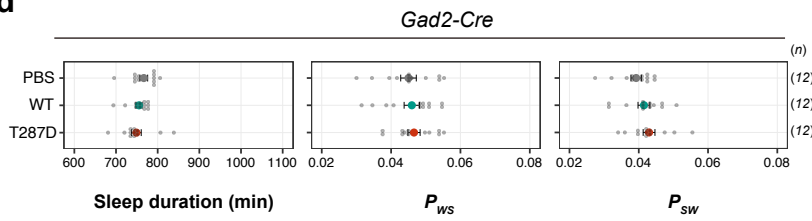
**b**



**c**



**d**



**e**

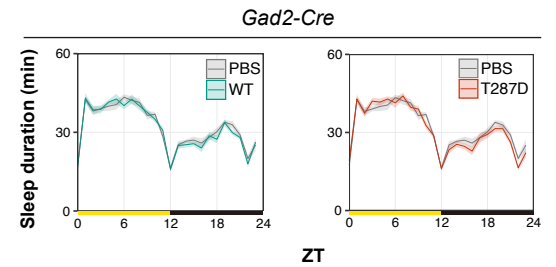


Figure 3



996 **Figure 3. Phosphorylation of CaMKII $\beta$  in excitatory neurons regulates sleep**  
997 **induction**

998 **(a)** Schematic diagram of cell type-specific expression of CaMKII $\beta$  using AAV and  
999 Cre-mice. Cre-mediated recombination of AAV genomes results in *Camk2b* gene  
1000 expression in the target cells.

1001 **(b-c)** Sleep/wake parameters **(b)** and sleep profiles **(c)** of *Vglut2-Cre*-mice  
1002 administrated with AAV-DIO-*Camk2b*, averaged over six days. Shaded areas  
1003 represent SEM. Multiple comparison tests were performed between all individual  
1004 groups.

1005 **(d-e)** Sleep/wake parameters **(d)** and sleep profiles **(e)** of *Gad2-Cre*-mice  
1006 administrated with AAV-DIO-*Camk2b*, averaged over six days. Multiple comparison  
1007 tests were performed between all individual groups.

1008 Error bars: SEM, \* $p < 0.05$ , \*\* $p < 0.01$ , \*\*\* $p < 0.001$ , n.s.: no significance.

1009

1010 **Figure 3-source data 1**

1011 Source data for Figure 3b-e

1012

1013

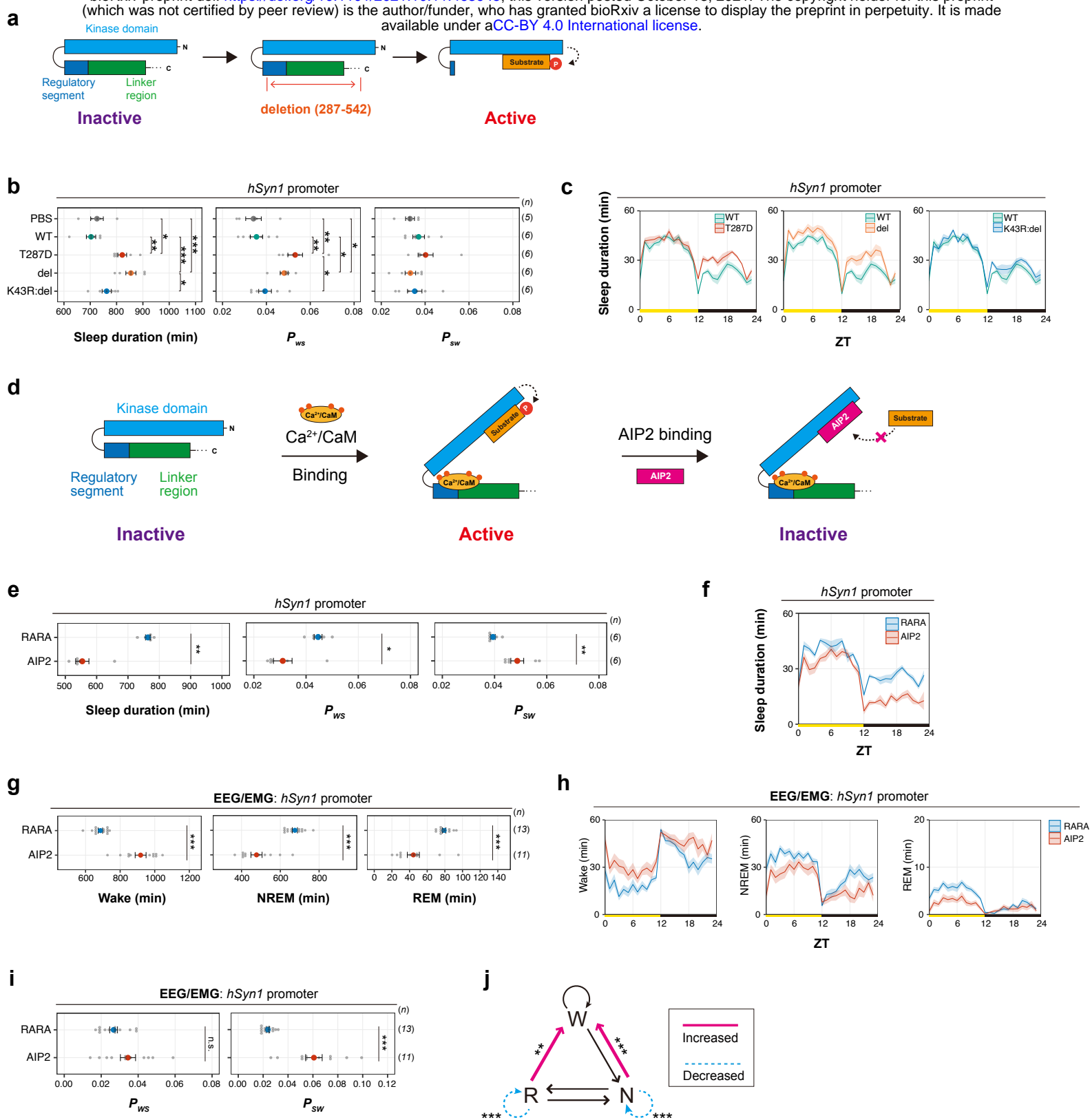


Figure 4

1014 **Figure 4. Perturbation on the kinase activity of CaMKII $\beta$  bidirectionally**  
1015 **affects sleep duration.**

1016 **(a)** Schematic diagram of CaMKII $\beta$  activation via deletion of its C-terminus. Deletion  
1017 of the regulatory segment and linker region exposes the kinase domain of the  
1018 CaMKII $\beta$  and makes the enzyme constitutively activated.

1019 **(b-c)** Sleep/wake parameters **(b)** and sleep profiles **(c)** of mice expressing the  
1020 CaMKII $\beta$  deletion mutant (del), averaged over six days. The shaded areas represent  
1021 SEM. Multiple comparison tests were performed between all individual groups.

1022 **(d)** Schematic diagram of CaMKII inhibition by AIP2 expression. AIP2 competitively  
1023 binds to the kinase domain and inhibits substrate phosphorylation.

1024 **(e-f)** Sleep/wake parameters **(e)** and sleep profiles **(f)** of mice expressing AIP2 or the  
1025 RARA mutant measured by the SSS, averaged over six days.

1026 **(g-i)** Sleep phenotypes **(g and i)** and sleep profiles **(h)** of mice expressing AIP2 or  
1027 the RARA mutant measured by EEG/EMG recordings.

1028 **(j)** Differences in transition probabilities (between wakefulness (W), NREM sleep (N),  
1029 and REM sleep (R)) between mice expressing AIP2 or the RARA mutant. Magenta  
1030 lines and dashed blue lines indicate when the values for the AIP2-expressing mice  
1031 are significantly ( $p < 0.05$ ) higher and lower, respectively.

1032 Error bars: SEM, \* $p < 0.05$ , \*\* $p < 0.01$ , \*\*\* $p < 0.001$ , n.s.: no significance.

1033

1034 **Figure 4-source data 1**

1035 Source data for Figure 4b, c, e, f, g, h, i, j

1036

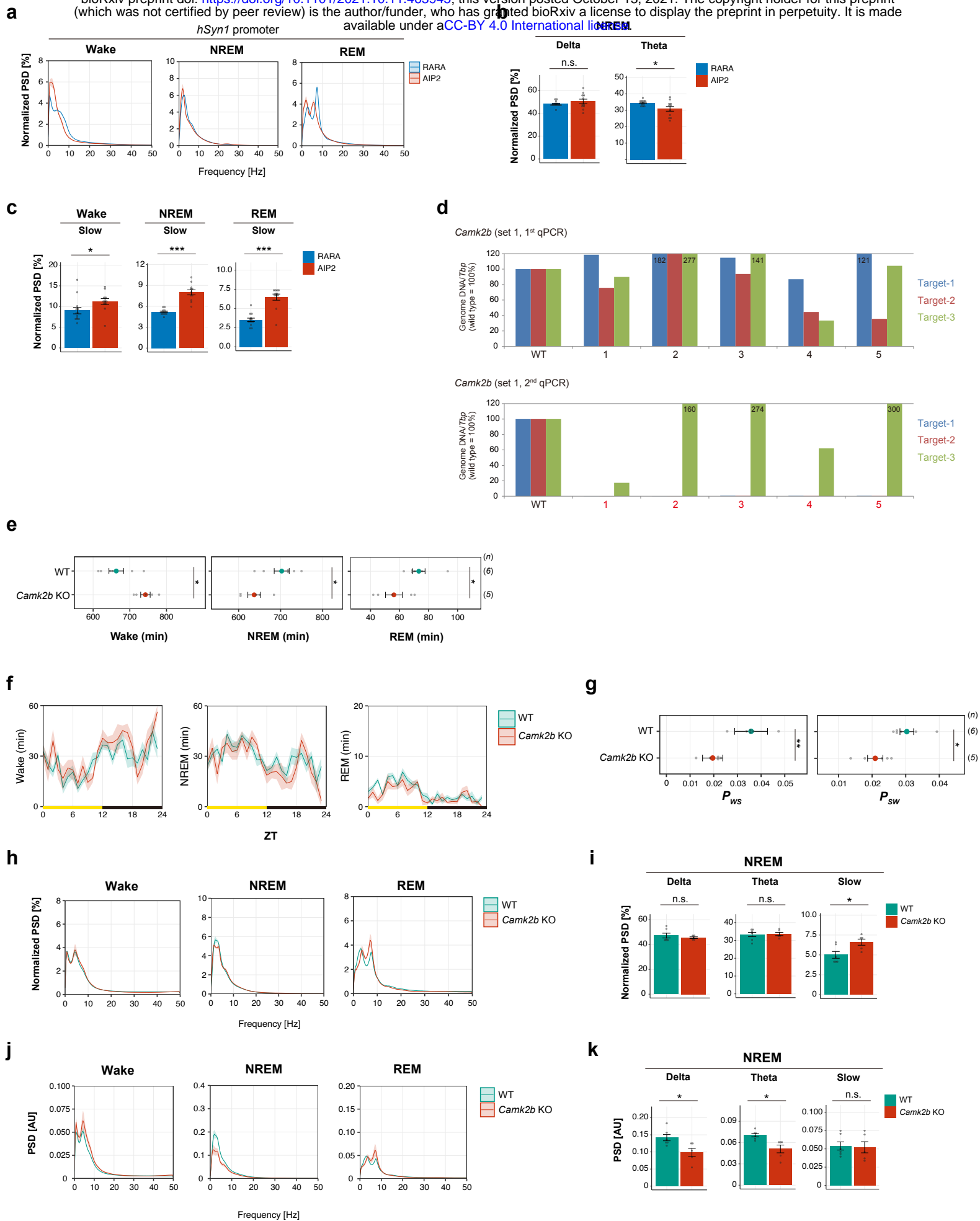


Figure 4-figure supplement 1

1037 **Figure 4-figure supplement 1. Sleep phenotypes of AIP2-expressing mice and**  
1038 ***Camk2b* KO mice**

1039 **(a-b)** EEG power spectra **(a)** and NREM power density in delta and theta domains  
1040 **(b)** of mice expressing AIP2 or the RARA mutant.

1041 **(c)** Power densities in slow domains of mice expressing AIP2 or the RARA mutant.

1042 **(d)** The genotype of *Camk2b* KO mice. The relative amount of intact DNA for each  
1043 target sequence was normalized to be 100% for wild-type mouse (WT). The qPCR  
1044 was performed with two independent primer sets (1<sup>st</sup> and 2<sup>nd</sup>) for the three target  
1045 sites. When the 0.5% criteria were met in either set, the mouse was considered a  
1046 KO mouse. All the mice (n=5) were confirmed as KO mice by the 2<sup>nd</sup> qPCR.

1047 **(e-g)** Sleep parameters **(e and g)** and sleep profiles **(f)** measured by EEG/EMG  
1048 recordings for *Camk2b* KO mice and wild-type C57BL/6N mice (WT).

1049 **(h-i)** Normalized EEG power spectra **(h)** and NREM power density in typical  
1050 frequency domains **(i)** of *Camk2b* KO mice and wild-type C57BL/6N mice (WT). EEG  
1051 Power was normalized relative to the total power in each frequency band.

1052 **(j-k)** EEG power spectra **(j)** and NREM power density in typical frequency domains  
1053 **(k)** of *Camk2b* KO mice and wild-type C57BL/6N mice (WT) without normalization.

1054 Error bars: SEM, \*p < 0.05, \*\*p < 0.01, \*\*\*p < 0.001, n.s.: no significance.

1055

1056 **Figure 4-figure supplement 1-source data 1**

1057 Source data for Figure 4-figure supplement 1a, b, c, d, e, f, g, h, i, j, k

1058



1059 **Figure 5. Multi-site phosphorylation of CaMKII $\beta$  can cancel sleep induction**

1060 **(a)** Daily sleep duration, averaged over six days, of mice expressing CaMKII $\beta$   
1061 double-phosphomimetic mutants (n = 5–12). The dashed green and red lines  
1062 represent the averaged sleep duration of mice expressing wild-type CaMKII $\beta$  (WT, n  
1063 = 71) and T287D mutants (T287D, n = 68), respectively. The plus sign in a mutant's  
1064 name indicates a combination with T287D. Multiple comparison test was performed  
1065 against WT (vs WT) or T287D (vs T287D). In the comparison with T287D mutant,  
1066 "n.s." labels are omitted for visibility.

1067 **(b-c)** Sleep/wake parameters **(b)** and sleep profiles **(c)**, averaged over six days, of  
1068 mice expressing CaMKII $\beta$  mutants with D or A substitutions of residues that cancel  
1069 the sleep-inducing effect of T287D in **(a)**. Measurements are independent from those  
1070 in **(a)**. The shaded areas represent SEM.

1071 Error bars: SEM, \*p < 0.05, \*\*p < 0.01, \*\*\*p < 0.001, n.s.: no significance.

1072

1073 **Figure 5-source data 1**

1074 Source data for Figure 5a-c

1075

1076

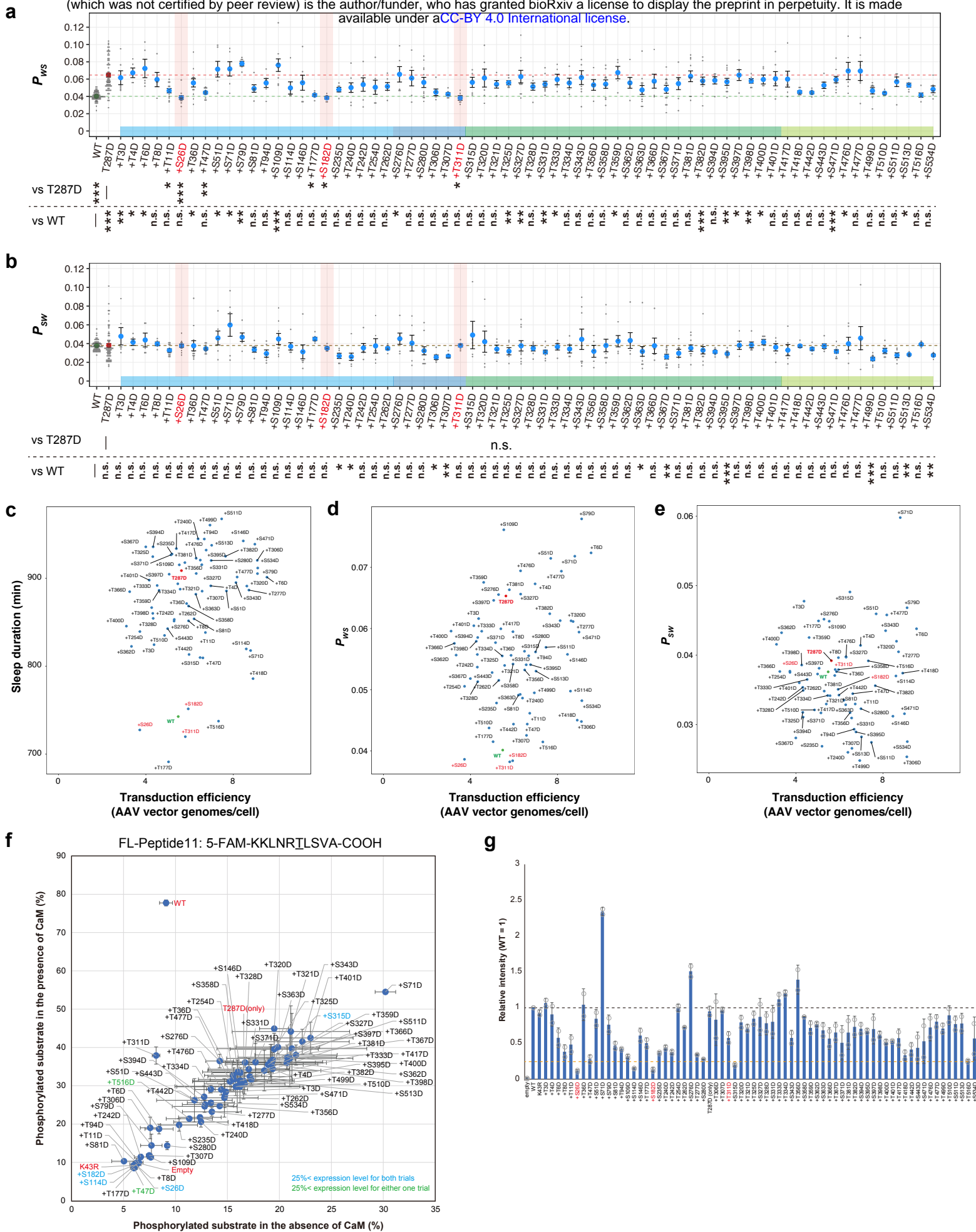


Figure 5-figure supplement 1



1077 **Figure 5-figure supplement 1. Multi-site phosphorylation of CaMKII $\beta$  can**  
1078 **cancel sleep induction**

1079 **(a-b)** Daily  $P_{WS}$  **(a)** and  $P_{SW}$  **(b)**, averaged over six days, of the mice expressing  
1080 CaMKII $\beta$  double-phosphomimetic mutants (n = 5–12) shown in **Figure 5a**. Dashed  
1081 green and red lines represent the averaged sleep duration of wild-type CaMKII $\beta$ -  
1082 expressing mice (WT, n = 71) and CaMKII $\beta$  T287D mutants-expressing mice (T287D,  
1083 n = 68), respectively. The plus sign in a mutant name indicates a combination with  
1084 T287D. Multiple comparison test was performed against WT (vs WT) or T287D (vs  
1085 T287). In the comparison with the T287D mutant, “n.s.” labels are omitted for visibility  
1086 in **(a)**.

1087 **(c-e)** Calculated transduction efficiency plotted against sleep duration **(c)**,  $P_{WS}$  **(d)**  
1088 and  $P_{SW}$  **(e)**. Transduction efficiency is an estimation of the number of AAV vector  
1089 genomes present per cell in a mouse brain. After the SSS measurements, we  
1090 purified the AAV vector genomes from the mice brains and then quantified them with  
1091 a WPRE-specific primer. The transduction efficiency is the quantification value  
1092 normalized to a TATA-binding protein (*Tbp*)-specific primer using qPCR.

1093 **(f-g)** *In vitro* kinase activity and expression level of CaMKII $\beta$  double-phosphomimetic  
1094 mutants. The data represented as in **Figure 1-figure supplement 2f** and **g**.

1095 Error bars except in **(f-g)**: SEM, \*p < 0.05, \*\*p < 0.01, \*\*\*p < 0.001, n.s.: no  
1096 significance.

1097

1098 **Figure 5-figure supplement 1-source data 1**

1099 Source data for Figure 5-figure supplement 1a-g.

1100

1101

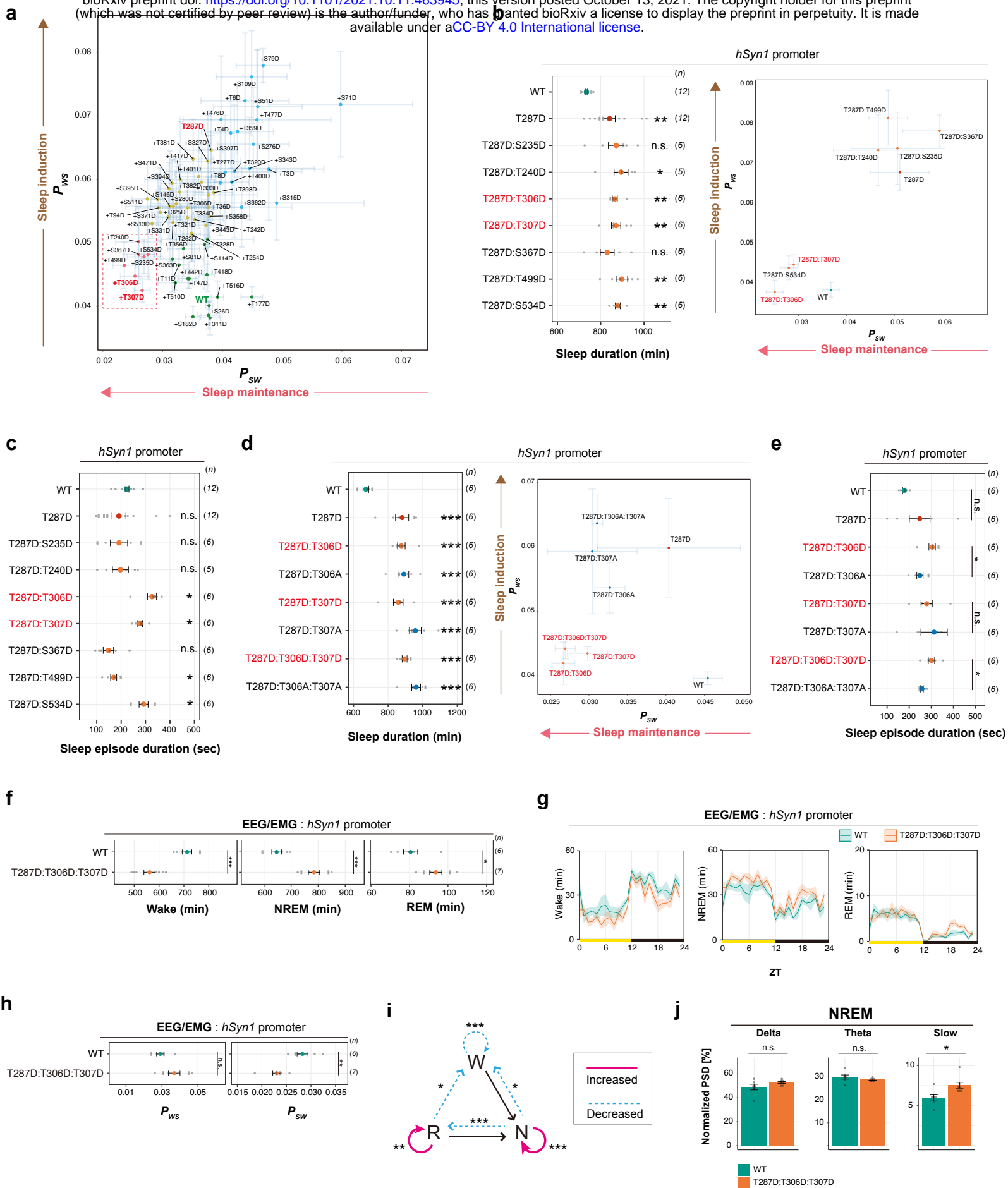


Figure 6

1102 **Figure 6. Multi-site phosphorylation of CaMKII $\beta$  regulates sleep stabilization**

1103 **(a)** Correlation diagram of daily  $P_{WS}$  and  $P_{SW}$  of mice expressing the CaMKII $\beta$   
1104 double-phosphomimetic mutants shown in **Figure 5a**, averaged over six days. The  
1105 color of the dots correspond to the result of the clustering shown in **Figure 6-figure**  
1106 **supplement 1a**. The mutants in the dotted magenta box had extended sleep  
1107 duration with lower  $P_{WS}$  and  $P_{SW}$  (i.e., higher sleep maintenance activity).

1108 **(b)** Sleep duration and correlation diagram of daily  $P_{WS}$  and  $P_{SW}$  of mice expressing  
1109 double-phosphomimetic mutants with sleep maintenance activity. Measurements  
1110 are independent from those in **Figure 5a**. For the comparisons of sleep duration,  
1111 multiple testing was performed against wild-type CaMKII $\beta$ -expressing mice (WT).

1112 **(c)** Sleep episode duration, averaged over six days, of mice expressing the double-  
1113 phosphomimetic mutants shown in **Figure 6b**

1114 **(d)** Sleep duration and correlation diagram of daily  $P_{WS}$  and  $P_{SW}$  of mice expressing  
1115 CaMKII $\beta$  mutants with D or A substitutions of sleep-stabilizing residues. For the  
1116 comparisons of sleep duration, multiple testing was performed against wild-type  
1117 CaMKII $\beta$ -expressing mice (WT).

1118 **(e)** Sleep episode duration, averaged over six days, of mice expressing CaMKII $\beta$   
1119 mutants with D or A substitutions of sleep-stabilizing residues shown in **Figure 6d**

1120 **(f-h)** Sleep phenotypes of mice expressing WT CaMKII $\beta$  or the T287D:T306D:T307D  
1121 mutant measured by EEG/EMG recordings.

1122 **(i)** Differences in transition probabilities (between wakefulness (W), NREM sleep (N),  
1123 and REM sleep (R)) between mice expressing WT CaMKII $\beta$  or the  
1124 T287D:T306D:T307D mutant. Magenta lines and dashed blue lines indicate when  
1125 the values for the T287D:T306D:T307D-expressing mice are significantly ( $p < 0.05$ )

1126 higher and lower, respectively.

1127 **(j)** NREM power density in typical frequency domains of mice expressing WT

1128 CaMKII $\beta$  and the T287D:T306D:T307D mutant.

1129 Error bars: SEM, \* $p < 0.05$ , \*\* $p < 0.01$ , \*\*\* $p < 0.001$ , n.s.: no significance.

1130

1131

1132 **Figure 6-source data 1**

1133 Source data for Figure 6b-j

1134

1135

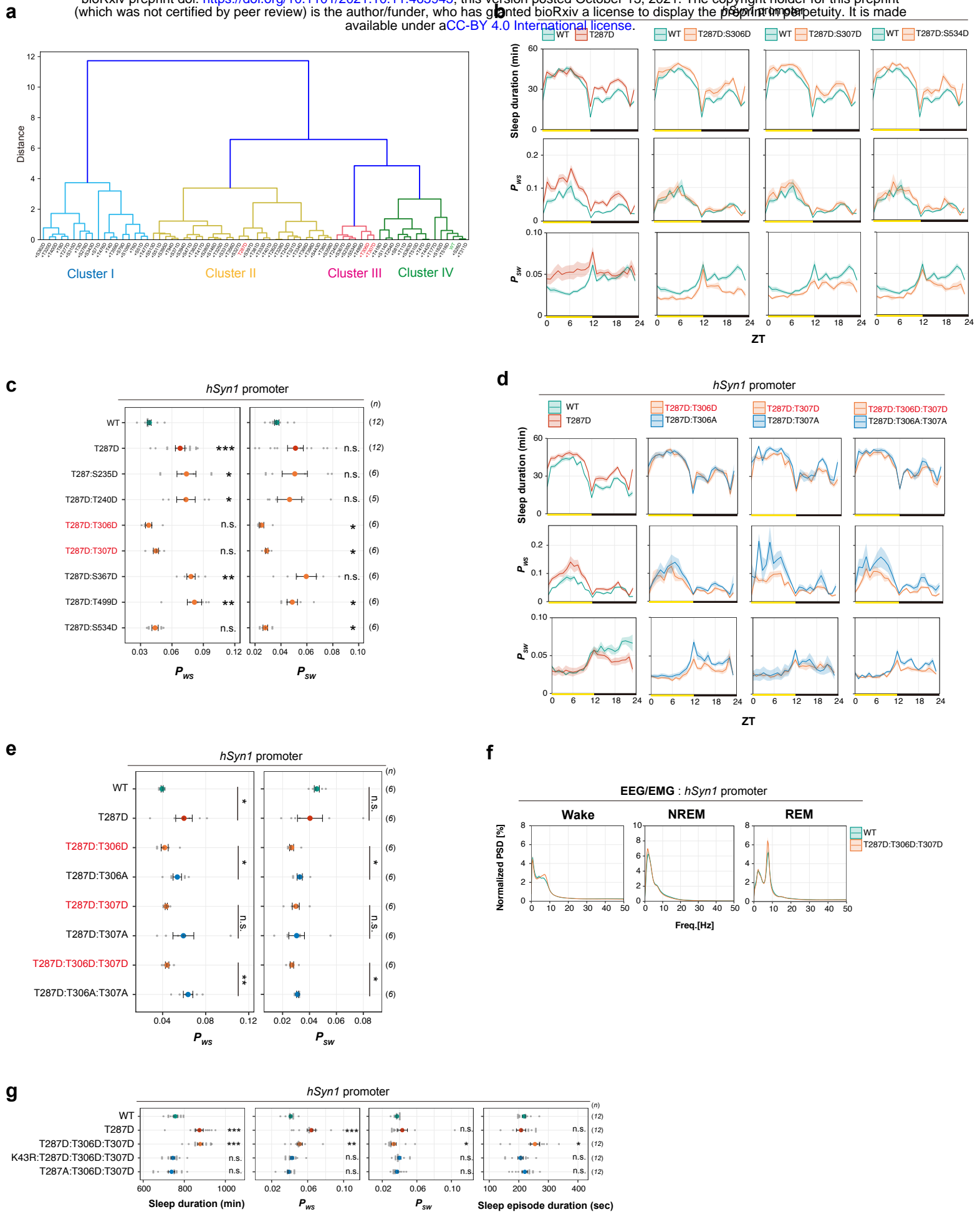


Figure 6-figure supplement 1

1136 **Figure 6-figure supplement 1. Multi-site phosphorylation of CaMKII $\beta$**   
1137 **regulates sleep stabilization**

1138 **(a)** Hierarchical clustering dendrogram from sleep profiles of mice expressing the  
1139 CaMKII $\beta$  double-phosphomimetic mutants shown in **Figure 6a**. Cluster I contains  
1140 mutants that increase  $P_{SW}$ , (sleep destabilizing). Cluster II, the largest cluster,  
1141 contains mutants that increase  $P_{WS}$ , similar to the T287D mutant. Cluster III contains  
1142 mutants that decrease  $P_{SW}$  (sleep stabilizing). Cluster IV contains mutants with  
1143 properties similar to WT. The "T287D-canceling" mutants such as +S26D, +S182D,  
1144 and +T311D belong to cluster IV. The vertical branch length represents the degree  
1145 of dissimilarity in sleep profiles among the mutants. Branch colors indicate clusters.

1146 **(b-c)** Profiles of sleep and transition probability **(b)** and  $P_{WS}$  and  $P_{SW}$  **(c)**, averaged  
1147 over six days, of mice expressing the double-phosphomimetic mutants shown in  
1148 **Figure 6b and 6c**. The shaded areas represent SEM. Multiple comparison test was  
1149 performed against wild-type CaMKII $\beta$ -expressing mice (WT).

1150 **(d-e)** Profiles of sleep and transition probability **(d)** and  $P_{WS}$  and  $P_{SW}$  **(e)**, averaged  
1151 over six days, of mice expressing the CaMKII $\beta$  mutants with sleep-stabilizing  
1152 residues substituted with D or A shown in **Figure 6d and 6e**. The shaded areas  
1153 represent SEM. Multiple comparison test was performed against wild-type CaMKII $\beta$ -  
1154 expressing mice (WT).

1155 **(f)** EEG power spectra of mice expressing WT CaMKII $\beta$  and the  
1156 T287D:T306D:T307D mutant shown in **Figure 6f-j**.

1157 **(g)** Sleep/wake parameters, averaged over six days, of mice expressing the  
1158 CaMKII $\beta$  T287D:T306D:T307D mutant with the K43R or T287A mutation. Multiple  
1159 comparison test was performed against wild-type CaMKII $\beta$ -expressing mice (WT).

1160 Error bars: SEM, \* $p < 0.05$ , \*\* $p < 0.01$ , \*\*\* $p < 0.001$ , n.s.: no significance.

1161

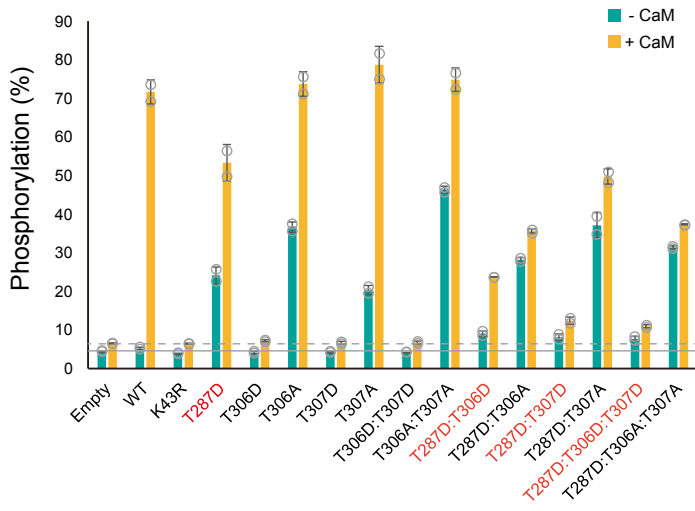
1162 **Figure 6-figure supplement 1-source data 1**

1163 Source data for Figure 6-figure supplement 1a-g

1164

1165

**a** FL-Peptide11: 5-FAM-KKLNRI<sub>L</sub>SVA-COOH



**b** Autocamide-2 Peptide : 5-FAM-KKALRRQE<sub>I</sub>VDAL-COOH

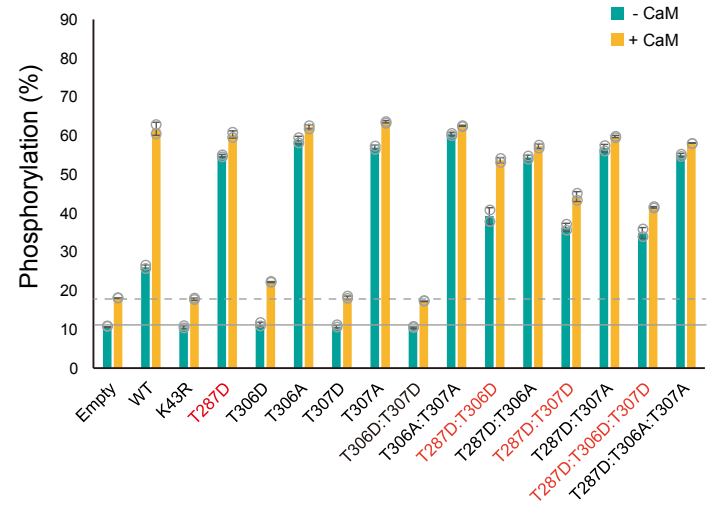


Figure 6-figure supplement 2



1166 **Figure 6-figure supplement 2. Ordered auto-phosphorylation of sleep-**  
1167 **controlling residues in CaMKII $\beta$**

1168 **(a-b)** *In vitro* kinase activity of CaMKII $\beta$  mutants against FL-Peptide 11 **(a)** or  
1169 autocamtide-2 peptide **(b)** in the absence (-CaM, green bar) or presence (+CaM,  
1170 yellow bar) of CaM. The amino acids phosphorylated by CaMKII $\beta$  are underlined in  
1171 the peptide sequences. Phosphorylation (%) indicates the percentage of the  
1172 phosphorylated substrate relative to the total peptide. The reported values are the  
1173 mean  $\pm$  SD (n = 2 independent experiments). The dashed and solid lines indicate  
1174 background signals measured in cell lysate transfected with the control empty vector  
1175 (Empty).

1176

1177 **Figure 6-figure supplement 2-source data 1**

1178 Source data for Figure 6-figure supplement 2a-b.

1179

1180

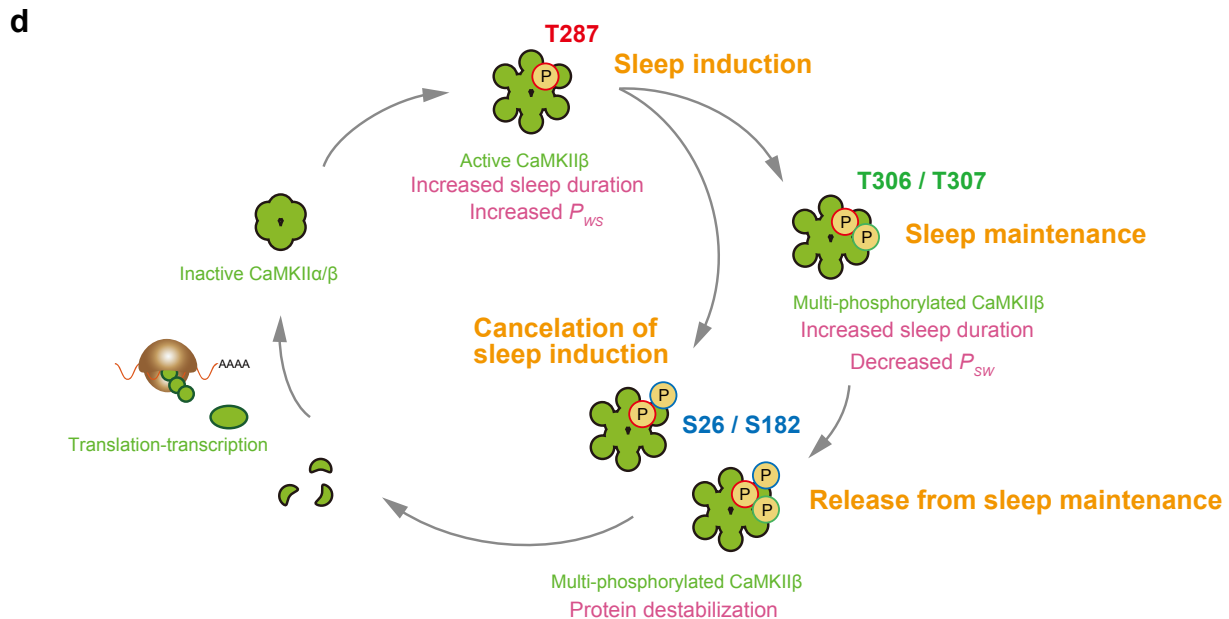
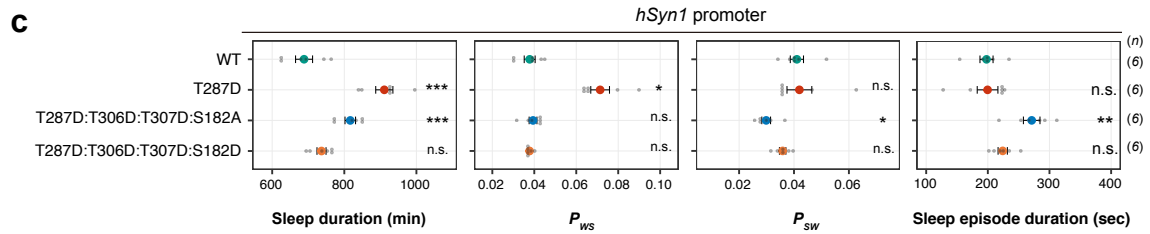
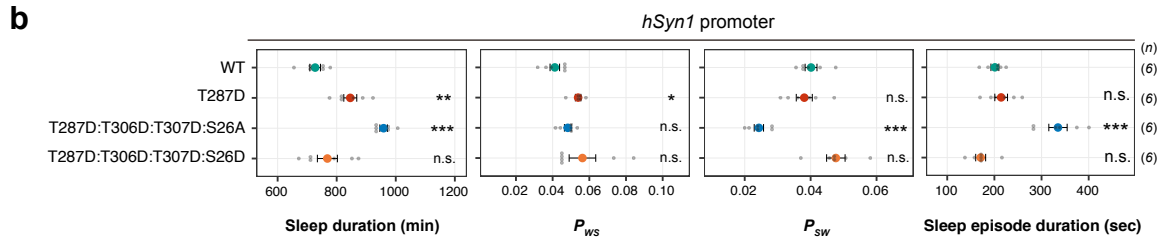
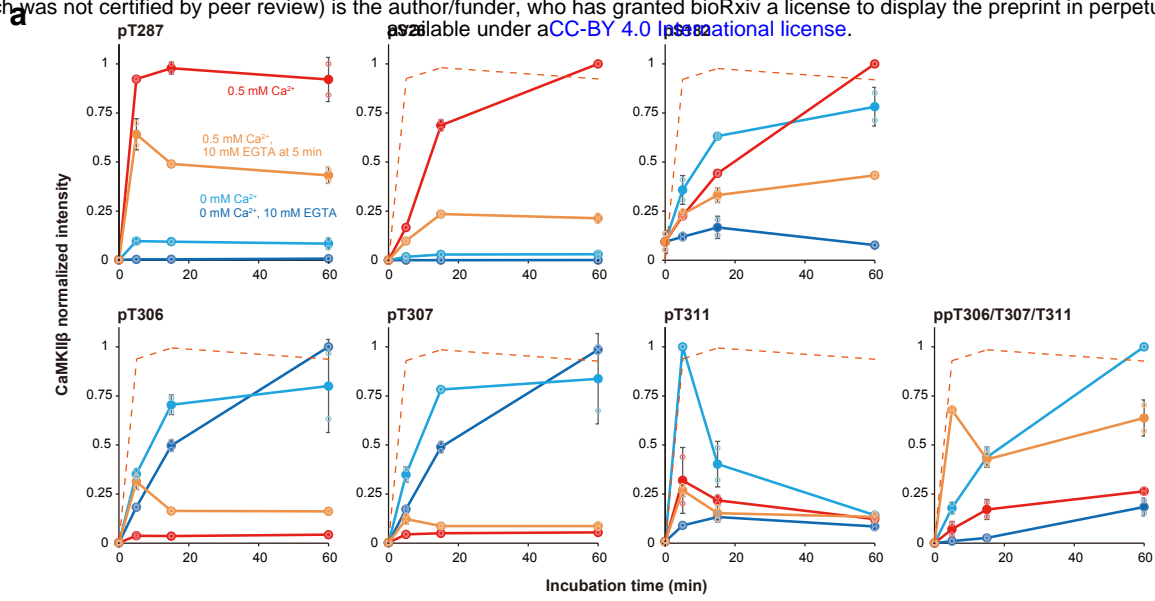


Figure 7

1181 **Figure 7. Ordered multi-site phosphorylation of CaMKII $\beta$  underlies multi-step**  
1182 **sleep regulation**

1183 **(a)** Time series changes of sleep-controlling residues phosphorylation under  
1184 different Ca<sup>2+</sup> conditions *in vitro*. The represented values are the mean  $\pm$  SD (n = 2  
1185 independent experiments). The signal intensity of the detected peptides was  
1186 normalized to the maximum value in the time series. The quantified values at 0 min  
1187 were obtained from the sample before adding CaM and were shared in every Ca<sup>2+</sup>  
1188 conditions. The dashed lines trace the dynamics of T287 phosphorylation in the 0.5  
1189 mM Ca<sup>2+</sup> condition.

1190 **(b-c)** Sleep/wake parameters of mice expressing quadruple-phosphomimetic  
1191 CaMKII $\beta$  mutants related to S26 **(b)** and S182 **(c)**. Multiple comparison test was  
1192 performed against wild-type CaMKII $\beta$ -expressing mice (WT). Error bars: SEM, \*p <  
1193 0.05, \*\*p < 0.01, \*\*\*p < 0.001, n.s.: no significance.

1194 **(d)** Ordered multi-site phosphorylation states of CaMKII $\beta$  in sleep regulation. Note  
1195 that this model only describes about the possible relationship between CaMKII $\beta$  and  
1196 the sleep-wake cycle without considering the difference between NREM and REM  
1197 sleeps.

1198

1199 **Figure 7-source data 1 and 2**

1200 Source data for Figure 7a.

1201

1202 **Figure 7-source data 3**

1203 Source data for Figure 7b-c.

1204

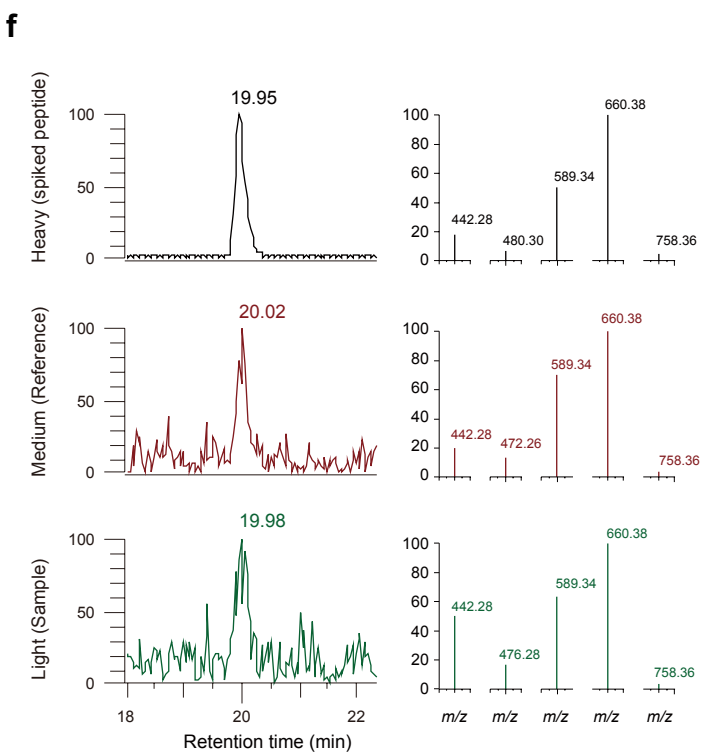
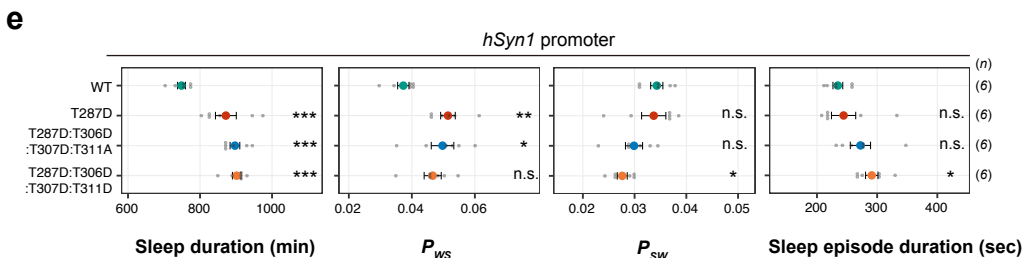
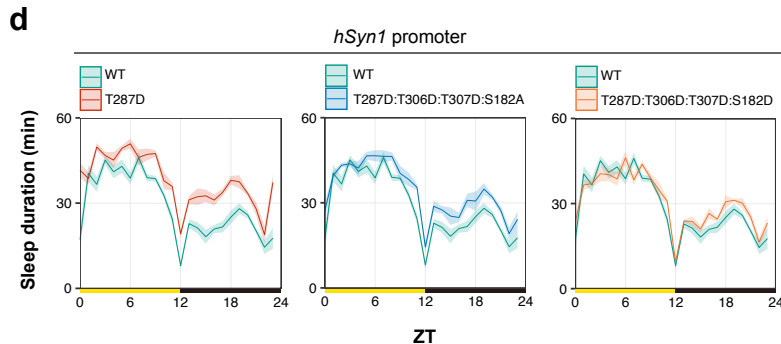
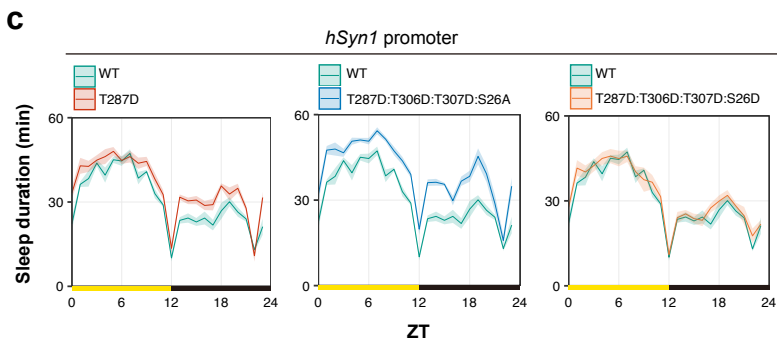
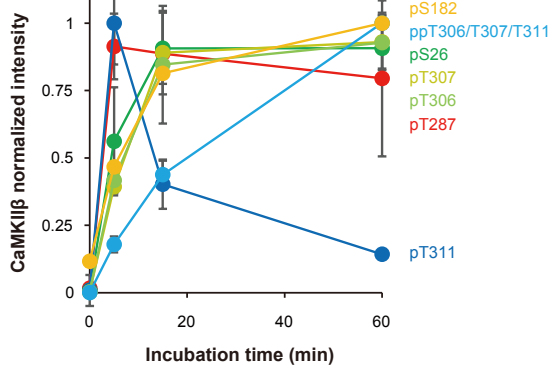
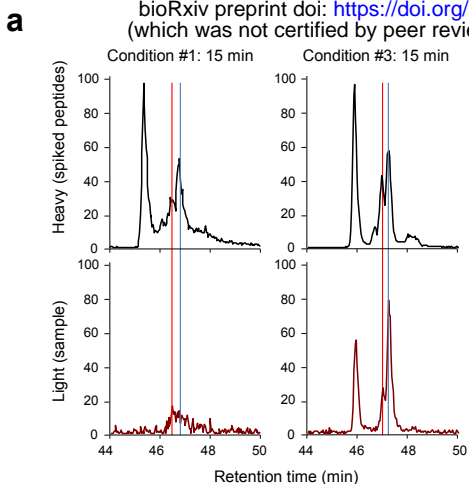


Figure 7-figure supplement 1

1205 **Figure 7-figure supplement 1. Ordered multi-site phosphorylation of CaMKII $\beta$**   
1206 **underlies multi-step sleep regulation**

1207 **(a)** Example chromatogram of SRM measurement for pS182 peptide. Red line  
1208 indicates the retention time of a peptide phosphorylated at S182. Red line indicates  
1209 the retention time of a peptide phosphorylated at T177.

1210 **(b)** Phosphorylation time course for sleep-controlling residues *in vitro*. Time series  
1211 changes of the residues in the condition #2 are extracted and overlaid from **Figure**  
1212 **7a**. The values are shown as relatives, with the maximum value of each residue in  
1213 the time course as 1.

1214 **(c)** Profiles of sleep, averaged over six days, of mice expressing the quadruple-  
1215 phosphomimetic CaMKII $\beta$  mutants related to S26 shown in **Figure 7b**. The shaded  
1216 areas represent SEM.

1217 **(d)** Profiles of sleep, averaged over six days, of mice expressing the quadruple-  
1218 phosphomimetic CaMKII $\beta$  mutants related to S182 shown in **Figure 7c**. The shaded  
1219 areas represent SEM.

1220 **(e)** Sleep/wake parameters of mice expressing the quadruple-phosphomimetic  
1221 CaMKII $\beta$  mutants related to T311. Multiple comparison test was performed against  
1222 wild-type CaMKII $\beta$ -expressing mice (WT).

1223 **(f)** Phosphorylation of S26 (CaMKII $\beta$ ) or S25 (CaMKII $\alpha$ ) residue in mice brain. Mice  
1224 brain samples shown in **Figure 1g and 1h** were also subjected to SRM analysis with  
1225 mass-spectrometry method for analyzing the phosphorylation of S26 (CaMKII $\beta$ ) or  
1226 S25 (CaMKII $\alpha$ ) residues. Representative chromatograms shown in left indicated that  
1227 a synthesized and heavy-labeled phosphorylated peptide, of which sequence is  
1228 identical to a trypsin-digested peptide sequence corresponding to S26 (CaMKII $\beta$ ) or

1229 S25 (CaMKII $\alpha$ ) was detected at retention time ~20 min. Medium-labeled peptide  
1230 sample (derived from internal control mixture) and light-labeled peptide sample  
1231 (derived from individual samples) also showed a peak at retention time ~20 min. The  
1232 product ion spectrum on the right shows that each product ion from the five different  
1233 transitions in the three samples has a similar intensity distribution. These results  
1234 suggest that a peptide corresponding to phosphorylated S26 (CaMKII $\beta$ ) or S25  
1235 (CaMKII $\alpha$ ) was included in trypsin-digested mice brain samples.

1236 Error bars: SEM, \* $p < 0.05$ , \*\* $p < 0.01$ , \*\*\* $p < 0.001$ , n.s.: no significance.

1237

1238

1239 **Figure 7-figure supplement 1-source data 1**

1240 Source data for Figure 7-figure supplement 1c-e

1241

1242 **Figure 7-source data 1 and 2**

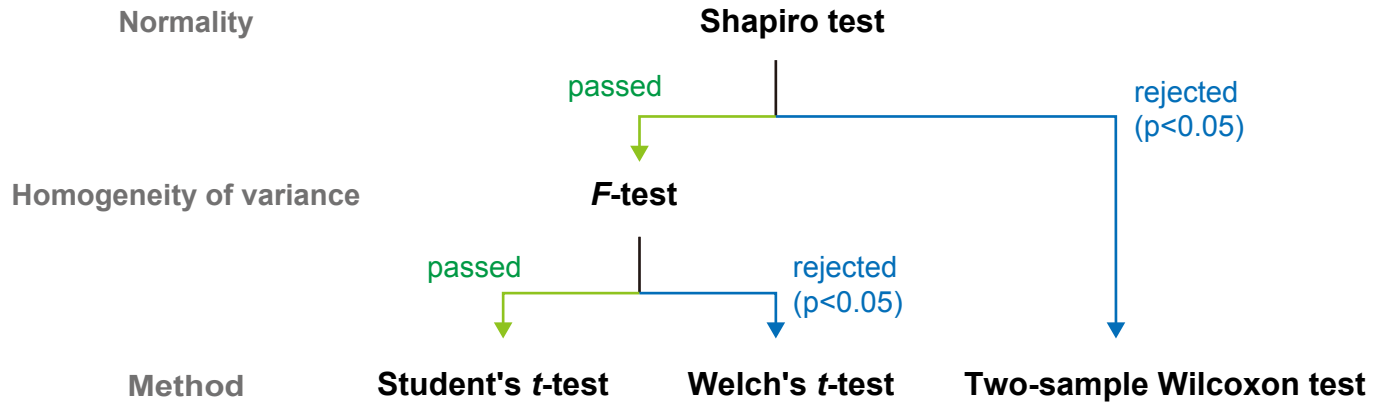
1243 These source data include source data for Figure 7-figure supplement 1a, b, f.

1244

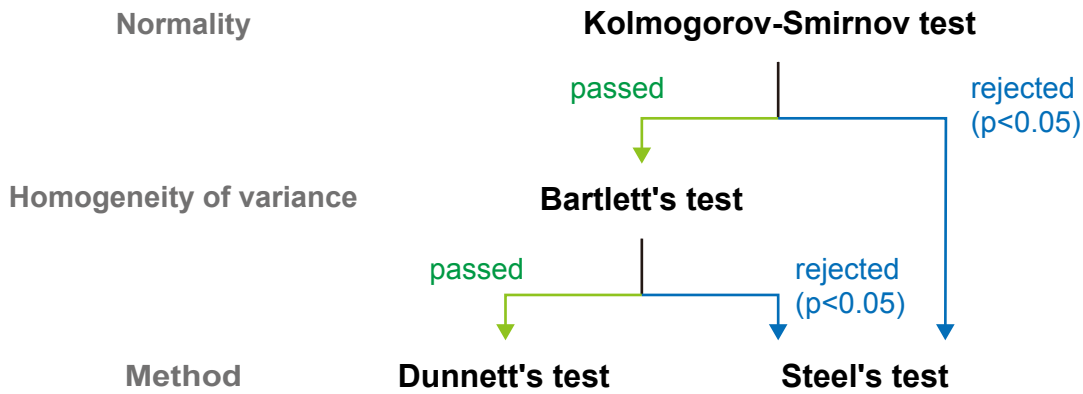
1245

1246

## Two unpaired samples



## More than two samples against identical sample (e.g., common control)



## Multiple comparisons between each group

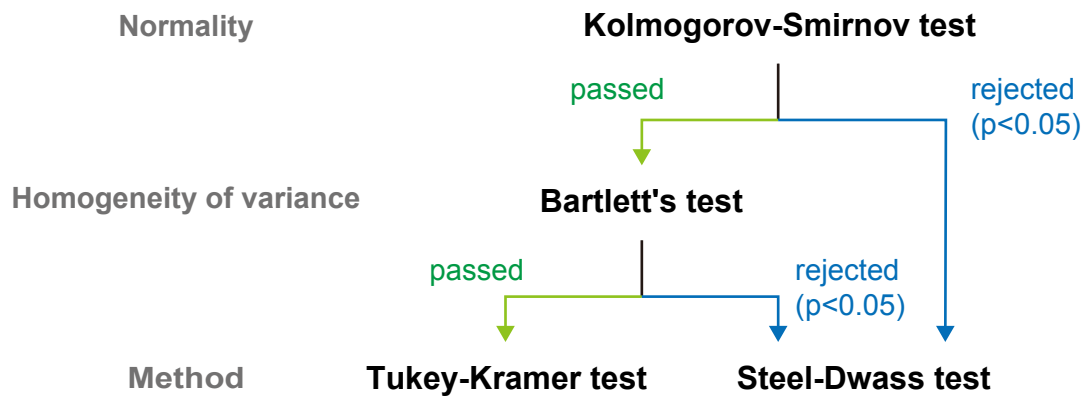


Figure 8

1247 **Figure 8. Workflow for selecting the statistical method**

1248 Workflow for selecting the statistical test methods used in this study. Based on the  
1249 purpose of the comparison, normality and equality of variance were checked, and  
1250 appropriate statistical method was selected. Details are provided in the Methods  
1251 section.

1252

1253

1254

1255 **TABLES**

1256 **Table 1. Summary of AAV applications and conditions**

1257

1258



**Table 1: Summary of AAV applications and conditions**

<b>Applications in the paper</b>	<b>Use cases</b>	<b>pAAV vector</b>	<b>Dosage (vg/mouse)</b>
Neuronal expression of <i>Camk2b</i>	Fig.1d-f, Fig.5, Fig.6, Fig.7b-c, Fig.1-Sup1b, Fig1-Sup2a-e, Fig.2-Sup1e-j, Fig.5-Sup1a-e, Fig.6-Sup1, Fig.7-Sup1a-c	P(hSyn1)-Camk2b-3'UTR-WPRE-SV40pA	5.0 x 10 <sup>10</sup>
Neuronal expression of H2B-mCherry	Fig.1c, Fig.1-Sup1a	P(hSyn1)-H2B-mCherry-3'UTR-WPRE-SV40pA	5.0 x 10 <sup>10</sup>
Camk2a promoter-driven expression of <i>Camk2b</i>	Fig.2, Fig.2-Sup1d	P(Camk2a)-Camk2b-3'UTR-WPRE-SV40pA	1.0 x 10 <sup>11</sup>
Camk2b promoter-driven expression of <i>Camk2b</i>	Fig.2-Sup1a-d	P(Camk2b)-Camk2b-3'UTR-WPRE-SV40pA	2.0 x 10 <sup>11</sup>
Cre-dependent expression of <i>Camk2b</i>	Fig.3b-e	P(hSyn1)-DIO-Camk2b-3'UTR-WPRE-SV40pA	2.0 x 10 <sup>11</sup>
Neuronal expression of <i>Camk2b</i> deletion mutant	Fig.4b-c	P(hSyn1)-Camk2b(del)-3'UTR-WPRE-SV40pA	2.5 x 10 <sup>10</sup>
Neuronal expression of AIP2	Fig.4e-j, Fig.4-Sup1a-c	P(hSyn1)-mCherry-AIP2-Map2DTE-WPRE-SV40pA	2.0 x 10 <sup>11</sup>

## 1259 **MATERIALS and METHODS**

### 1260 **Plasmids**

1261 Mouse *Camk2b* cDNA (NM\_007595) was subcloned into the pMU2 vector <sup>71</sup> that  
1262 expresses genes under the CMV promoter. Note that the FLAG-tag involved in the  
1263 original pMU2 vector was removed in the construct used in this study. Mutagenesis  
1264 of pMU2-*Camk2b* was conducted by inverse PCR with Mighty Cloning Reagent Set  
1265 (Blunt End) (Takara Bio, Japan) following to the manufacturer's protocol.

1266 For pAAV construction, the *Camk2b* sequence was transferred into the pAAV  
1267 vector (kindly provided by Dr. Hirokazu Hirai) along with the *hSyn1* promoter <sup>72</sup>,  
1268 FLAG tag, *Camk2b* 3'UTR, WPRE, and SV40 polyA sequences as illustrated in  
1269 Figure 1b. For the *Camk2b* 3'UTR used in this study, the evolutionarily conserved  
1270 ~350 bp (chr11:5,971,489-5,971,827, GRCm38/mm10) and ~650 bp  
1271 (chr11:5,969,672-5,970,313, GRCm38/mm10) regions in the mouse *Camk2b* 3'UTR  
1272 was cloned and assembled tandemly. For double-floxed inverted open reading frame  
1273 (DIO) constructs, the inverted FLAG-*Camk2b* sequence flanked by lox2272 and loxP  
1274 was inserted between the *hSyn1* promoter and the *Camk2b* 3'UTR of the pAAV  
1275 vector as illustrated in **Figure 3a**. For more targeted gene expression, the *hSyn1*  
1276 promoter was replaced with other promoters (Figure 2 and Figure 1-figure  
1277 supplement 2a). A vector containing *Camk2a* promoter sequence was a kind gift  
1278 from Drs. Masamitsu Iino and Yohei Okubo (The University of Tokyo). For the  
1279 *Camk2b* promoter, ~1300 bp region (chr11:6,065,706-6,066,972, GRCm38/mm10)  
1280 upstream of the TSS of the *Camk2b* gene was cloned using a pair of primers (5'-  
1281 AGCACTCTGTCAAATGTACCTTTAG-3'; 5'-AGATCTGCTCGCTCTGTCCC-3').

1282 The mCherry-AIP2 was constructed by fusing the AIP2 sequence  
1283 (KKKLRRQEAFDAL) to the C-terminus of mCherry via a (GGGGS)<sub>3</sub> linker. To

1284 construct pAAV, the mCherry-AIP2 sequences were inserted into the pAAV vector  
1285 with the *hSyn1* promoter, dendritic targeting element (DTE) of mouse *Map2* gene,  
1286 WPRE, and SV40 polyA sequences. The DTE of *Map2* were amplified and cloned  
1287 from C57BL/6N mouse genomic DNA <sup>73</sup>.

1288 pUCmini-iCAP-PHP.eB for PHP.eB production was a gift from Dr. Viviana  
1289 Gradinaru (Addgene plasmid # 103005).

1290

### 1291 **Animals and sleep phenotyping**

1292 All experimental procedures and housing conditions were approved by the  
1293 Institutional Animal Care and Use Committee of RIKEN Center for Biosystems  
1294 Dynamics Research and the University of Tokyo. All the animals were cared for and  
1295 treated humanely in accordance with the Institutional Guidelines for Experiments  
1296 using Animals. All mice had *ad libitum* access to food and water, and were  
1297 maintained at ambient temperature and humidity conditions under a 12 h light/dark  
1298 cycle. All C57BL/6N mice were purchased from CLEA Japan (Tokyo, Japan). The  
1299 mice used in each experiment were randomly chosen from colonies. EEG/EMG  
1300 recording for the *Camk2b* KO mice (**Figure 4-figure supplement 1**) were conducted  
1301 at the University of Tokyo. Other animal experiments were performed in the RIKEN  
1302 Center for Biosystems Dynamics Research.

1303

### 1304 **Mass spectrometry and western blotting of mice brain samples**

1305 C57BL/6N mice (CLEA Japan, Japan) were housed in a light-dark controlling rack  
1306 (Nippon Medical & Chemical instruments, Japan) and habituated to a 12 h light/dark  
1307 cycle for at least one week. At eight weeks old, half of the mice were subjected to  
1308 the sleep deprivation protocol from ZT0 to ZT6. The sleep deprivation was conducted

1309 by gentle handling and cage changing <sup>42</sup> at every 2 h. The other mice were housed  
1310 under *ad lib* sleep conditions. At ZT6, the mice were sacrificed by cervical dislocation  
1311 and their forebrain was immediately frozen in liquid nitrogen. The brain samples were  
1312 stored at  $-80^{\circ}\text{C}$ . The frozen brains were cryo-crushed with a Coolmil (Tokken, Japan)  
1313 pre-cooled in liquid nitrogen, and the brain powders were stored at  $-80^{\circ}\text{C}$ .

1314 The brain powders were then lysed and digested according to the phase-  
1315 transfer surfactant (PTS) method <sup>74</sup>. Approximately 10 mg of brain powder was  
1316 added to the 500  $\mu\text{l}$  of Solution B (12 mM sodium deoxycholate, 12 mM N-  
1317 lauroylsarcosine sodium salt, 50 mM ammonium hydrogen carbonate) containing  
1318 phosphatase inhibitors (1 mM sodium orthovanadate, 1 mM  $\beta$ -glycerophosphoric  
1319 acid disodium salt pentahydrate, 4 mM sodium (+)-tartrate dihydrate, 2.5 mM sodium  
1320 fluoride, 1.15 mM disodium molybdate (VI) dihydrate) pre-heated at  $98^{\circ}\text{C}$  and  
1321 sonicated extensively. After further incubation at  $98^{\circ}\text{C}$  for 30 min, the samples were  
1322 reduced with 10 mM dithiothreitol (FUJIFILM Wako Pure Chemical, Japan) at room  
1323 temperature for 30 min, and then alkylated with 100 mM iodoacetamide (Sigma-  
1324 Aldrich, U.S.A.) at room temperature for 30 min. The samples were then diluted to  
1325 five-fold by adding Solution A (50 mM ammonium hydrogen carbonate) and digested  
1326 them by adding 5  $\mu\text{g}$  of lysyl endopeptidase (Lys-C) (FUJIFILM Wako Pure Chemical,  
1327 Japan). After  $37^{\circ}\text{C}$  overnight incubation, 5  $\mu\text{g}$  of trypsin (Roche, Switzerland) was  
1328 added and the mixture was further incubated at  $37^{\circ}\text{C}$  overnight. After the digestion,  
1329 an equal volume of ethyl acetate was added to the sample, which was acidified with  
1330 0.5% TFA and well mixed to transfer the detergents to the organic phase. The sample  
1331 was then centrifuged at  $2,380 \times g$  for 15 min at room temperature, and an aqueous  
1332 phase containing peptides was collected and dried with a SpeedVac (Thermo Fisher  
1333 Scientific, U.S.A.).

1334           The dried peptides were solubilized in 1 mL of 2% acetonitrile and 0.1% TFA.  
1335 We prepared an internal control by mixing 500  $\mu$ L of each peptide solution. The  
1336 individual samples were the remaining 500  $\mu$ L of each peptide solution. The internal  
1337 control and individual samples were trapped and desalted on a Sep-Pak C18  
1338 cartridge (Waters, U.S.A.). Dimethyl-labeling was then applied to the peptides on the  
1339 cartridge as previously described <sup>75</sup>. Formaldehyde (CH<sub>2</sub>O, Nacalai Tesque, Japan)  
1340 and NaBH<sub>3</sub>CN (Sigma-Aldrich, U.S.A.) were added to the individual samples (light  
1341 label), and isotope-labeled formaldehyde (CD<sub>2</sub>O, Cambridge Isotope Laboratories,  
1342 U.S.A.) and NaBH<sub>3</sub>CN (Sigma-Aldrich, U.S.A.) were added to the internal control  
1343 mixture (medium label). The dimethyl-labeled peptides on the Sep-Pak cartridge  
1344 were eluted with an 80% acetonitrile and 0.1% TFA solution. Then, equal amount of  
1345 medium-labeled internal control mixture was added to each light-labeled individual  
1346 sample. This allowed us to compare the relative amount of peptides in the individual  
1347 samples with each other using the equally-added medium-labeled internal control  
1348 mixture as a standard.

1349           A one-hundredth of the mixture underwent LC-MS analysis to quantify the  
1350 amount of CaMKII $\alpha/\beta$  and total proteins. The remaining mixture was applied to High-  
1351 Select™ Fe-NTA Phosphopeptide Enrichment Kit (Thermo Fisher Scientific, U.S.A.)  
1352 to enrich the phosphorylated peptides following the manufacture's protocol.

1353           All analytical samples were dried with a SpeedVac (Thermo Fisher Scientific,  
1354 U.S.A.) and dissolved in 2% acetonitrile and 0.1% TFA. Mass-spectrometry-based  
1355 quantification of CaMKII $\alpha/\beta$ -derived peptides was carried out by selected reaction  
1356 monitoring (SRM) analysis using a TSQ Quantiva triple-stage quadrupole mass  
1357 spectrometer (Thermo Fisher Scientific, U.S.A.). The following parameters were  
1358 selected: positive mode, Q1 and Q3 resolutions of 0.7 full width of half maximum

1359 (FWHM), cycle time of 2 s, and gas pressure of 1.5 Torr. The mass spectrometer  
1360 was equipped with an UltiMate 3000 RSLCnano nano-high performance liquid  
1361 chromatography (HPLC) system (Thermo Fisher Scientific, U.S.A.), and a PepMap  
1362 HPLC trap column (C18, 5  $\mu$ m, 100 A; Thermo Fisher Scientific, U.S.A.) for loading  
1363 samples. Samples were separated by reverse-phase chromatography using a  
1364 PepMap rapid separation liquid chromatography (RSLC) EASY-Spray column (C18,  
1365 3  $\mu$ m, 100 A, 75  $\mu$ m x 15 cm; Thermo Fisher Scientific, U.S.A.) using mobile phases  
1366 A (0.1% formic acid/H<sub>2</sub>O) and B (0.1% formic acid and 100% acetonitrile) at a flow  
1367 rate of 300 nl/min (4% B for 5 min, 4%–35% B in 55 min, 35%–95% B in 1 min, 95%  
1368 B for 10 min, 95%–4% B in 0.1 min and 4% B for 9.9 min). The eluted material was  
1369 directly electro-sprayed into the MS. The SRM transitions of the target peptides were  
1370 determined based on the pre-analysis of several samples including mice brains,  
1371 293T cells expressing CaMKII $\beta$ , and synthesized peptides, and optimized using  
1372 Pinpoint software, version 1.3 (Thermo Fisher Scientific, U.S.A.). The Quan Browser  
1373 of the Quan Browser data system, version 3.0.63 (Thermo Fisher Scientific, U.S.A.)  
1374 was used for data processing and quantification.

1375 To estimate the relative amount of total peptides involved in each brain sample,  
1376 approximately half of the light/medium mixture sample without the enrichment of  
1377 phosphopeptides was analyzed by data-dependent MS/MS with a mass  
1378 spectrometer (Q-Exactive Mass Spectrometer, Thermo Fisher Scientific, U.S.A.)  
1379 equipped with an HPLC system containing nano HPLC equipment (Advance UHPLC,  
1380 Bruker Daltonics, U.S.A.) and an HTC-PAL autosampler (CTC Analytics,  
1381 Switzerland) with a trap column (0.3 x 5 mm, L-column, ODS, Chemicals Evaluation  
1382 and Research Institute, Japan). An analytical sample were loaded into the LC-MS  
1383 system to be separated by a gradient using mobile phases A (0.1% formic acid) and

1384 B (0.1% formic acid and 100% acetonitrile) at a flow rate 300 nL/min (4% to 32% B  
1385 in 190 min, 32% to 95% B in 1 min, 95% B for 2 min, 95% to 4% B in 1 min and 2%  
1386 B for 6 min) with a homemade capillary column (200 mm length, 100  $\mu$ m inner  
1387 diameter) packed with 2  $\mu$ m C18 resin (L-column2, Chemicals Evaluation and  
1388 Research Institute, Japan). The eluted peptides were then electrosprayed (1.8- 2.3  
1389 kV) and introduced into the MS equipment (positive ion mode, data-dependent  
1390 MS/MS). MS data were analyzed by Proteome Discoverer version 2.2 (Thermo  
1391 Fisher Scientific, U.S.A.) with the Swiss-Prot section of UniProtKB mouse database  
1392 (as of August 9<sup>th</sup>, 2018). The relative amount of CaMKII $\alpha$ / $\beta$  protein was normalized  
1393 to the median of all quantified proteins for each sample, with the effect derived from  
1394 different amounts of start materials being excluded.

1395 For the western-blotting analysis, brain powder was lysed in the 3x Laemmli  
1396 sample buffer (20% glycerol, 2.25% sodium dodecyl sulphate (SDS), 187.5 mM Tris-  
1397 HCl at pH 6.8, 0.015% bromophenol blue) pre-heated at 98 °C and sonicated  
1398 extensively. Approximately 0.1 mg of brain powder (~ 10  $\mu$ g protein) was subjected  
1399 to each lane of hand-made polyacrylamide gel. The samples were separated by  
1400 SDS-polyacrylamide gel electrophoresis and then transferred to a polyvinylidene  
1401 difluoride (PVDF) membrane (Hybond-P PVDF membranes, Merck, Germany) by a  
1402 wet-transfer apparatus (Vep-3, Thermo Fisher Scientific, U.S.A.). The membrane  
1403 was washed by TTBS (0.9% NaCl, 0.1% Tween-20, and 100 mM Tris-HCl at pH 7.5)  
1404 and non-specific protein binding was blocked by incubating with Blocking One  
1405 solution (Nacalai Tesque, Japan) for 1 hr at room temperature. FLAG-tagged protein  
1406 was detected by an anti-FLAG M2 antibody conjugated with horseradish peroxidase  
1407 (A8592, Sigma-Aldrich, U.S.A.). CaMKII $\beta$  and  $\alpha$ -Tubulin were detected by primary  
1408 antibodies anti-CaMK2 $\beta$  (#139800, Thermo Fisher Scientific, U.S.A.) or anti-alpha

1409 Tubulin [DM1A] (ab7291, Abcam), respectively, followed by the incubation with a  
1410 secondary antibody anti-mouse IgG HRP conjugate (W4021, Promega, U.S.A.). All  
1411 the primary antibodies were diluted 1/3000 in 10% Blocking One/TTBS (50 mM Tris,  
1412 0.5 M NaCl, 0.05% Tween-20, pH 7.4) and incubated with the membrane for  
1413 overnight at 4 °C. The secondary antibody was diluted 1/2000 in 10% Blocking  
1414 One/TTBS (50 mM Tris, 0.5 M NaCl, 0.05% Tween-20, pH 7.4) and incubated with  
1415 the membrane for 1 hr at room temperature. Immunoreactivities were detected with  
1416 Clarity Western ECL Substrate for Chemiluminescent Western Blot Detection (Bio-  
1417 rad, U.S.A.) and ChemiDoc XRS+ system (Bio-rad, U.S.A.).

1418

#### 1419 **Tissue clearing and LSFM imaging**

1420 AAV-administrated mice were perfusion-fixed under anesthesia, and brains were  
1421 isolated. Isolated brains were fixed overnight in 4% PFA and then washed with PBS.  
1422 For clearing the mouse brain, second-generation CUBIC protocols were used. The  
1423 detailed protocol can be found in a previous report <sup>76</sup>. For delipidation, the brain was  
1424 treated with CUBIC-L (10% (w/w) N-butyldiethanolamine and 10% (w/w) Triton X-  
1425 100) solution at 37°C for 5 days. For nuclear staining, the brain was rinsed with PBS  
1426 and incubated in 1:250 diluted RedDot2 (Biotium, 40061) in staining buffer (10%  
1427 (w/w) Triton X-100, 10% (w/w) Urea, 5% (w/w) *N,N,N',N'*-Tetrakis(2-  
1428 hydroxypropyl)ethylenediamine, 500mM NaCl) for 3 days at 37°C. The stained brain  
1429 sample was washed with PBS and then treated in CUBIC-R+ solution (45% (w/w)  
1430 antipyrine, 30% (w/w) nicotinamide, 0.5% (v/v) *N*-butyldiethanolamine) for 3 days at  
1431 25°C for RI matching. For whole-brain imaging, the cleared brain sample was  
1432 embedded in a CUBIC-R+ gel, which contains 2% (w/w) agarose in the CUBIC-R+  
1433 solution and set in a customized light-sheet microscopy (LSFM) <sup>76</sup>. Dual-colored



1434 images were simultaneously acquired with illumination objective lens (MVPLAPO 1×,  
1435 Olympus, Japan), 10× detection objective lens (XLPLN10XSVMP, Olympus, Japan),  
1436 Dichroic mirror (DMSP650L, Thorlabs, U.S.A.) and following laser and fluorescence  
1437 filters: RedDot2 [Ex: 594 nm, Em: 700 nm bandpass (FB700-40, Thorlabs, U.S.A.)],  
1438 mCherry [Ex: 594 nm, Em: 625 nm bandpass (ET625/30m, Chroma Technology,  
1439 U.S.A.)]. Stacked brain images were reconstructed and visualized by the Imaris  
1440 software (Bitplane).

1441

#### 1442 **CaMKII $\beta$ kinase assay**

1443 293T cells were grown in culture medium consisting of Dulbecco's Modified Eagle  
1444 Medium (DMEM) (high glucose, Thermo Fisher Scientific, U.S.A.), 10% FBS (Sigma-  
1445 Aldrich) and 100 U/ml penicillin-streptomycin (Thermo Fisher Scientific, U.S.A.) at  
1446 37°C with 5% CO<sub>2</sub>. The cells were plated at  $2 \times 10^4$  cells per well in 24-well plates  
1447 24 h before transfection. The cells in each well were transfected with 1.6  $\mu$ g PEI  
1448 (Polyethylenimine, Linear, MW 25000, Polysciences, U.S.A.) and 400 ng of pMU2-  
1449 *Camk2b* plasmids. 24 hr after the transfection, the medium in each well was replaced  
1450 with fresh culture medium. The cells were stayed for another 48 h, and collected by  
1451 removing all the culture medium. The remaining cells on the 24-well plate were  
1452 stored at -80 °C.

1453 The cells were lysed with 200  $\mu$ l of cell lysis buffer (50 mM HEPES-NaOH pH  
1454 7.6, 150 mM NaCl, 0.5 mM CaCl<sub>2</sub>, 1 mM MgCl<sub>2</sub>, and 0.25% (v/v) NP-40) containing  
1455 protease inhibitors (100 mM phenylmethanesulfonyl fluoride, 0.1 mM Aprotinin, 2  
1456 mM Leupeptin hemisulfate, 1 mM Pepstatin A, and 5 mM Bestatin). Followed by  
1457 extensive sonication, the cell lysates were collected and stored at -80 °C.

1458 The relative expression levels of CaMKII $\beta$  in each cell lysate was estimated

1459 by dot blot. A PVDF membrane (Hybond-P PVDF membranes, Merck, Germany)  
1460 was immersed in 100% methanol (Nacalai Tesque, Japan) and then soaked in water  
1461 for at least 10 min. Excess water was removed from the membrane, 2  $\mu$ l of four-fold  
1462 diluted cell lysate was spotted on the membrane. The membrane was then dried  
1463 completely, immersed in 100% Methanol and equilibrated in water. The membrane  
1464 was incubated in Blocking One solution (Nacalai Tesque, Japan) for 1 hr at room  
1465 temperature. After the blocking reaction, the membrane was incubated for 2 hr with  
1466 the primary antibody anti-CaMK2 $\beta$  (#139800, Thermo Fisher Scientific, U.S.A.)  
1467 diluted at 1/3000 in 10% Blocking One/TTBS (50 mM Tris, 0.5 M NaCl, 0.05%  
1468 Tween-20, pH 7.4). The membrane was washed with TTBS, and incubated for 1 h  
1469 with the secondary antibody anti-mouse IgG HRP conjugate (W4021, Promega,  
1470 U.S.A.) diluted at 1/3000 in 10% Blocking One/TTBS. Immunoreactivities of the  
1471 blotted proteins were detected with Clarity Western ECL Substrate for  
1472 Chemiluminescent Western Blot Detection (Bio-rad, U.S.A.) and ChemiDoc XRS+  
1473 system (Bio-rad, U.S.A.). The images were analyzed with Image Lab software  
1474 (version 6.01, Bio-rad, U.S.A.). For each dot-blot experiment, serial dilution of cell  
1475 lysate expressing the WT CaMKII $\beta$  was spotted to confirm that the quantification of  
1476 the dot blot signal was within the linear range of detection.

1477       The kinase activity of CaMKII $\beta$ -expressed cell lysate was calibrated as follows.  
1478 First, a serial dilution of cell lysate expressing WT CaMKII $\beta$  was prepared. Then 5  $\mu$ l  
1479 of each diluted cell lysate was mixed with 15  $\mu$ l of cell lysis buffer containing 0.33  
1480 mM ATP and 5  $\mu$ M ProfilerPro Kinase Peptide Substrate 11 5-FAM-KKLNRTLSVA-  
1481 COOH (PerkinElmer, U.S.A.) in the presence or absence of 0.66  $\mu$ M CaM (Sigma-  
1482 Aldrich, U.S.A.). After incubating at 37°C for 10 min, and the reaction was stopped  
1483 by incubating at 98°C for 10 min. 100  $\mu$ L of 2% ACN/0.1% TFA was added to the

1484 reaction mixture and the mixture was analyzed by mobility shift assay (LabChip EZ  
1485 Reader II; PerkinElmer, U.S.A.). The kinase activity is the percentage of  
1486 phosphorylated peptide signal over the total substrate peptide signal. Based on the  
1487 kinase activity obtained from the serial dilution of cell lysate, we determined two  
1488 critical dilution ratios. One is a dilution rate that gives the ~50% kinase activity in the  
1489 calibration curve in the presence of CaM (called “half-max dilution rate”). The other  
1490 dilution rate (called “background dilution rate”) is based on the calibration curve in  
1491 the absence of CaM, where most of the kinase activity should come from the  
1492 endogenous proteins in 293T cells. We determined the “background dilution rate” to  
1493 give the phosphorylation rate around 10% or less in the absence of CaM.

1494         With these two critical dilution rates, we normalized the relative expression  
1495 levels of each WT or mutant CaMKII $\beta$ . First, all the cell lysates were diluted to the  
1496 “background dilution rate” in a cell lysis buffer. We also prepared a lysate of the cells  
1497 treated with the PEI transfection procedure without vector plasmid (called PEI-  
1498 treated cell lysate) and diluted it to the same “background dilution rate.” Next, the  
1499 diluted cell lysate expressing the WT CaMKII $\beta$  was further diluted to reach the final  
1500 dilution rate (equivalent to the “half-max dilution rate”) by mixing with diluted PEI-  
1501 treated cell lysate. For the CaMKII $\beta$  mutants (except those with 25% or lower  
1502 expression levels compared to WT CaMKII $\beta$ ), the mixing ratio between CaMKII $\beta$ -  
1503 expressed lysate and PEI-treated lysate were adjusted based on the relative  
1504 expression level of CaMKII $\beta$  mutants quantified by dot blot. Through these  
1505 processes, we obtained a series of diluted cell lysates with the same background  
1506 kinase activity level and the same relative expression levels of WT or mutant  
1507 CaMKII $\beta$ . The kinase activity of WT CaMKII $\beta$  is expected to be around 50%.

1508         The quantification of kinase activity was carried out by mixing 5  $\mu$ l of cell

1509 lysates (diluted as described above) and 15  $\mu$ l of cell lysis buffer containing 0.33 mM  
1510 (**Figure 1-figure supplement 3**) or 3.3 mM (**Figure 5-figure supplement 1 and 8**)  
1511 ATP and 5  $\mu$ M ProfilerPro Kinase Peptide Substrate 11 5-FAM-KKLNRTLVA-  
1512 COOH (PerkinElmer, U.S.A.), in the presence or absence of 0.66  $\mu$ M CaM (Sigma-  
1513 Aldrich, U.S.A.). FAM-labeled autocalmitide-2 5-FAM-KKALRRQETVDAL-COOH,  
1514 synthesized with a peptide synthesizer Syro Wave (Biotage, Sweden) using Fmoc  
1515 solid-phase chemistry, was used in the experiment shown in Figure 6j. After  
1516 incubating at 37°C for 10 min, and the reaction was stopped by incubating at 98°C  
1517 for 10 min. 100  $\mu$ L of 2% ACN/0.1% TFA was added to the reaction mixture and the  
1518 mixture was analyzed by mobility shift assay (LabChip EZ Reader II and operation  
1519 software version 2.2.126.0; PerkinElmer, U.S.A.).

1520

#### 1521 **Mass spectrometry of purified CaMKII $\beta$**

1522 The spike peptides were synthesized with a peptide synthesizer Syro Wave (Biotage,  
1523 Sweden) using Fmoc solid-phase chemistry. The synthesized peptides were treated  
1524 with dithiothreitol and iodoacetamide as described above. The peptides were  
1525 desalted by using hand-made C18 StageTips<sup>77</sup>. The desalted peptides on the  
1526 StageTips were subjected to dimethyl-labeling with isotope-labeled formaldehyde  
1527 (<sup>13</sup>CD<sub>2</sub>O, ISOTECH, U.S.A.) and NaBD<sub>3</sub>CN (Cambridge Isotope Laboratories, U.S.A.)  
1528 (heavy label) as described previously<sup>75</sup>. The dimethyl-labeled spike peptides were  
1529 eluted with an 80% acetonitrile and 0.1% TFA solution, and dried with a SpeedVac  
1530 (Thermo Fisher Scientific, U.S.A.).

1531 For the time course sampling for autophosphorylation detection, one  
1532 timepoint sample contains 0.3  $\mu$ M purified GST-CaMKII $\beta$  protein (Carna Biosciences,  
1533 Japan), 50 mM HEPES-NaOH pH 7.6, 150 mM NaCl, 1 mM MgCl<sub>2</sub>, 0.25% (v/v) NP-

1534 40 and 2.5 mM ATP. The sample without CaM was sampled and used as “0 min”  
1535 time point. Then, 0.5 mM CaCl<sub>2</sub> and 10 mM EGTA were added to the indicated  
1536 conditions shown in Figure 7a. The kinase reaction was initiated by adding 0.5 μM  
1537 CaM to each sample. During the time course sampling, 10 mM EGTA was added for  
1538 the condition named “0.5 mM Ca<sup>2+</sup>, 10 mM EGTA at 5 min (Condition #4)”. Note that  
1539 for the quantification of S182 phosphorylation, 10-fold higher concentration of  
1540 purified GST-CaMKIIβ and CaM were used because of the low signal sensitivity of  
1541 the corresponding phosphorylated peptide.

1542         The kinase reaction was terminated by adding an equal volume of Solution B  
1543 and incubating at 98 °C for 30 min. The samples were reduced, alkylated, and  
1544 digested by proteases according to the PTS method <sup>74</sup> as described above except  
1545 that 1 μg of Lys-C and 1 μg of trypsin were used for most of the samples, and 1 μg  
1546 of Lys-C and 1 μg of Glu-C (Promega, U.S.A.) were used for the sample for  
1547 quantifying S182 phosphorylation.

1548         The dried peptides were solubilized in 1 mL of a 2% acetonitrile and 0.1% TFA  
1549 solution, and trapped on C18 StageTips <sup>77</sup>. The trapped peptides were subjected to  
1550 dimethyl-labeling with formaldehyde (light label) as described above. An additional  
1551 GST-CaMKIIβ sample independent from the time course sampling were prepared as  
1552 an internal control reference, and subjected to dimethyl-labeling with CD<sub>2</sub>O (medium  
1553 label). The dimethyl-labeled peptides on the tip were eluted with an 80% acetonitrile  
1554 and 0.1% TFA solution. Then, 1/30 volume of the light-labeled samples were isolated  
1555 and mixed with equal amounts of medium label peptides. This allowed us to compare  
1556 the relative amount of GST-CaMKIIβ in the individual time course samples with each  
1557 other using the medium-labeled internal control.

1558         The remainder of the light-labeled samples were mixed with the mixture of

1559 heavy labeled spike peptides and applied to High-Select™ Fe-NTA Phosphopeptide  
1560 Enrichment Kit (Thermo fisher Scientific, U.S.A.) to enrich the phosphorylated  
1561 peptides. This allowed us to compare the relative amount of phosphorylated peptides  
1562 in the individual time course samples with each other using the heavy labeled spike  
1563 peptides.

1564 All analytical samples were dried with a SpeedVac (Thermo Fisher Scientific,  
1565 U.S.A.) and dissolved in a 2% acetonitrile and 0.1% TFA solution. Mass-  
1566 spectrometry-based quantification was carried out by SRM analysis using a TSQ  
1567 Quantiva triple-stage quadrupole mass spectrometer (Thermo Fisher Scientific,  
1568 U.S.A.) as described above. The amount of each phosphorylated peptide was  
1569 normalized to the amount of total GST-CaMKII $\beta$  quantified using the average  
1570 amounts of several non-phosphorylated peptides.

1571

#### 1572 **Production of *Camk2b* KO mice**

1573 *Camk2b* KO mice were generated using the Triple-target CRISPR method described  
1574 previously <sup>24</sup>. C57BL/6N females (4–6 weeks old, CLEA Japan, Japan) were  
1575 superovulated and mated with C57BL/6N males (CLEA Japan, Japan). The fertilized  
1576 eggs were collected from the ampulla of the oviduct of plugged C57BL/6N females  
1577 by micro-dissection and kept in KSOM medium (Merck, Germany or ARK Resource,  
1578 Japan) in a 5% CO<sub>2</sub> incubator at 37°C. The design of gRNAs for *Camk2b* was  
1579 previously shown as set 1 in a previous study <sup>10</sup>. In the previous study, an  
1580 independent set of gRNA called set 2 was also tested. A significant decrease in the  
1581 sleep duration was observed both in set 1 and set 2 gRNA-injected mice, suggesting  
1582 that at least a major part of sleep phenotype is not due to the off-target effect of  
1583 injected gRNAs <sup>10</sup>. The synthesized gRNAs for *Camk2b* (150 ng/ $\mu$ l in total) and *Cas9*

1584 mRNA (100 ng/μl) were co-injected into the cytoplasm of fertilized eggs in M2  
1585 medium (Merck, Germany or ARK Resource, Japan) at room temperature. After  
1586 microinjection, the embryos were cultured for 1 h in KSOM medium (Merck, Germany,  
1587 or ARK Resource, Japan) in a 5% CO<sub>2</sub> incubator at 37°C. 15–30 embryos were then  
1588 transferred to the oviducts of pseudopregnant female ICR mice.

1589 Genotyping of KO mice was conducted with the same protocol described  
1590 previously<sup>24</sup>. qPCR was performed using genomic DNA purified from tails of WT and  
1591 KO mice and primers which were annealed to the target sequences. The target site  
1592 abundance was calculated using a standard curve obtained from wild-type genomic  
1593 DNA. The amount of *Tbp*<sup>78</sup> was quantified with a pair of primers (5'-  
1594 CCCCTCTGCACTGAAATCA-3'; 5'-GTAGCAGCACAGAGCAAGCAA-3') and  
1595 used as an internal control. When the amplified intact DNA by qPCR is less than 0.5%  
1596 of wild-type genome, we judged that the target DNA is not detectable. When any of  
1597 three targets was not detected, we classified the animal as a KO. When we could  
1598 not confirm KO genotype by the qPCR, we performed 2nd qPCR using the  
1599 alternative primer which was independent of 1st qPCR. In the case of *Camk2b* set 1  
1600 KO, first and second targets of triple CRISPR gRNA were judged as not detectable  
1601 by 2nd qPCR. The result of qPCR is shown in **Figure 4-figure supplement 1d** and  
1602 the primer list used for the qPCR is shown below.

1603

1604 1st qPCR primer pairs:

1605 *Camk2b* set 1, target #1

1606 Forward: 5'-CCACAGGGGTGATCCTGTATATCCTGC-3'

1607 Reverse: 5'-CTGCTGGTACAGCTTGTGTTGGTCCTC-3'

1608 *Camk2b* set 1, target #2



1609 Forward: 5'- GGAAAATCTGTGACCCAGGCCTGAC-3'

1610 Reverse: 5'- TCTGTGGAAATCCATCCCTTCGACC-3'

1611 *Camk2b* set 1, target #3

1612 Forward: 5'- GAACCCGCACGTGCACGTCATTGGC-3'

1613 Reverse: 5'- CCCTGGCCATCGATGTACTGTGTG-3'

1614

1615 2nd qPCR primer pairs:

1616 *Camk2b* set 1, target #1

1617 Forward: 5'- CAGAAAGGTGGGTAGCCCACCAGCAGG-3'

1618 Reverse: 5'- CTATGCTGCTCACCTCCCCATCCACAG-3'

1619 *Camk2b* set 1, target #2

1620 Forward: 5'- GCCTGAAGCTCTGGGCAACCTGGTTCG-3'

1621 Reverse: 5'- CCACCCCAGCCTTTTCACTCACGGTTCTC-3'

1622 *Camk2b* set 1, target #3

1623 Forward: 5'- GCATCGCCTACATCCGCCTCACAC-3'

1624 Reverse: 5'- CGGTGCCACACACGGGTCTCTTCGGAC-3'

1625

1626 **Production of *Camk2b*<sup>FLAG/FLAG</sup> mice**

1627 FLAG-tag sequence was inserted into the endogenous *Camk2b* locus (prior to the  
1628 stop codon) by single-stranded oligodeoxynucleotide (ssODN) and CRISPR/Cas9-  
1629 mediated knock-in. The gRNA target sequence and a donor sequence were selected  
1630 according to previous study <sup>79</sup>. Preparation of gRNA and Cas9, and general  
1631 procedures for obtaining the genetically modified mouse were conducted according  
1632 to previous study <sup>10</sup>. Following primer sequences were used to produce gRNA  
1633 targeting the *Camk2b* locus.



1634 *Camk2b*-FLAG gRNA primer forward #1

1635 5'-CACTATAGGCAGTGGCCCCGCTGCAGTGGTTTTAGAGCTAGAAATAGC -3'

1636 *Camk2b*-FLAG gRNA primer forward #2

1637 5'-GGGCCTAATACGACTCACTATAGGCAGTGGCCCCGCTGCAGTGG -3'

1638 *Camk2b*-FLAG gRNA primer reverse #1

1639 5'-AAAAGCACCGACTCGGTGCC -3'

1640 A donor ssODN (*sequence*) was synthesized by Integrated DNA Technologies.

1641 *Camk2b*-FLAG ssODN (capital letter: FLAG tag sequence)

1642 5'-aagagaccgctgtgtggcaccgccgacgcaagtggcagaatgtacatttccactgctcgggcgct

1643 ccagtggccccgctgcagGACTACAAGGACGACGATGACAAGtgaggtgagtcacctgcggt

1644 gtgcgtagggcagtgccgcatgctgtggacagtgacgctgcatgggggtgtggcccagtgacgctgc -3'

1645 1~2 pL of RNase free water (Nacalai Tesque Inc.) containing 100 ng/μl gRNA, 100

1646 ng/μl Cas9 mRNA and 100 ng/μl ssODN was injected into the cytoplasm of fertilized

1647 eggs in M2 medium (Merck, Germany or ARK Resource, Japan) at room

1648 temperature. After microinjection, the embryos were cultured for 1 h in KSOM

1649 medium (Merck, Germany, or ARK Resource, Japan) in a 5% CO<sub>2</sub> incubator at 37°C.

1650 15–30 embryos were then transferred to the oviducts of pseudopregnant female ICR

1651 mice.

1652 Genomic DNA of F<sub>0</sub> mice tails was extracted with NucleoSpin Tissue kit

1653 (Takara Bio, Japan) according to the manufacturer's protocol. The genotyping PCR

1654 was conducted by using following primer pairs to select heterozygous or

1655 homozygous FLAG knock-in offspring. Genotyping was based on the size and direct

1656 sequencing of the PCR amplicon. The obtained heterozygous or homozygous FLAG

1657 knock-in F<sub>0</sub> mice were crossed with wildtype C57BL/6N mice to obtain heterozygous

1658 FLAG knock-in F<sub>1</sub> mice.

1659

1660 *Camk2b*-FLAG genotyping primer pairs:

1661 Pair #1

1662 Forward: 5'- ACGACCAACTCCATTGCTGAC -3'

1663 Reverse: 5'- CTACATCCGCCTCACACAGTACATC -3'

1664 Pair #2

1665 Forward: 5'- ACGACCAACTCCATTGCTGAC -3'

1666 Reverse: 5'- GACTACAAGGACGACGATGACAAG -3'

1667 Pair #3

1668 Forward: 5'- CTTGTCATCGTCGTCCTTGTAGTC -3'

1669 Reverse: 5'- CTACATCCGCCTCACACAGTACATC -3'

1670

### 1671 **Sleep measurement with the SSS**

1672 The SSS system enables fully automated and noninvasive sleep/wake phenotyping

1673 <sup>24</sup>. The SSS recording and analysis were carried out according to the protocol

1674 described previously <sup>24</sup>. The light condition of the SSS rack was set to light/dark (12

1675 h periods) or constant dark. Mice had *ad libidum* access to food and water. In the

1676 normal measurement, eight-week-old mice were placed in the SSS chambers for

1677 one to two weeks for sleep recordings. For data analysis, we excluded the first day

1678 and used six days of measurement data. For the *Cry1/2* DKO and *Per1/2* DKO

1679 mutant mice, recordings were performed under light/dark conditions for two weeks

1680 followed by constant dark conditions for two weeks. For data analysis, we excluded

1681 the first day and used four days of measurement data under each light condition.

1682 Sleep staging was performed in every 8-second epoch.

1683 Sleep parameters, such as sleep duration,  $P_{WS}$ , and  $P_{SW}$  were defined

1684 previously<sup>24</sup>. In the SSS, sleep staging was performed every 8 seconds, which is  
1685 the smallest unit called “epoch”. When we focus on two consecutive epochs, there  
1686 are four combinations: keeping awake state (wake to wake), keeping sleep state  
1687 (sleep to sleep), transition from wakefulness to sleep (wake to sleep), and transition  
1688 from sleep to wakefulness (sleep to wake). Transition probabilities were calculated  
1689 from all two consecutive epochs in the measurement period. The definition of  
1690 transition probabilities are as follows:  $P_{WS}$  (transition probability from wake to sleep)  
1691 is defined as  $P_{WS} = N_{WS} / (N_{WS} + N_{WW})$ , and  $P_{SW}$  (transition probability from sleep to  
1692 wake) is defined as  $P_{SW} = N_{SW} / (N_{SW} + N_{SS})$ , where  $N_{mn}$  is the number of transitions  
1693 from state  $m$  to  $n$  ( $m, n \in \{\text{sleep, awake}\}$ ) in the observed period. The balance  
1694 between  $P_{WS}$  and  $P_{SW}$  determines the total sleep time, i.e., mice with longer sleep  
1695 time tend to have increased  $P_{WS}$  and/or decreased  $P_{SW}$ .  $P_{WS}$  and  $P_{SW}$  are  
1696 independent of each other, and it can be deduced from the definition that  $P_{WS} + P_{WW}$   
1697 = 1 and  $P_{SW} + P_{SS} = 1$ . The sleep episode duration is the average of the time spent  
1698 in each consecutive sleep phase during the observed period.

1699

### 1700 **Sleep measurement with EEG/EMG recording**

1701 For EEG/EMG recording, AAV-administrated six-week-old C57BL/6N mice were  
1702 used for surgery. For the recording of *Camk2b* KO mice, 16-17-week-old *Camk2b*  
1703 KO mice and WT control mice at the same age were used for surgery. Wired and  
1704 wireless recording method are used in parallel for EEG/EMG measurements, and  
1705 we have confirmed that these two methods give qualitatively comparable results.

1706 For wireless recordings, anesthetized mice were implanted a telemetry  
1707 transmitter (DSI, U.S.A). As EEG electrodes, two stainless steel screws were  
1708 connected with lines from the transmitter and embedded in the skull of the cortex  
1709 (anteroposterior, +1.0 mm; right, +1.5 mm from bregma or lambda). As EMG  
1710 electrodes, two lines from the transmitter were placed in the trapezius muscles. After

1711 the surgery, the mice were allowed to recover for at least ten days. EEGs and EMGs  
1712 were recoded wirelessly. The mice had access to food and water. The sampling rate  
1713 was 100 Hz for both EEG and EMG. The detailed methods were described  
1714 previously<sup>80</sup>.

1715 For wired recordings, mice were implanted with EEG and EMG electrodes for  
1716 polysomnographic recordings. To monitor EEG signals, two stainless steel EEG  
1717 recording screws with 1.0 mm in diameter and 2.0 mm in length were implanted on  
1718 the skull of the cortex (anterior, +1.0 mm; right, +1.5 mm from bregma or lambda).  
1719 EMG activity was monitored through stainless steel, Teflon-coated wires with 0.33  
1720 mm in diameter (AS633, Cooner Wire, California, U.S.A) placed into the trapezius  
1721 muscle. The EEG and EMG wires were soldered to miniature connector with four  
1722 pins in 2 mm pitch (Hirose Electric, Japan). Finally, the electrode assembly was fixed  
1723 to the skull with dental cement (Unifast III, GC Corporation, Japan). After 10 days of  
1724 recovery, the mice were placed in experimental cages with a connection of spring  
1725 supported recording leads. The EEG/EMG signals were amplified (Biotex, Japan),  
1726 filtered (EEG, 0.5–60 Hz; EMG, 5–128 Hz), digitized at a sampling rate of 128 Hz,  
1727 and recorded using VitalRecorder software (KISSEI Comtec, Japan).

1728 For the sleep staging, we used the FASTER method<sup>80</sup> with some  
1729 modifications to automatically annotate EEG and EMG data. 24 h of recording data  
1730 were used for the analysis. Sleep staging was performed every 8-second epoch.  
1731 Finally, the annotations were manually checked.

1732 The power spectrum density was calculated for each epoch by fast Fourier  
1733 transformation (FFT) with Welch's averaging method. Briefly, each 8 s segment was  
1734 further divided into eight overlapping sequences. The overlapping length was 50%  
1735 of each sequence. The Hamming window was applied onto the sequences before

1736 the FFT and the obtained spectrum was averaged over the eight sequences. The  
1737 dirty segments were excluded from the subsequent processes<sup>80</sup>. The power  
1738 spectrum of each behavioral state (Wake, NREM, REM) was calculated by  
1739 averaging the power spectra (1-50 Hz) of segments within each state over the  
1740 observation period. The calculated power spectra were normalized by the total power.  
1741 The power density in typical frequency domains were calculated as the summation  
1742 of the powers in each frequency domain (slow, 0.5-1 Hz; delta, 0.5-4 Hz; theta, 6-10  
1743 Hz).

1744 Transition probabilities between wakefulness, NREM sleep, and REM sleep  
1745 were calculated same as previously reported<sup>81</sup>. For example,  $P_{NW} = N_{NW} / (N_{NW}$   
1746  $+ N_{NR} + N_{NN})$ , where  $N_{mn}$  is the number of transitions from state  $m$  to  $n$  ( $m, n \in \{\text{wake,}$   
1747  $\text{NREM sleep, REM sleep}\}$ ) in the observed period.

1748

#### 1749 **Cage change experiment**

1750 For cage change experiment (**Figure 2-figure supplement 1**), AAV-administrated  
1751 mice (9-week-old) were placed in the SSS chambers and habituated to the  
1752 environment for three days. On the fourth day, the SSS chamber was replaced with  
1753 a new one at ZT0. The sleep data of the fourth day was analyzed. The data of the  
1754 first three days were used for baseline calculation.

1755

#### 1756 **ES-mice production**

1757 Genetically modified mice were produced using the previously reported ES-mouse  
1758 method, which allows us to analyze the behavior of F0 generation mice without  
1759 crossing<sup>82,83</sup>. Mouse ES cells (ESCs) were established from blastocysts in 3i  
1760 medium culture conditions as described previously<sup>84</sup>. Mouse strains used for the

1761 ESC establishment were as follows: *Cry1<sup>-/-</sup>:Cry2<sup>-/-</sup>*, *Cry1<sup>-/-</sup>:Cry2<sup>-/-</sup>* mouse <sup>38</sup>; *Per1<sup>-/-</sup>*  
1762 *:Per2<sup>-/-</sup>*, *Per1<sup>-/-</sup>:Per2<sup>-/-</sup>* mouse <sup>40</sup>; *Vglut2-Cre*, heterozygous *Slc17a6<sup>tm2(cre)Lowl/J</sup>*/  
1763 mouse (The Jackson Laboratory, JAX stock #016963) <sup>85</sup>; *Gad2-Cre*, heterozygous  
1764 *Gad2<sup>tm2(cre)Zjh/J</sup>* mouse (The Jackson Laboratory, JAX stock #010802) <sup>86</sup>.

1765 Male ESCs were cultured as described previously <sup>82,83</sup>. Before cultivation,  
1766 PURECoat™ amine dishes (Beckton-Dickinson, NJ, U.S.A.) was treated with a  
1767 medium containing LIF plus 6-bromoindirubin-30-oxime (BIO) <sup>87</sup> for more than 5 h at  
1768 37°C with 5% CO<sub>2</sub>. ESCs were seeded at 1 × 10<sup>5</sup> cells per well and maintained at  
1769 37°C in 5% CO<sub>2</sub> under humidified conditions with a 3i culture medium (Y40010,  
1770 Takara Bio, Japan) without feeder cells. The expanded ESCs were collected by  
1771 adding 0.25% trypsin-EDTA solution and prepared as a cell suspension. 10–30  
1772 ESCs were injected into each ICR (CLEA Japan, Japan) 8-cell-stage embryo and  
1773 the embryos were transferred into the uterus of pseudopregnant ICR female mice  
1774 (SLC, Japan). We determined the contribution of the ESCs in an obtained ES-mouse  
1775 by its coat color following a previously reported protocol <sup>82,83</sup>. The ES mice  
1776 uncontaminated with ICR-derived cells were used for the experiment.

1777

## 1778 **AAV production**

1779 The protocol for AAV production was based on the previously reported protocol <sup>88</sup>  
1780 with some modifications. AAV pro 293T (Takara Bio, Japan) was cultured in 150 mm  
1781 dishes (Corning, USA) in a culture medium containing DMEM (high glucose)  
1782 (Thermo Fisher Scientific, U.S.A.), 10% (v/v) FBS, and penicillin-streptomycin  
1783 (Thermo Fisher Scientific, U.S.A.) at 37°C in 5% CO<sub>2</sub> under humidified conditions.  
1784 pAAV, pUCmini-iCAP-PHPeB and pHelper plasmid (Agilent, U.S.A.) were  
1785 transfected into cells at 80%–90% confluency using polyethyleneimine

1786 (Polysciences, U.S.A.). We employed a pAAV: pUCmini-iCAP-PHPeB: pHelper  
1787 plasmid ratio of 1:4:2 based on micrograms of DNA (e.g. 5.7  $\mu\text{g}$  of pAAV, 22.8  $\mu\text{g}$  of  
1788 pUCmini-iCAP-PHP, and 11.4  $\mu\text{g}$  of pHelper). On the day following the transfection,  
1789 the culture medium was replaced with 20 ml of a culture medium containing DMEM  
1790 (high glucose, Glutamax) (Thermo Fisher Scientific, U.S.A.), 2% (v/v) FBS, MEM  
1791 Non-Essential Amino Acids solution (NEAA) (Thermo Fisher Scientific, U.S.A.), and  
1792 penicillin-streptomycin. On the third day following the transfection, the culture  
1793 medium was collected and replaced with 20 ml of new culture medium containing  
1794 DMEM (high glucose, Glutamax), 2% (v/v) FBS, MEM NEAA, and penicillin-  
1795 streptomycin. The collected culture medium was stored at 4°C. On the fifth day  
1796 following the transfection, the cells and the culture medium were collected and  
1797 combined with the stored medium. The suspension was separated into supernatant  
1798 and cell pellet by centrifugation (2000  $\times$  g, 20min). From the supernatant, AAVs were  
1799 concentrated by adding polyethylene glycol at a final concentration of 8% followed  
1800 by centrifugation. From the cells, AAVs were extracted in a Tris-MgCl<sub>2</sub> buffer (10 mM  
1801 Tris pH 8.0, 2 mM MgCl<sub>2</sub>) by repetitive freeze-thaw cycles. The obtained extract  
1802 containing AAV was treated with Benzonase (100 U/ml) in a Tris-MgCl<sub>2</sub> buffer, and  
1803 then AAVs were purified by ultracentrifugation at 350,000  $\times$  g for 2 h 25 min (himac  
1804 CP80WX and P70AT rotor, HITACHI, Japan) with Iodixanol density gradient  
1805 solutions (15%, 25%, 40%, and 60% (wt/vol)). Viral particles were contained in a 40%  
1806 solution, and this solution was ultrafiltered with an Amicon Ultra-15 device (100 kDa,  
1807 Merck, Germany) to obtain the AAV stock solution for administration to mice.

1808 To determine the AAV titer, virus solution was treated with Benzonase (50  
1809 U/ml, 37°C, 1 h) followed by Proteinase K (0.25 mg/ul, 37°C, 1 h). Subsequently, the  
1810 viral genome was obtained by phenol-chloroform-isoamyl alcohol extraction followed

1811 by isopropanol precipitation. The AAV titer (vg/ml) was calculated by quantifying the  
1812 number of WPRE sequences in the sample by qPCR using plasmid as a standard.  
1813 The qPCR protocol was 60 s at 95°C for preheating (initial denaturation) and 45  
1814 cycles from 10 s at 95°C to 30 s at 60°C using TB Green *Premix Ex Taq*<sup>TM</sup> GC  
1815 (Takara Bio, Japan).

1816

### 1817 **Retro orbital injection of AAV to mice**

1818 Six-week-old male mice were anesthetized with 2%–4% isoflurane and injected with  
1819 100 µl of AAV in their retro orbital sinus. **Table 1** summarizes the AAVs used in this  
1820 study and their administration conditions. The AAV-administrated mice were  
1821 subjected to sleep phenotyping at eight-week-old.

1822

### 1823 **Estimation of transduction efficiency**

1824 Transduction efficiency was estimated based on previous reports <sup>89,90</sup>. After the  
1825 sleep phenotyping, the brain hemisphere except for the olfactory bulb and  
1826 cerebellum was collected from the AAV administrated mouse. Brain DNA was  
1827 purified using an Agencourt DNAdvance (BECKMAN COULTER, U.S.A.). The copy  
1828 numbers of both the AAV vector genomes and mouse genomic DNA were quantified  
1829 with a standard curve generated from known amounts of DNA. Vector genomes per  
1830 cell were calculated by dividing the copy number of AAV vector genomes by diploid  
1831 copies of the *Tbp* gene in the sample. The copy number of the AAV vector genomes  
1832 and the *Tbp* gene were determined with WPRE-binding primers (5'-  
1833 CTGTTGGGCACTGACAATTC-3', 5'-GAAGGGACGTAGCAGAAGGA-3') and *Tbp*-  
1834 binding primers (5'-CCCCCTCTGCACTGAAATCA-3'; 5'-  
1835 GTAGCAGCACAGAGCAAGCAA-3') <sup>78</sup>, respectively. The qPCR protocol was 60 s



1836 at 95°C for preheating (initial denaturation) and 45 cycles from 10 s at 95°C to 30 s  
1837 at 60°C using a TB Green *Premix Ex Taq*<sup>TM</sup> GC (Takara Bio, Japan).

1838

### 1839 **Clustering analysis**

1840 The character of each mutant was extracted by principal component analysis using  
1841 the values of  $P_{WS}$  and  $P_{SW}$ . The first and second principal components were used for  
1842 hierarchical clustering using Ward's algorithm. The threshold was set to 40% of the  
1843 distance between the farthest clusters (**Figure 6-figure supplement 1a**). The  
1844 principal component analysis and clustering were performed using Python 3.8.0 with  
1845 the numpy 1.18.5, scikit-learn 0.23.1 and scipy 1.5.0 libraries.

1846

### 1847 **Statistics**

1848 No statistical method was used to predetermine the sample size. The sample sizes  
1849 were determined based on previous experiences and reports. Experiments were  
1850 repeated at least two times with the independent sets of the animals or  
1851 independently prepared cell lysates. The series of single/double phosphomimetic  
1852 screening was not repeated, but the mutants we focused on from the screening  
1853 results were further analyzed in detail through additional independent experiments.  
1854 In the sleep analysis, individuals with abnormal measurement signals or weakened  
1855 individuals were excluded from the sleep data analyses because of their difficulties  
1856 in accurate sleep phenotyping.

1857 Statistical analyses were performed by Microsoft Excel and R version 3.5.2.  
1858 Statistical tests were performed by two-sided. To compare two unpaired samples,  
1859 the normality was tested using the Shapiro test at a significance level of 0.05. When  
1860 the normality was not rejected in both groups, the homogeneity of variance was

1861 tested using the *F*-test at a significance level of 0.05. When the null hypothesis of a  
1862 normal distribution with equal variance for the two groups was not rejected, a  
1863 Student's *t*-test was used. When the normality was not rejected but the null  
1864 hypothesis of equal variance was rejected, a Welch's *t*-test was used. Otherwise, a  
1865 two-sample Wilcoxon test was applied.

1866 To compare more than two samples against an identical sample, the normality  
1867 was tested with the Kolmogorov-Smirnov test at a significance level of 0.05. When  
1868 the normality was not rejected in all groups, the homogeneity of variance was tested  
1869 with Bartlett's test at a significance level of 0.05. When the null hypothesis of a  
1870 normal distribution with equal variance was not rejected for all groups, Dunnett's test  
1871 was used. Otherwise, Steel's test was applied.

1872 For multiple comparisons between each group, the Tukey-Kramer test was  
1873 used when the null hypothesis of a normal distribution with equal variance was not  
1874 rejected for all groups. Otherwise, Steel-Dwass test was applied.

1875 In this study,  $p < 0.05$  was considered significant ( $*p < 0.05$ ,  $**p < 0.01$ ,  $***p <$   
1876  $0.001$ , and n.s. for not significant). **Figure 8** summarizes the workflow for selecting  
1877 statistical method and the statistical analyses used in each experiment of this study  
1878 and *P* values.

1879  
1880

## 1881 **ACKNOWLEDGMENTS**

1882

1883 We thank all the lab members at RIKEN Center for Biosystems Dynamics Research  
1884 (BDR) and the University of Tokyo, in particular, Masazumi Tanaka, Jun-ichi Kuroda,  
1885 and Ayaka Saito for technical assistance of the biochemical analysis; Etsuo A.  
1886 Susaki, Rurika Itofusa, Takeyuki Miyawaki, Chika Shimizu and Kimiko Itayama for  
1887 AAV preparation; Masako Kunimi and Ruriko Inoue, Sachiko Tomita, for help with  
1888 sleep phenotyping; Yumika Sugihara, Natsumi Hori, Eriko Matsushita, and Yuichi  
1889 Uranyu for animal experiment. We also thank members at LARGE, RIKEN BDR for  
1890 help with ES-mouse production; Chiaki Masuda for kind instructions on AAV  
1891 production; Hirokazu Hirai for providing pAAV plasmid and helpful suggestions on  
1892 the experiment.

1893

1894 This work was supported by grants from the Brain/MINDS JP20dm0207049, Science  
1895 and Technology Platform Program for Advanced Biological Medicine  
1896 JP21am0401011, AMED-CREST 18gm0610006h0006 (AMED/MEXT) (H.R.U.),  
1897 Grant-in-Aid for Scientific Research (S) JP25221004 (JSPS KAKENHI) (H.R.U.) and  
1898 Scientific Research (C) JP20K06576 (JSPS KAKENHI) (K.L.O.), Grant-in-Aid for  
1899 Early-Career Scientists JP19K16115 (JSPS KAKENHI) (D.T.), HFSP Research  
1900 Grant Program RGP0019/2018 (HFSP) (H.R.U.), ERATO JPMJER2001 (JST)  
1901 (H.R.U.) and an intramural Grant-in-Aid from the RIKEN BDR (H.R.U.). The authors  
1902 would like to thank Enago ([www.enago.jp](http://www.enago.jp)) for the English language review.

1903

1904 **COMPETING INTERESTS**

1905 H.R.U conducted a collaborative research project with Thermo Fisher Scientific Inc.

1906 Y.N. is an employee of Thermo Fisher Scientific, Inc. The company provided support

1907 in the form of salary for Y.N., and technical advice on the setup of mass

1908 spectrometers. However, the company did not have any additional role in the study

1909 design, data collection and analysis, decision to publish, or preparation of the

1910 manuscript.

1911

1912

## 1913 REFERENCES

1914

- 1915 1 Partch, C. L. Orchestration of Circadian Timing by Macromolecular Protein  
1916 Assemblies. *J Mol Biol*, (2020).
- 1917 2 Ode, K. L. & Ueda, H. R. Design Principles of Phosphorylation-Dependent  
1918 Timekeeping in Eukaryotic Circadian Clocks. *Cold Spring Harb Perspect Biol*  
1919 **10**, (2018).
- 1920 3 Millius, A., Ode, K. L. & Ueda, H. R. A period without PER: understanding 24-  
1921 hour rhythms without classic transcription and translation feedback loops.  
1922 *F1000Res* **8**, (2019).
- 1923 4 Konopka, R. J. & Benzer, S. Clock mutants of *Drosophila melanogaster*. *Proc*  
1924 *Natl Acad Sci U S A* **68**, 2112-2116, (1971).
- 1925 5 Toh, K. L. *et al.* An hPer2 phosphorylation site mutation in familial advanced  
1926 sleep phase syndrome. *Science* **291**, 1040-1043, (2001).
- 1927 6 Xu, Y. *et al.* Modeling of a human circadian mutation yields insights into clock  
1928 regulation by PER2. *Cell* **128**, 59-70, (2007).
- 1929 7 Masuda, S. *et al.* Mutation of a PER2 phosphodegron perturbs the circadian  
1930 phosphoswitch. *Proc Natl Acad Sci U S A* **117**, 10888-10896, (2020).
- 1931 8 Isojima, Y. *et al.* CKIepsilon/delta-dependent phosphorylation is a  
1932 temperature-insensitive, period-determining process in the mammalian  
1933 circadian clock. *Proc Natl Acad Sci U S A* **106**, 15744-15749, (2009).
- 1934 9 Frank, M. G. & Heller, H. C. The Function(s) of Sleep. *Handb Exp Pharmacol*  
1935 **253**, 3-34, (2019).
- 1936 10 Tatsuki, F. *et al.* Involvement of Ca(2+)-Dependent Hyperpolarization in Sleep  
1937 Duration in Mammals. *Neuron* **90**, 70-85, (2016).
- 1938 11 Diering, G. H. *et al.* Homer1a drives homeostatic scaling-down of excitatory  
1939 synapses during sleep. *Science* **355**, 511-515, (2017).
- 1940 12 Wang, Z. *et al.* Quantitative phosphoproteomic analysis of the molecular  
1941 substrates of sleep need. *Nature* **558**, 435-439, (2018).
- 1942 13 Bruning, F. *et al.* Sleep-wake cycles drive daily dynamics of synaptic  
1943 phosphorylation. *Science* **366**, (2019).
- 1944 14 Ode, K. L. & Ueda, H. R. Phosphorylation Hypothesis of Sleep. *Front Psychol*  
1945 **11**, 575328, (2020).

- 1946 15 Funato, H. *et al.* Forward-genetics analysis of sleep in randomly mutagenized  
1947 mice. *Nature* **539**, 378-383, (2016).
- 1948 16 Park, M. *et al.* Loss of the conserved PKA sites of SIK1 and SIK2 increases  
1949 sleep need. *Sci Rep* **10**, 8676, (2020).
- 1950 17 Mikhail, C., Vaucher, A., Jimenez, S. & Tafti, M. ERK signaling pathway  
1951 regulates sleep duration through activity-induced gene expression during  
1952 wakefulness. *Sci Signal* **10**, (2017).
- 1953 18 Bayer, K. U. & Schulman, H. CaM Kinase: Still Inspiring at 40. *Neuron* **103**,  
1954 380-394, (2019).
- 1955 19 Coultrap, S. J. & Bayer, K. U. CaMKII regulation in information processing  
1956 and storage. *Trends Neurosci* **35**, 607-618, (2012).
- 1957 20 Miller, S. G., Patton, B. L. & Kennedy, M. B. Sequences of  
1958 autophosphorylation sites in neuronal type II CaM kinase that control Ca<sup>2+</sup>-  
1959 independent activity. *Neuron* **1**, 593-604, (1988).
- 1960 21 Meyer, T., Hanson, P. I., Stryer, L. & Schulman, H. Calmodulin trapping by  
1961 calcium-calmodulin-dependent protein kinase. *Science* **256**, 1199-1202,  
1962 (1992).
- 1963 22 Mullasseril, P., Dosemeci, A., Lisman, J. E. & Griffith, L. C. A structural  
1964 mechanism for maintaining the 'on-state' of the CaMKII memory switch in the  
1965 post-synaptic density. *J Neurochem* **103**, 357-364, (2007).
- 1966 23 Thornquist, S. C., Langer, K., Zhang, S. X., Rogulja, D. & Crickmore, M. A.  
1967 CaMKII Measures the Passage of Time to Coordinate Behavior and  
1968 Motivational State. *Neuron* **105**, 334-345 e339, (2020).
- 1969 24 Sunagawa, G. A. *et al.* Mammalian Reverse Genetics without Crossing  
1970 Reveals Nr3a as a Short-Sleeper Gene. *Cell Rep* **14**, 662-677, (2016).
- 1971 25 Chemelli, R. M. *et al.* Narcolepsy in orexin knockout mice: molecular genetics  
1972 of sleep regulation. *Cell* **98**, 437-451, (1999).
- 1973 26 Griffith, L. C. Regulation of calcium/calmodulin-dependent protein kinase II  
1974 activation by intramolecular and intermolecular interactions. *J Neurosci* **24**,  
1975 8394-8398, (2004).
- 1976 27 Patton, B. L., Miller, S. G. & Kennedy, M. B. Activation of type II  
1977 calcium/calmodulin-dependent protein kinase by Ca<sup>2+</sup>/calmodulin is inhibited  
1978 by autophosphorylation of threonine within the calmodulin-binding domain. *J*

- 1979 *Biol Chem* **265**, 11204-11212, (1990).
- 1980 28 Colbran, R. J. & Soderling, T. R. Calcium/calmodulin-independent  
1981 autophosphorylation sites of calcium/calmodulin-dependent protein kinase II.  
1982 Studies on the effect of phosphorylation of threonine 305/306 and serine 314  
1983 on calmodulin binding using synthetic peptides. *J Biol Chem* **265**, 11213-  
1984 11219, (1990).
- 1985 29 Lou, L. L. & Schulman, H. Distinct autophosphorylation sites sequentially  
1986 produce autonomy and inhibition of the multifunctional Ca<sup>2+</sup>/calmodulin-  
1987 dependent protein kinase. *J Neurosci* **9**, 2020-2032, (1989).
- 1988 30 Baicum, A. J., 2nd, Shonesy, B. C., Rose, K. L. & Colbran, R. J. Quantitative  
1989 proteomics analysis of CaMKII phosphorylation and the CaMKII interactome  
1990 in the mouse forebrain. *ACS Chem Neurosci* **6**, 615-631, (2015).
- 1991 31 Myers, J. B. *et al.* The CaMKII holoenzyme structure in activation-competent  
1992 conformations. *Nat Commun* **8**, 15742, (2017).
- 1993 32 Vyazovskiy, V. V., Cirelli, C., Pfister-Genskow, M., Faraguna, U. & Tononi, G.  
1994 Molecular and electrophysiological evidence for net synaptic potentiation in  
1995 wake and depression in sleep. *Nat Neurosci* **11**, 200-208, (2008).
- 1996 33 Blanco, W. *et al.* Synaptic Homeostasis and Restructuring across the Sleep-  
1997 Wake Cycle. *PLoS Comput Biol* **11**, e1004241, (2015).
- 1998 34 Chan, K. Y. *et al.* Engineered AAVs for efficient noninvasive gene delivery to  
1999 the central and peripheral nervous systems. *Nat Neurosci* **20**, 1172-1179,  
2000 (2017).
- 2001 35 Torres-Ocampo, A. P. *et al.* Characterization of CaMKIIalpha holoenzyme  
2002 stability. *Protein Sci* **29**, 1524-1534, (2020).
- 2003 36 Nathanson, J. L., Yanagawa, Y., Obata, K. & Callaway, E. M. Preferential  
2004 labeling of inhibitory and excitatory cortical neurons by endogenous tropism  
2005 of adeno-associated virus and lentivirus vectors. *Neuroscience* **161**, 441-450,  
2006 (2009).
- 2007 37 Kon, N. *et al.* CaMKII is essential for the cellular clock and coupling between  
2008 morning and evening behavioral rhythms. *Genes Dev* **28**, 1101-1110, (2014).
- 2009 38 van der Horst, G. T. *et al.* Mammalian Cry1 and Cry2 are essential for  
2010 maintenance of circadian rhythms. *Nature* **398**, 627-630, (1999).
- 2011 39 Vitaterna, M. H. *et al.* Differential regulation of mammalian period genes and



- 2012 circadian rhythmicity by cryptochromes 1 and 2. *Proc Natl Acad Sci U S A* **96**,  
2013 12114-12119, (1999).
- 2014 40 Bae, K. *et al.* Differential functions of mPer1, mPer2, and mPer3 in the SCN  
2015 circadian clock. *Neuron* **30**, 525-536, (2001).
- 2016 41 Zheng, B. *et al.* Nonredundant roles of the mPer1 and mPer2 genes in the  
2017 mammalian circadian clock. *Cell* **105**, 683-694, (2001).
- 2018 42 Suzuki, A., Sinton, C. M., Greene, R. W. & Yanagisawa, M. Behavioral and  
2019 biochemical dissociation of arousal and homeostatic sleep need influenced  
2020 by prior wakeful experience in mice. *Proc Natl Acad Sci U S A* **110**, 10288-  
2021 10293, (2013).
- 2022 43 Zou, D. J. & Cline, H. T. Expression of constitutively active CaMKII in target  
2023 tissue modifies presynaptic axon arbor growth. *Neuron* **16**, 529-539, (1996).
- 2024 44 Ishida, A. *et al.* Critical amino acid residues of AIP, a highly specific inhibitory  
2025 peptide of calmodulin-dependent protein kinase II. *FEBS Lett* **427**, 115-118,  
2026 (1998).
- 2027 45 Murakoshi, H. *et al.* Kinetics of Endogenous CaMKII Required for Synaptic  
2028 Plasticity Revealed by Optogenetic Kinase Inhibitor. *Neuron* **94**, 37-47 e35,  
2029 (2017).
- 2030 46 Kool, M. J. *et al.* CAMK2-Dependent Signaling in Neurons Is Essential for  
2031 Survival. *J Neurosci* **39**, 5424-5439, (2019).
- 2032 47 Colbran, R. J. Inactivation of Ca<sup>2+</sup>/calmodulin-dependent protein kinase II by  
2033 basal autophosphorylation. *J Biol Chem* **268**, 7163-7170, (1993).
- 2034 48 Takao, K. *et al.* Visualization of synaptic Ca<sup>2+</sup> /calmodulin-dependent protein  
2035 kinase II activity in living neurons. *J Neurosci* **25**, 3107-3112, (2005).
- 2036 49 Bhattacharyya, M. *et al.* Flexible linkers in CaMKII control the balance  
2037 between activating and inhibitory autophosphorylation. *Elife* **9**, (2020).
- 2038 50 Wang, Z., Palmer, G. & Griffith, L. C. Regulation of Drosophila  
2039 Ca<sup>2+</sup>/calmodulin-dependent protein kinase II by autophosphorylation  
2040 analyzed by site-directed mutagenesis. *J Neurochem* **71**, 378-387, (1998).
- 2041 51 Lu, C. S., Hodge, J. J., Mehren, J., Sun, X. X. & Griffith, L. C. Regulation of  
2042 the Ca<sup>2+</sup>/CaM-responsive pool of CaMKII by scaffold-dependent  
2043 autophosphorylation. *Neuron* **40**, 1185-1197, (2003).
- 2044 52 Hanson, P. I. & Schulman, H. Inhibitory autophosphorylation of multifunctional



- 2045 Ca<sup>2+</sup>/calmodulin-dependent protein kinase analyzed by site-directed  
2046 mutagenesis. *J Biol Chem* **267**, 17216-17224, (1992).
- 2047 53 Wayman, G. A., Lee, Y. S., Tokumitsu, H., Silva, A. J. & Soderling, T. R.  
2048 Calmodulin-kinases: modulators of neuronal development and plasticity.  
2049 *Neuron* **59**, 914-931, (2008).
- 2050 54 Okamoto, K., Narayanan, R., Lee, S. H., Murata, K. & Hayashi, Y. The role of  
2051 CaMKII as an F-actin-bundling protein crucial for maintenance of dendritic  
2052 spine structure. *Proc Natl Acad Sci U S A* **104**, 6418-6423, (2007).
- 2053 55 Borgesius, N. Z. *et al.* betaCaMKII plays a nonenzymatic role in hippocampal  
2054 synaptic plasticity and learning by targeting alphaCaMKII to synapses. *J*  
2055 *Neurosci* **31**, 10141-10148, (2011).
- 2056 56 Bayer, K. U., De Koninck, P., Leonard, A. S., Hell, J. W. & Schulman, H.  
2057 Interaction with the NMDA receptor locks CaMKII in an active conformation.  
2058 *Nature* **411**, 801-805, (2001).
- 2059 57 Strack, S., McNeill, R. B. & Colbran, R. J. Mechanism and regulation of  
2060 calcium/calmodulin-dependent protein kinase II targeting to the NR2B subunit  
2061 of the N-methyl-D-aspartate receptor. *J Biol Chem* **275**, 23798-23806, (2000).
- 2062 58 Honda, T. *et al.* A single phosphorylation site of SIK3 regulates daily sleep  
2063 amounts and sleep need in mice. *Proc Natl Acad Sci U S A* **115**, 10458-10463,  
2064 (2018).
- 2065 59 Cheng, D. *et al.* Relative and absolute quantification of postsynaptic density  
2066 proteome isolated from rat forebrain and cerebellum. *Mol Cell Proteomics* **5**,  
2067 1158-1170, (2006).
- 2068 60 Takeuchi, Y., Yamamoto, H., Fukunaga, K., Miyakawa, T. & Miyamoto, E.  
2069 Identification of the isoforms of Ca(2+)/Calmodulin-dependent protein kinase  
2070 II in rat astrocytes and their subcellular localization. *J Neurochem* **74**, 2557-  
2071 2567, (2000).
- 2072 61 Jewett, K. A. *et al.* Tumor necrosis factor enhances the sleep-like state and  
2073 electrical stimulation induces a wake-like state in co-cultures of neurons and  
2074 glia. *Eur J Neurosci* **42**, 2078-2090, (2015).
- 2075 62 Saberi-Moghadam, S., Simi, A., Setareh, H., Mikhail, C. & Tafti, M. In vitro  
2076 Cortical Network Firing is Homeostatically Regulated: A Model for Sleep  
2077 Regulation. *Sci Rep* **8**, 6297, (2018).

- 2078 63 Valk, E. *et al.* Multistep phosphorylation systems: tunable components of  
2079 biological signaling circuits. *Mol Biol Cell* **25**, 3456-3460, (2014).
- 2080 64 Wright, P. E. & Dyson, H. J. Intrinsically disordered proteins in cellular  
2081 signalling and regulation. *Nat Rev Mol Cell Biol* **16**, 18-29, (2015).
- 2082 65 Karandur, D. *et al.* Breakage of the oligomeric CaMKII hub by the regulatory  
2083 segment of the kinase. *Elife* **9**, (2020).
- 2084 66 Cook, S. G., Buonarati, O. R., Coultrap, S. J. & Bayer, K. U. CaMKII  
2085 holoenzyme mechanisms that govern the LTP versus LTD decision. *Sci Adv*  
2086 **7**, (2021).
- 2087 67 Gangopadhyay, S. S., Gallant, C., Sundberg, E. J., Lane, W. S. & Morgan, K.  
2088 G. Regulation of Ca<sup>2+</sup>/calmodulin kinase II by a small C-terminal domain  
2089 phosphatase. *Biochem J* **412**, 507-516, (2008).
- 2090 68 Yilmaz, M., Gangopadhyay, S. S., Leavis, P., Grabarek, Z. & Morgan, K. G.  
2091 Phosphorylation at Ser(2)(6) in the ATP-binding site of Ca(2+)(+)/calmodulin-  
2092 dependent kinase II as a mechanism for switching off the kinase activity.  
2093 *Biosci Rep* **33**, (2013).
- 2094 69 Fustin, J. M. *et al.* Two Ck1delta transcripts regulated by m6A methylation  
2095 code for two antagonistic kinases in the control of the circadian clock. *Proc*  
2096 *Natl Acad Sci U S A* **115**, 5980-5985, (2018).
- 2097 70 Narasimamurthy, R. *et al.* CK1delta/epsilon protein kinase primes the PER2  
2098 circadian phosphoswitch. *Proc Natl Acad Sci U S A* **115**, 5986-5991, (2018).
- 2099 71 Ukai, H. *et al.* Melanopsin-dependent photo-perturbation reveals  
2100 desynchronization underlying the singularity of mammalian circadian clocks.  
2101 *Nat Cell Biol* **9**, 1327-1334, (2007).
- 2102 72 Thiel, G., Greengard, P. & Sudhof, T. C. Characterization of tissue-specific  
2103 transcription by the human synapsin I gene promoter. *Proc Natl Acad Sci U S*  
2104 *A* **88**, 3431-3435, (1991).
- 2105 73 Blichenberg, A. *et al.* Identification of a cis-acting dendritic targeting element  
2106 in MAP2 mRNAs. *J Neurosci* **19**, 8818-8829, (1999).
- 2107 74 Masuda, T., Tomita, M. & Ishihama, Y. Phase transfer surfactant-aided trypsin  
2108 digestion for membrane proteome analysis. *J Proteome Res* **7**, 731-740,  
2109 (2008).
- 2110 75 Boersema, P. J., Raijmakers, R., Lemeer, S., Mohammed, S. & Heck, A. J.

- 2111 Multiplex peptide stable isotope dimethyl labeling for quantitative proteomics.  
2112 *Nat Protoc* **4**, 484-494, (2009).
- 2113 76 Matsumoto, K. *et al.* Advanced CUBIC tissue clearing for whole-organ cell  
2114 profiling. *Nat Protoc* **14**, 3506-3537, (2019).
- 2115 77 Rappsilber, J., Mann, M. & Ishihama, Y. Protocol for micro-purification,  
2116 enrichment, pre-fractionation and storage of peptides for proteomics using  
2117 StageTips. *Nat Protoc* **2**, 1896-1906, (2007).
- 2118 78 Tsujino, K. *et al.* Establishment of TSH beta real-time monitoring system in  
2119 mammalian photoperiodism. *Genes Cells* **18**, 575-588, (2013).
- 2120 79 Mikuni, T., Nishiyama, J., Sun, Y., Kamasawa, N. & Yasuda, R. High-  
2121 Throughput, High-Resolution Mapping of Protein Localization in Mammalian  
2122 Brain by In Vivo Genome Editing. *Cell* **165**, 1803-1817, (2016).
- 2123 80 Sunagawa, G. A., Sei, H., Shimba, S., Urade, Y. & Ueda, H. R. FASTER: an  
2124 unsupervised fully automated sleep staging method for mice. *Genes Cells* **18**,  
2125 502-518, (2013).
- 2126 81 Niwa, Y. *et al.* Muscarinic Acetylcholine Receptors Chrm1 and Chrm3 Are  
2127 Essential for REM Sleep. *Cell Rep* **24**, 2231-2247 e2237, (2018).
- 2128 82 Ukai, H., Kiyonari, H. & Ueda, H. R. Production of knock-in mice in a single  
2129 generation from embryonic stem cells. *Nat Protoc* **12**, 2513-2530, (2017).
- 2130 83 Ode, K. L. *et al.* Knockout-Rescue Embryonic Stem Cell-Derived Mouse  
2131 Reveals Circadian-Period Control by Quality and Quantity of CRY1. *Mol Cell*  
2132 **65**, 176-190, (2017).
- 2133 84 Kiyonari, H., Kaneko, M., Abe, S. & Aizawa, S. Three inhibitors of FGF  
2134 receptor, ERK, and GSK3 establishes germline-competent embryonic stem  
2135 cells of C57BL/6N mouse strain with high efficiency and stability. *Genesis* **48**,  
2136 317-327, (2010).
- 2137 85 Vong, L. *et al.* Leptin action on GABAergic neurons prevents obesity and  
2138 reduces inhibitory tone to POMC neurons. *Neuron* **71**, 142-154, (2011).
- 2139 86 Taniguchi, H. *et al.* A resource of Cre driver lines for genetic targeting of  
2140 GABAergic neurons in cerebral cortex. *Neuron* **71**, 995-1013, (2011).
- 2141 87 Sato, H., Amagai, K., Shimizukawa, R. & Tamai, Y. Stable generation of  
2142 serum- and feeder-free embryonic stem cell-derived mice with full germline-  
2143 competency by using a GSK3 specific inhibitor. *Genesis* **47**, 414-422, (2009).

- 2144 88 Challis, R. C. *et al.* Systemic AAV vectors for widespread and targeted gene  
2145 delivery in rodents. *Nat Protoc* **14**, 379-414, (2019).
- 2146 89 Deverman, B. E. *et al.* Cre-dependent selection yields AAV variants for  
2147 widespread gene transfer to the adult brain. *Nat Biotechnol* **34**, 204-209,  
2148 (2016).
- 2149 90 Liguore, W. A. *et al.* AAV-PHP.B Administration Results in a Differential  
2150 Pattern of CNS Biodistribution in Non-human Primates Compared with Mice.  
2151 *Mol Ther* **27**, 2018-2037, (2019).
- 2152
- 2153
- 2154

2155 **LIST OF SOURCE FILES**

2156 **Figure1-sourcedata 1**

2157 Sleep phenotypes of mice expressing CaMKII $\beta$  single D mutants.

2158

2159 **Figure1-sourcedata 2**

2160 Quantified values of CaMKII $\alpha/\beta$ -derived peptides.

2161

2162 **Figure1-sourcedata 3**

2163 SRM transition list for the MS-based quantification of CaMKII $\alpha/\beta$ -derived peptides.

2164

2165 **Figure1-figure-supplement 1-sourcedata 1**

2166 Uncropped image of western blotting data.

2167

2168 **Figure1-figure-supplement 1-sourcedata 2**

2169 Raw image files of western blotting data.

2170

2171 **Figure1-figure-supplement 2-sourcedata 1**

2172 Sleep phenotypes of mice expressing CaMKII $\beta$  single D mutants.

2173

2174 **Figure1-figure-supplement 3-sourcedata 1**

2175 *In vitro* expression levels and kinase activities of CaMKII $\beta$  single D mutants.

2176

2177 **Figure2-sourcedata 1**

2178 Sleep phenotypes of mice expressing CaMKII $\beta$  T287D-related mutants.

2179

2180 **Figure2-figure-supplement 1-sourcedata 1**

2181 Sleep phenotypes of mice expressing CaMKII $\beta$  T287D-related mutants.

2182

2183 **Figure3-sourcedata 1**

2184 Sleep phenotypes of Cre-mice expressing CaMKII $\beta$  T287D mutant.

2185

2186 **Figure4-sourcedata 1**

2187 Sleep phenotypes of mice expressing kinase domain of CaMKII $\beta$  or CaMKII inhibitor  
2188 peptide.

2189

2190 **Figure4-figure-supplement 1-sourcedata 1**

2191 EEG/EMG data of *Camk2b* knockout mice or mice expressing CaMKII inhibitor  
2192 peptide.

2193

2194 **Figure5-sourcedata 1**

2195 Sleep phenotypes of mice expressing CaMKII $\beta$  double D mutants.

2196

2197 **Figure5-figure-supplement 1-sourcedata 1**

2198 Sleep phenotypes and *in vitro* kinase activities of CaMKII $\beta$  double D mutants.

2199

2200 **Figure6-sourcedata 1**

2201 Sleep phenotypes of mice expressing CaMKII $\beta$  T306D:T307D-related mutants.

2202

2203 **Figure6-figure-supplement 1-sourcedata 1**

2204 Sleep phenotypes of mice expressing CaMKII $\beta$  T306D:T307D-related mutants.

2205

2206 **Figure6-figure-supplement 2-sourcedata 1**

2207 *In vitro* kinase activities of CaMKII $\beta$ T306D:T307D-related mutants.

2208

2209 **Figure7-sourcedata 1**

2210 Quantified values of peptides derived from purified CaMKII $\beta$ .

2211

2212 **Figure7-sourcedata 2**

2213 SRM transition list for the MS-based quantification of CaMKII $\beta$ -derived peptides.

2214

2215 **Figure7-sourcedata 3**

2216 Sleep phenotypes of mice expressing CaMKII $\beta$  with the combined mutation at sleep  
2217 maintenance and cancelation of sleep induction residues.

2218

2219 **Figure7-figure-supplement 1-sourcedata 1**

2220 Sleep phenotypes of mice expressing CaMKII $\beta$  with the combined mutation at sleep  
2221 maintenance and cancelation of sleep induction residues.  
2222